

Copyright Undertaking

This thesis is protected by copyright, with all rights reserved.

By reading and using the thesis, the reader understands and agrees to the following terms:

1. The reader will abide by the rules and legal ordinances governing copyright regarding the use of the thesis.
2. The reader will use the thesis for the purpose of research or private study only and not for distribution or further reproduction or any other purpose.
3. The reader agrees to indemnify and hold the University harmless from and against any loss, damage, cost, liability or expenses arising from copyright infringement or unauthorized usage.

IMPORTANT

If you have reasons to believe that any materials in this thesis are deemed not suitable to be distributed in this form, or a copyright owner having difficulty with the material being included in our database, please contact lbsys@polyu.edu.hk providing details. The Library will look into your claim and consider taking remedial action upon receipt of the written requests.

**DEVELOPMENT OF AN INTERACTIVE ROBOTIC
MANNEQUIN FOR FASHION INDUSTRY**

PENG SIXIANG

Ph.D

The Hong Kong Polytechnic University

2013

THE HONG KONG POLYTECHNIC UNIVERSITY

INSTITUTE OF TEXTILES AND CLOTHING

DEVELOPMENT OF AN INTERACTIVE ROBOTIC

MANNEQUIN FOR FASHION INDUSTRY

PENG SIXIANG

**A thesis submitted in partial fulfilment of the
requirements for the degree of Doctor of Philosophy**

March 2013

CERTIFICATE OF ORIGINALITY

I hereby declare that this thesis is my own work and that, to the best of my knowledge and belief, it reproduces no material previously published or written, nor material that has been accepted for the award of any other degree or diploma, except where due acknowledgement has been made in the text.

_____ (Signed)

Peng Sixiang (Name of student)

ABSTRACT

This thesis describes the development of a robotic mannequin for fashion dressing. Mannequins are indispensable tools in fashion industry. They are used for apparel design, fitting, alteration, and size gradation. There are set-sized and mechanical adjustable mannequins on the market, however a number of set-sized ones are needed for one complete size range, which can be expensive, moreover, a place is needed to store the mannequins. The adjustable ones are complicated in structure yet clumsy to use and they can only change in limited parts. Thus, there is a need for a revolutionary robotic mannequin system to overcome these deficiencies, which is the main goal of this research project.

The robotic mannequin system consists of three part, a personal computer (PC), control unit and robotic mannequin. A user-friendly graphical user-interface software was developed on Windows platform, so the user can control the robotic mannequin easily. The control unit received the control signal from the PC and driven the actuators in the robotic mannequin. The robotic mannequin has 20 degree of freedom which is able to cover the common size range used in the fashion industry. It can change its shape, size and dimension precisely and quickly. The accuracy achieves ± 0.1 cm which is better than what the industry is accepting, i.e. ± 0.5 cm. The

maximum time for transformation is 8.1 s.

The entire research process followed the stages of innovative product design, to develop an idea into a realistic and workable product. First stage was the understanding of opportunity and market need from the literature review. Second stage was defining the design specification according to the market requirements. For investigating the human body shape variation, a data base of 130 Chinese female profiles was built using a 3-D body scanner. Statistic analyses were performed to analyze the body variation quantitatively. For a more comprehensive understanding of regularities of the body variation, the anthropometric surveys of other population were also studied. Third stage was concept design. A virtual mannequin which is able to decrease/increase its body size for simulating the appearance and function of the real robotic mannequin was developed. The fourth stage was the "robotic mannequin system detailed design stage", which involved an in-depth discussion and design of the physical robotic mannequin based on the virtual parametric mannequin. Standardized design and modular design were adopted in the design of mechanism. Finite element analysis (FEA) was adopted to ensure the safety of the structure. The fifth stage was the manufacturing and integration, where the parts were produced and integrated into the system. The final stage was the system validation, where the

performance of variation range and precision of the robotic mannequin were tested.

The feedbacks from the professionals indicate that the robotic mannequin system is practical for the fashion industry, the dimensional variation range is sufficient, and the shape variation is realistic. The system can be used for garment design, quality control relating to garment fitting, garment factories, customized garment design. E-retailing and on-line purchase.

LIST OF PUBLICATIONS

Referred Journal Papers

Peng Sixiang, Chan Chee-kooi, and W.H. Ip. 2011. Waist-Hip Section Surface Profile Data Automatic Analyzing System: WHS. *The International Journal of Human Factors Modelling and Simulation*, Volume 2, Number 4, PP.267-275.

Peng Sixiang, Chan Chee-kooi, Ameersing Luximon and W.H. Ip. 2012. Parametric Body Model Development. *Computer Technology and Application*, Volume 3, Number 3, PP.209-210.

Kuan-Sheng Zou, Chee-Kooi Chan, Si-Xiang Peng, Ameersing Luximon, Zeng-Qiang Chen, Wai-Hung Ip. 2012. Shape-based Retrieval and Analysis of 3D Models Using Fuzzy Weighted Symmetrical Depth Images. *Neurocomputing*, Volume 89, PP. 114-121.

Kuan-Sheng Zou, Chee-Kooi Chan, Si-Xiang Peng, Wai-Hung Ip and Zeng-Qiang Chen. 2011. Efficient 3D Model Retrieval by Using Symmetrical Depth Images. *ICICEL*, Volume 5, Number 8, PP. 2889-2894.

Conference Papers

Peng Sixiang, Chan Chee-kooi, Ameersing Luximon and W.H. Ip. 2011 July. 3D Parametric Body Model Based On Chinese Female Anthropometric Analysis. *HCI international 2011 proceeding*, PP. 22-29, Orlando, USA.

Peng Sixiang, Chan Chee-kooi, Ameersing Luximon & W.H. Ip. 2012

December. Evolution and development of mannequin for the fashion industry.

8th International Shibori Symposium proceeding, PP 210-213, Hong Kong

S.A.R.

Peng Sixiang, Chan Chee-kooi, Ameersing Luximon and W.H. I. 2012

April. Shape Map Method for 3D Body Scanning Information Storage. *Asian*

Workshop on 3D Body Scanning Technologies proceeding, PP 71-76, Tokyo.

Japan.

Patent applied

China (201210279971.5)

Hong Kong (12111456.0)

ACKNOWLEDGEMENTS

This project began in 2009 with the support of industry. It is also partly funded by the General Research Fund of the Research Grants Council.

I would like to express my deepest gratitude and appreciation to my chief supervisor, Dr. Chan Chee-kooi, who provide me with his guidance and patient support throughout this project. His excellent ideas are indispensable in this robotic mannequin project, And his firm support and patience help me to overcome the difficulties encountered. I am also thankful to my co-supervisors, Dr. Ameersing Luximon and Dr. W.H. Ip, who offered me help during my research.

I would like to express my special appreciation and love to my parents and Fang Siyan, who strongly supported me through this period of study.

Special thanks are also due to Win Hanverky Ltd. For their kind donation and Ms. Agnes Yeung for her support and help in this project.

Last but not least, I am thankful to the staffs and students in the Institute of Textile & Clothing of the Hong Kong Polytechnic University.

TABLE OF CONTENTS

ABSTRACT	i
LIST OF PUBLICATIONS	iv
ACKNOWLEDGEMENTS	vi
TABLE OF CONTENTS	vii
LIST OF FIGURES.....	xii
LIST OF TABLES.....	xxi
Chapter 1 Introduction	1
1.1. Background of study	1
1.2. Objectives.....	5
1.3. Significance of study.....	6
1.4. Organization of the thesis.....	8
Chapter 2 Literature Review	9
2.1. Mannequin history and development.....	9
2.1.1. From 1350 BC to the 21 st century	9
2.1.2. Adjustable mannequin design.....	17
2.2. Recent technique in mannequin development.....	26
2.2.1. 3-D scanning technology in fashion industry	26

2.2.2. Fixed dress form manufacture process and company currently	35
2.2.3. Virtual mannequins in fashion industry.....	40
2.3. Robotic mannequin background and prospect.....	46
2.3.1. Robot development.....	46
2.3.2. Robotic mannequin.....	54
Chapter 3 Research Methodology	57
3.1 Introduction.....	57
3.2 Research Framework	57
3.3 Research methodology.....	60
3.3.1 Understanding of opportunity and requirements.....	60
3.3.2 Design specifications.....	60
3.3.3 Concept design	61
3.3.4 Robotic mannequin system detailed design	62
3.3.5 Manufacturing and integration	63
3.3.6 System validation	63
Chapter 4 Design Specifications	64
4.1 Introduction.....	64
4.2 Body morphological variation analysis	65
4.2.1 Anthropometric survey of Chinese female.....	65

4.2.2	Anthropometric analysis result.....	66
4.3	Variation range definition.....	74
4.3.1.	Mannequin size.....	74
4.3.2.	Anthropometric data of Japanese and American studies	77
4.3.3.	Robotic mannequin size variation range	79
Chapter 5	Concept design	81
5.1	Introduction	81
5.2	Initial shape design.....	81
5.2.1	3-D scanning body profile data preparation	82
5.2.2	Cross-section level design	88
5.2.3	B-spline curve construction	90
5.2.4	Initial shape Generation.....	100
5.3	Panel and kinematics design	101
5.3.1.	Primary panels design.....	101
5.3.2.	Major panel movement simulation and kinematic design	106
5.3.3.	Style panel design and modification.....	110
5.3.4.	Pilot validation result and comment	112
Chapter 6	Detailed design of the robotic mannequin.....	118
6.1.	Introduction	118

6.2. Mechanical part.....	119
6.2.1. Mechanical module design.....	120
6.2.2. Mechanism design.....	121
6.3. Electrical & Electronic part	155
6.3.1. Rotation actuator system	156
6.3.2. Linear actuator system.....	161
6.4. Cladding part.....	166
6.5. Controlling Software part	167
6.6. Production and integration.....	172
6.6.1. Production	172
6.6.2. Integration	172
6.7. Summary of chapter.....	174
Chapter 7 System validation	175
7.1. Introduction.....	175
7.2. Range of dimensional variation and transformation time.....	175
7.3. Accuracy and repeatability	179
7.4. Cladding elasticity test.....	184
7.5. Summary of chapter.....	188
Chapter 8 Conclusion and future work	189

8.1. Summary of research project	189
8.2. Feedback from professionals.....	190
8.3. Discussion	193
8.4. Future work	196
Appendices	198
Appendix I. Anthropometric measurements of Chinese female.....	198
Appendix II. Pilot survey result of concept design	202
Appendix III. Cladding pattern.....	206
Bibliographies	207

LIST OF FIGURES

Figure 1-1. A dress form used in the fashion industry	1
Figure 2-1. A wooden torso found in King Tutankhamen's tomb.....	10
Figure 2-2. Mannequins from various periods.....	11
Figure 2-3. Pierre Imans' wax mannequins form the early 20th century.....	12
Figure 2-4. Lester Gaba repairs an arm on his mannequin named Cynthia.....	14
Figure 2-5. One of the "New look" Mannequins.	15
Figure 2-6. A belt type adjustable mannequin	21
Figure 2-7. A panel type adjustable mannequin.....	22
Figure 2-8. A flexible type adjustable mannequin	23
Figure 2-9. The first example of the simple type adjustable mannequins	24
Figure 2-10. The second example of the simple type adjustable mannequins.....	25
Figure 2-11. Examples of exploitation of human body digitization for styling applications. Source: "3-D body scanning technology for fashion and fashion industry"(N. D'Apuzzo, 2006).....	29
Figure 2-12. An example of the laser-based unit using triangulation method. Source: "3-D scanning instruments" (W. Böhler and A. Marbs, 2002)	33
Figure 2-13. An example of the light-based unit using triangulation method. Source: "3-D scanning instruments"(W. Böhler and A. Marbs, 2002)	35

Figure 2-14. Moulds used to make dress form.....	36
Figure 2-15. Coat the wet card boards with plaster and glue.....	37
Figure 2-16. Feathering process.....	38
Figure 2-17. Press the card boards into the mould.....	38
Figure 2-18 Overlap the card board edges.	39
Figure 2-19. Review the dress form when opening the moulds.....	40
Figure 2-20. Parametric mannequin development procedures: (a) obtain the point cloud data and locate the mark points; (b) construct the wireframe; (c) generate the surface. Source: "Parameterization and parametric design of mannequins"(CCL Wang, 2005)	43
Figure 2-21. Cross-section profiles generated using Graham convex hull generation method. Source: “Parametric body model generation for garment drape simulation”(S Kim and CK Park, 2004)	44
Figure 2-22. Water clock built by Su Song.	47
Figure 2-23. A tea-serving Karakuri.....	48
Figure 2-24. Left: A Talon 3B robot unit removes a mine. Right: A MQ-1 Predator equipped two laser-guided Hellfire anti-tank missiles.....	51
Figure 2-25. A KR 16 ARC HW robot.....	52
Figure 2-26. Curiosity Mars Rover relies on the radioisotope power system and	

numerous tools equipped to access the habitability of Mars.	53
Figure 2-27. a: The ASIMO robot (Y. Sakagami, R. Watanabe et al., 2002). b: The Jules robot. Source: a: Photo courtesy of Honda Motor Co., Ltd. b: Photo courtesy of Daily Mail Co. UK, Ltd.	53
Figure 2-28. A robotic mannequin system for online shopping.....	56
Figure 2-29. Male robotic mannequin from Fits.me can shift between small and extra large.....	56
Figure 3-1. Frame work of project.....	59
Figure 4-1. A plane determined by the left, right waist point and crotch point.	68
Figure 4-2. Comparison of the increasing rate between the front part and back part of the waist girth.....	69
Figure 4-3. Comparison of the increasing rate between the front part and back part of the hip girth.	70
Figure 4-4. Alvanon’s Missy Miss series full body mannequin.....	76
Figure 4-5. K&L’s WED series dress form.....	76
Figure 5-1. 3-D body scan data.....	83
Figure 5-2. Comparison of one slice before and after the alignment process.....	85
Figure 5-3. From left to right, three different subjects with a slightly backward, straight, slightly forward posture. The two points are the shoulder point and crotch	

point.	87
Figure 5-4. A plane is defined by the two shoulder points and crotch point. The body angle is the angle between the x axial and the plane.....	88
Figure 5-5. Layout of the cross-sections for the initial shape. All units are in millimetre.	89
Figure 5-6. The cross-section at the bust level constructed by the points and B-spline curve. Left shows the proximate level to the bust level. Right shows the average shape represented by B-spline curve.....	91
Figure 5-7. The front, top, back and bottom view of the initial shape profile	100
Figure 5-8. Major body sections of UK size 12 and 22 superimposed on each other (P.J. Taylor and M.M. Shoben, 1993).....	102
Figure 5-9. Dotted line shows waist cross- sections of 62cm and 80cm in waist girth superimposed on each other according to the center point. The curve and arrow shows that the general shape can be represented by move 4 panels in 4 different directions.....	102
Figure 5-10. Left shows the bust point's horizontal variation. Right shows the bust point's vertical variation when the body size increases (P.J. Taylor and M.M. Shoben, 1993).	103
Figure 5-11. Virtual robotic mannequin shell	104

Figure 5-12. Front and back view of the virtual robotic mannequin panels.	104
Figure 5-13. Side view of the virtual robotic mannequin panels.	105
Figure 5-14. Top view of the virtual robotic mannequin panels.	105
Figure 5-15. The front, side and top view of modified neck panels.	111
Figure 5-16. Front and side view of modified abdomen panels.	111
Figure 5-17. The front, side and top view of the additional part added to the shoulder.	112
Figure 5-18. virtual robotic mannequin imitates the shape of an Asian Size 10 mannequin. Top left is the front view, top right is the back view, bottom left is the side view, and bottom right is the right view.	114
Figure 5-19. Virtual robotic mannequin imitates the shape of an Asian Size 12 mannequin. Top left is the front view, top right is the back view, bottom left is the side view, and bottom right is the right view.	115
Figure 5-20: Virtual robotic mannequin imitates the shape of a US Size 8 mannequin. Top left is the front view, top right is the back view, bottom left is the side view, and bottom right is the right view.	116
Figure 6-1. Top-down design procedure for robotic mannequin development.	119
Figure 6-2. Layout of modules.	120
Figure 6-3. Support module overview. All units are in mm.	122

Figure 6-4. Top view of the support module (Unit: mm).....	123
Figure 6-5. Von Mises stress distribution of the support module. The green arrow represents the fixture. The purple arrow represents the external force.	125
Figure 6-6. Neck model overview.....	126
Figure 6-7. Von Mises stress distribution on the support part of the neck module. The blue line with a dot in the end represents a connector.....	128
Figure 6-8. Link mechanism schematic diagram. The solid arrow shows the movement direction. The circle of the gear represents the reference circle. All the linear dimensions are in mm.	130
Figure 6-9. Front chest overview	131
Figure 6-10. Back chest overview.....	131
Figure 6-11. Chest plate part overview	133
Figure 6-12. A circular pattern of screws on the flange to assist in fixing.....	133
Figure 6-13. Von Mises stress distribution on the support part of the chest plate part	134
Figure 6-14. Front chest mechanism schematic diagram. The solid arrow shows the movement direction. All the linear dimensions are in mm.	135
Figure 6-15. Back chest mechanism schematic diagram. The solid arrow shows the movement direction. All the linear dimensions are in mm.	136

Figure 6-16. Bust mechanism schematic diagram. The solid arrow shows the movement direction. All the linear dimensions are in mm.	138
Figure 6-17. Side view of the right bust slider and panel, the movement of left bust panel is identical. All the linear dimensions are in mm.	138
Figure 6-18. Front waist overview	140
Figure 6-19. Chest plate part overview	142
Figure 6-20. Von Mises stress distribution on waist plate part	143
Figure 6-21. Front waist mechanism schematic diagram. The solid arrow shows the movement direction. All the linear dimensions are in mm.	144
Figure 6-22. Back waist mechanism schematic diagram. The solid arrow shows the movement direction. All the linear dimensions are in mm.	145
Figure 6-23. Upper abdomen mechanism schematic diagram. The solid arrow shows the movement direction. All the linear dimensions are in mm.	147
Figure 6-24. Front 45 degree angle overview of the hip module.....	148
Figure 6-25. Rear overview of the hip module	148
Figure 6-26. Hip plate part overview	150
Figure 6-27. Von Mises stress distribution on hip plate part	151
Figure 6-28. Front hip mechanism schematic diagram. The solid arrow shows the movement direction. All linear dimensions are in mm.	152

Figure 6-29. Back hip mechanism schematic diagram. The solid arrow shows the movement direction. All linear dimensions are in mm.	153
Figure 6-30. Lower abdomen mechanism schematic diagram. The solid arrow shows the movement direction. All linear dimensions are in mm.	155
Figure 6-31. RobotBase RB-150MG RC servo	156
Figure 6-32. Schematic block diagram for RC servo system.....	158
Figure 6-33. Input pulse for RC servo	159
Figure 6-34. RobotBase Co. Ltd RC servo control board.....	160
Figure 6-35. Hybrid linear stepper actuators (DINGS' electrical & mechanical Co., Ltd product brochure, 2012)	162
Figure 6-36. Thrust diagram for hybrid linear captive stepper actuator. Lines with different label are corresponding to different model of linear actuator. The values in lower table stand for the linear speed (mm/s), pulse speed (pps) and rotary speed (rpm) (DINGS' electrical & mechanical Co., Ltd product brochure, 2012).	164
Figure 6-37 JMDM-COMTSM double stepper controller from JMDM Co., Ltd ...	166
Figure 6-38. Soft films are attached to the edge of panels so it can support the cladding over the gap when the cladding is covered on them.....	167
Figure 6-39. Robotic mannequin control software flowchart	169
Figure 6-40. GUI for robotic mannequin	171

Figure 6-41. Preset mannequin sizes in the "Mannequin size" drop-down list	171
Figure 6-42. From left to right, the front, side and back view of the robotic mannequin with panels installed	173
Figure 6-43. From left to right, the front, side and back view of the robotic mannequin with panels and cladding	173
Figure 7-1. Front view of the robotic mannequin of the minimum and maximum size.	176
Figure 7-2. Side view of the robotic mannequin of the minimum and maximum size	176
Figure 7-3. Back view of the robotic mannequin of the minimum and maximum size	177
Figure 7-4. The Accuracy and repeatability measurements	180
Figure 7-5. Elastic fabric used for cladding	187
Figure 7-6. Elasticity test using Instron 5566 device	187

LIST OF TABLES

Table 2-1. Flexible mannequins' designs	19
Table 2-2. 3-D scanners classified by Wolfgang Boehler and Andreas Marbs (C.L. Istook and S.J. Hwang, 2001).	31
Table 2-3. 3-D scanners classified by Nicola D'Apuzzo (N. D'Apuzzo, 2007a)	32
Table 4-1. Mean, standard deviation, and range of the anthropometric measurements of 130 female subjects.....	67
Table 4-2 Correlation coefficients between critical body dimensions. The correlation relationship for 130 Chinese female is shown as the value without brackets. The correlation relationship of U.S. females is shown as the value with brackets (J Cheverud, CC Gordon et al., 1988). "-" means the two part of body are irrelevant in robotic mannequin panel design.....	72
Table 4-3. ISO DIS 4416 standard bra cup size specification.....	73
Table 4-4. Bust size distribution of the 130 Chinese females	73
Table 4-5. Major size range for existing mannequins. The neck base girth measurements are not available on the K&L website.	77
Table 4-6. Body measurements of Japanese (Makiko Kouchi and Masaaki Mochimaru, 2002) and U.S. (M. Handbook, 1991) anthropometric surveys. N.A. means the values are not available in the result of the study.	79

Table 4-7. Variation range the robotic mannequin compared to existing mannequin and anthropometric survey of Chinese, Japanese and U.S. female. All units are in cm.	
" N.A." means the value is not available in the original source.....	80
Table 5-1. Robotic mannequin variation range and dimension for initial shape	92
Table 5-2. Cross-section design	99
Table 5-3. Panel movement direction and distance control	110
Table 5-4. Size table for the size 10, 12 and US Size 8 mannequin	113
Table 6-1 Ductile iron mechanical properties	123
Table 6-2. Mechanical properties of 6061 Aluminium alloy and stainless steel	127
Table 6-3. Forces on the thread head of the linear motor of the waist module.....	143
Table 6-4. Forces on the thread head of the linear motor of the hip module	151
Table 6-5. Specification for RobotBase RB-150MG RC servo (RB-150MG product homepage).....	160
Table 6-6. Specification for 14C2047D4-200-915 hybrid linear captive stepper actuator (DINGS' electrical & mechanical Co., Ltd product brochure, 2012)	164
Table 7-1. Range of dimensional variation of the robotic mannequin. All units are in cm.....	177
Table 7-2. Comparison between the designed and actual range of dimensional range of the robotic mannequin. All units are in cm.....	178

Table 7-3. Transformation time testing result	179
Table 7-4. Accuracy and repeatability for neck girth (all units in cm)	181
Table 7-5. Accuracy and repeatability for bust girth (all units in cm)	182
Table 7-6. Accuracy and repeatability for waist girth (all units in cm).....	182
Table 7-7. Accuracy and repeatability for hip girth (all units in cm).....	183
Table 7-8. Accuracy and repeatability for bust to waist vertical length (all units in cm)	183
Table 7-9. Accuracy and repeatability for waist to hip vertical length (all units in cm)	184
Table 7-10. Stretch properties test result. A is the original distance between jaw faces (250 mm). B is the distance between jaw faces measured while the specimens under 1814 ± 1.0 g. C is the distance between jaw faces measured after removal of slack.	187
Table 8-1. Feedbacks for professionals about the robotic mannequin system	192

Chapter 1 Introduction

1.1. Background of study

Mannequins (Figure 1-1), also known as model forms, dummies, manikins and body forms, were first made in the fourteenth century. They were three-quarter wooden torso forms with detachable arms and used for presentation of the dress for religious festivals. Nowadays, mannequins are essential in both fashion industry and for visual merchandising. In the early 1800s, retail mannequins were made of carved wood or metal and covered in fabric. Then, in the late 1800s, as ready-to-wear became more and more popular, a larger assortment of mannequins became available (R. Colborne, 1996).



Figure 1-1. A dress form used in the fashion industry

After the World War II, the age of mass production came, inspiring a new growth

in mannequins requirement. Since then, mannequins were much used in both the fashion industry , visual merchandising and retailing.

The fashion industry relies very much on the availability of the “mannequin” for many of the tasks involved in apparel design, fitting and alteration, and size gradation. The Mannequin is a prototype body on which apparel size designations are based and used as a fit model to suit sizes and styles (JE Workman and ES Lentz, 2000). However, throughout the history of the fashion industry, all of the mannequins adopted are fixed-sized. In every individual country, the fashion industry uses a range of fixed-size model forms produced based on their national anthropometric surveys, e.g. in the UK, the range of sizes for women’s wear can be listed as 6, 8,10, 12, 14, 16, etc. Also, there is other array of many adaptations according to the physical differences in the mix of population. Hence, each and every country and industry have their own model form design based on their needs, making entities like international designers, manufacturers and retailers are in a dilemma in owning many different fit models.

The visual merchandising or merchandising presentation is an effective means of substantially increasing business and sales. Mannequins in display windows and in

store interior present the store's newest fashion garments to attract the customers. At the same time, customers look to mannequins to learn how to combine separates and coordinates and how to wear new colours, silhouettes, textures, textiles, and accessories (R. Colborne, 1996). Thus, a mannequin that has a similar body shape to the customers will best create the image in customers' minds. And, this is the reason that garment stores need to hold a great number of mannequins to cover all the different body sizes of their targeting customers.

The main disadvantages of the traditional mannequin are set-sized and expensive. Adequate money should be budgeted for them in annual purchases for both garment designers and retailers. Moreover, a place is needed to store the mannequins.

Customized mannequins supposedly are duplicates of the human body shape. In the earlier days, body dimensions are taken manually from the human body for each customized mannequin, then made with specific mould or sculpture, resulting in a long production time, high skill requirements and cost. Nowadays, to make such a mannequin, body information is firstly collected by a 3-D body scanner. Then specific mannequin mould is designed and built according to the body information. Lastly, the mannequin is made from the mould. It is still much more expensive compared to the

traditional mannequin and the production time can take eight to ten weeks (Alvanon mannequins).

Another solution is an adjustable mannequin. Companies provide mechanically adjustable mannequins, which can change at the location of neck, bust, waist and hip. Such early mannequin's construction focused on mechanical parts such as wire frame, metal rod, screw and adjustable slots (E.R. Arthur, 1974; I. Greenberg, 1935). Their design features were complicated in structure yet clumsy to use. In recent mannequin development, it has become simple in structure by using the panels design and acrylic material so their adjustable mechanism tends to be simple at the critical location such as bust, waist and hip (M. Barra and J. Ralston, 2007; M. Bentham, G. Bingham et al., 2004; S.J. Claas, 1994; J. Jiang, 1993).

With the advancement in Computer-aided design (CAD) and computer-aided manufacture (CAM), virtual mannequins began to be adopted in various areas such as garment drape simulation (S. Kim and C.K. Park, 2004), female figure identification (K. Simmons, C.L. Istook and P. Devarajan, 2004) and virtual garment design (C.H.M. Hardaker and G.J.W. Fozzard, 1997). Nicola D'Apuzzo (N. D'Apuzzo, 2007b) reviewed the existing market usage of 3-D body scanning technology for the fashion

industry. Virtual-try-on is now possible for the industry. Using 3-D scanning data for digital model development, researchers still tend to use standard mannequins to perform their garment fabrication analysis (S. Petrak and D. Rogale, 2006), however, the virtual mannequin cannot replace the real mannequin for their inability to try on an item for size fitting (R. Greenspan, 2003). In other words, mannequins are essential tools used by the fashion industry and visual merchandising, but the conventional mannequins are costly and occupy a lot of storage space, while the alternatives, such as: customized mannequins, adjustable mannequins and virtual mannequins have limitations. Thus, there is a need for a revolutionary robotic mannequin system to overcome these deficiencies, which is the main goal of this research project.

1.2. Objectives

1. To study the morphological and topological profiles of the Chinese female figure in Hong Kong using the data obtained from the 3-D body scanner owned by the Institute of Textiles and Clothing, The Hong Kong Polytechnic University.

2. To study the mannequins of various standard sizes used by the fashion industry in countries, like U.S. and U.K.

3. To build a virtual mannequin based on the real human body shape data base, anthropometric survey, existing mannequins, to simulate the trunk profile of human body and the shape transformation between different body shapes.

4. To develop and build a prototype of an interactive robotic mannequin with the ability to increase/decrease automatically over a size range which is suitable for different commercial size systems, with the purpose to be used in garment design, fitting and display.

1.3. Significance of study

A revolutionary robotic mannequin system will be able to provide solution to various problems encountered. Mannequins are much used in a variety of domains in the global apparel community. Firstly, in the fashion industry, mannequins are used widely in apparel design, fitting and alteration, and size gradation. However, the model forms are available in a range of sizes in various body configurations making it necessary for apparel companies like design houses, manufacturers and retailers having to stock a wide range of model forms in their arsenal of equipments. Secondly, the mannequins play an important part in the visual merchandising as well. In the

fashion shop, well-dressed mannequins are used to make an impressive apparel presentation, far more than do any other display props (R. Colborne, 1996). Hence, these companies have to own various sizes of mannequins to display diverse range of garments. Besides, mannequins are expensive and needed to be updated from time to time, making it a "headache" for the users.

There are companies that produce custom-made mannequins to fulfil the demand of the market, but they can be rather expensive. As a result, there is indeed a need to have an intelligent and workable solution in the form of an automatic robotic mannequin system that can allow measurements to be keyed into the system and the said mannequin can automatically adjust to the required body configuration, thus saving on cost, space and the problem of stocking many model forms of multiple sizes.

Furthermore, online visual merchandising is showing a very promising future. A study (L. Khakimdjanova and J. Park, 2005) showed that in the past few years, e-commerce has been taking place other than the traditional shopping channel. L. Khakimdjanova and J. Park reported, by 2008, online buying is projected to reach an estimated 63 million household, while the apparel has reported higher sales than other

products. But online apparel shopping still faces obstacle, about 85 percent of women on-line shoppers avoided buying apparel because of the inability to try on an item for size fitting (R. Greenspan, 2003). With the help of a robotic mannequin system, online purchaser can indicate the robotic mannequin to change into their own body shape, then “try on” the selected item on the robotic mannequin and “see” for themselves the performance through webcam, and they can then shop with better confidence.

1.4. Organization of the thesis

Chapter 1 provides a general introduction including background, objectives and significance of the present study. Chapter 2 reviews the relevant fundamental knowledge as well as the related work done by previous researchers. Chapter 3 describes the research methodology of the novel robotic mannequin. Chapter 4 determined the design specifications according to the market needs. Chapter 5 shows the design of a virtual robotic mannequin. Chapter 6 reports the design and development of robotic mannequin’s mechanism, control and user-interface in detail. Chapter 7 presents the experiments results verifying the robotic mannequin’s performance. Finally, Chapter 8 presents the discussions, conclusions and suggestions for future work.

Chapter 2 Literature Review

2.1. Mannequin history and development

2.1.1. From 1350 BC to the 21st century

According to the American Heritage Dictionary, mannequin can be traced back to the French word *mannequin*, which means “an artist’s jointed model”(B.A. Beatie). The terms “doll”, “figure”, “dummy”, “manikin” and “dress form” often refer as alternatives of mannequin, among which, the dress form is the first kind of mannequin. The "Dress form" which is the mannequin with only the torso has been found since the time of the Egyptian pharaohs. It was documented that when Carter opened King Tutankhamen's tomb in 1922, he discovered a wooden torso (Figure 2-1) not far from a clothing chest. Dating from 1350 B.C., it might have been the world's first dress form (E. D'Aulaire and P.O. D'Aulaire, 1991).



Figure 2-1. A wooden torso found in King Tutankhamen's tomb
Source: The Politics of Mannequins, Part I,
<http://www.threadforthought.net/2010/02/16/politics-mannequins-part>

There are not many written records about the development of the mannequin, which go from the dress form to the life-size mannequin as shown as Figure 2-2. Ancestors of today's mannequins, the fashion dolls of the mid-18th Century were originally circulated in France as a mean to publish the latest fashion. Ranging from 12 inches to life size, they were "stylishly" clothed and exchanged freely by the royals and merchant class (J. Peers, 2004). As the fashion dolls were first made in France, it was believed that the first life-size mannequin was also made in France.



Figure 2-2. Mannequins from various periods

Source: James David Buckley, *the Drama of Display*, 1953

The establishment of the great department stores in Europe and America in the mid-19th Century, and the introduction of ready-made clothing sold in those stores, created a great demand for mannequins (E. D'Aulaire and P.O. D'Aulaire, 1991). Dressmaker's dummies and tailor's draping forms, which had been used to display and sell draped yard goods, were soon appropriated to effectively display and sell the new ready-made merchandise. The dress forms were a good beginning, but they lacked the arms and heads deemed necessary to create a realistic display (H. Costume and G. Strege, 1999).

In 1880, Fred Stockman used *papier-mâché* and wax to produce a more life-like mannequin. He commissioned mask houses to make heads and install joints in the

hands, arms, and legs to give the mannequin more flexibility (M. Thesander, 1997).

A metal screen was designed at the bottom of the torso for skirt draping, which was supported by a wooden tripod that was fixed. It became a common way to construct female mannequins until the beginning of the 20th century.

In the beginning of the 20th century, mannequin workshops existed in Brussels, Rome, Berlin, London, and Paris, employing wood carvers, cabinet makers, varnishes, painters, and dressmakers (H. Costume and G. Strege, 1999). Among these, Pierre Imans was considered to be the most famous of his profession due to his systematic use of wax and his skills in mesmerizing the public with his life-like creatures. Figure 2-3 shows one of his wax mannequin.



Figure 2-3. Pierre Imans' wax mannequins from the early 20th century
Source: Bibliotheque des Arts decoratifs, Paris, Maciet Collection.

Historians agreed that display mannequin evolved from four separate figures around the 20th century (1) the dressmaker form; (2) the artist's model; (3) the European fashion dolls as described in the previous paragraph; and (4) the wax sculptures (M. Davis, 1999). The dressmaker form was made according to the exact measurement of the customer to assist the garment design process. The artist's model was used to express the idea of the artist rather than for the use of garment display, they were expensive and not suitable for visual merchandising. The wax sculpture was an extension of the art of sculpting. Wax was just another medium, same as wood or stone (M. Davis, 1999). With the knowledge and technology developed with these four different forms of mannequin, the mannequin came out with a more realistic outlook. They were made of *papier-mâché* and fitted with realistic glass eyes making them looked like real humans.

During the 1930s, Cynthia made by Lester Gaba (Figure 2-4) became the representative of realistic mannequins. “And speaking of fetishes and mannequins: All the sculpted perfection at the Rootstein party—whether fibreglass or flesh—made us think back to our favourite mannequin story of all, that of the 1930s soap-sculptor-turned-mannequin-designer Lester Gaba. Gaba once became so enamoured with one of his pieces, a socialite-like mannequin named Cynthia, that

she accompanied him on ‘dates’ to the Stork Club and the opera. Cynthia lived a life of fame and fortune most young New York women only dream of: Cartier and Tiffany sent her jewels; designers gave her clothes. It was the perfect romance—until one fateful day at the beauty salon, when poor Cynthia slipped from a chair and broke into a million pieces.” (C. Zappia, 2006).



Figure 2-4. Lester Gaba repairs an arm on his mannequin named Cynthia.
Source: Model Girlfriend, Life magazine, New York 1937.

By the mid-30s, the realistic mannequin appeared frequently in store windows, most of which were made according to the famous film stars and members of American high society (T. Gronberg, 1997).

During the World War II, mannequins were made of plaster due to the rationing of supplies, making them very heavy (L. Taylor, 2002). After the war, mannequins were again produced out of the *papier-mâché*. In the late 1940s due to the shortage of material shortage, Mary Brosnan designed mannequins reflecting the silhouette of Christian Dior's revolutionary new style show as Figure 2-5 (M. Brosnan, 1947; H. Costume and G. Strege, 1999).



Figure 2-5. One of the "New look" Mannequins.
Source: Display World, 1947.

The modern mannequin came out with a technological innovation: fibreglass. The first commercial production of fibre glass was in 1936. In 1938 Owens-Illinois Glass Company and Corning Glass Works joined to form the Owens-Corning

Fiberglas Corporation to produce and promote fibre glass (K.L. Loewenstein, 1983).

As the fibre glass can provide a high ratio of surface area to weight and strong properties, it was an ideal material for mannequins (P.I. Frank and P.D.W. David, 1996). From 1950s to 1960s, a blend of fibre glass and polyester took the place of *papier-mâché* to be the new mannequin material. These mannequins were lighter in weight but stronger than the old ones, and could be taken apart and stored easily (H. Costume and G. Strege, 1999).

From 1970s to 1990s, mannequin technology has become mature. Major changes took place in the mannequin's outlook, body shape, make-up, pose, types, etc. During the 1970s, the female mannequins adopted a more natural body shape with the breasts taking on an unsupported "bra-less" look while the male mannequin change from a muscular to a more natural form, which were very similar to nowadays (H. Costume and G. Strege, 1999). Make-up has been changed from time to time to keep up with fashionable style and pose became diverse. And the mannequin developed into different types for modelling clothing as followings,

1. The life-size mannequin is the most common type of mannequins. They were of the same size as the human, with arms, hands, feet, legs, and head. They were made as male, female, children, or abstracted minimalist forms. They were

designed to be detachable and there were movable joints so they could be posed in different positions. They were used to model various types of clothing, including pants, shirts, dresses, shoes, underwear and so on.

2. The dress form is a mannequin has only the torso and stand which is mainly for clothes fitting and can also be used to display shirts, blouses or underwear, etc. Compared to the life-size mannequin, they are cheaper and need less storage space.

3. Adjustable mannequin is a mannequin that can change its body shape mechanically at the location of neck, bust, waist and hip. In view of the mannequin's construction, various designs are adopted, such as wire frame, metal rod, screw, adjustable slots, panels design and acrylic material. These designs provide valuable information for the anthropometric design, and in this study 29 different flexible mannequin designs were studied.

2.1.2. Adjustable mannequin design

A number of researches have been carried out on the adjustable mannequin design, as it can change its shape and try to simulate every unique customer's body shape and they are regarded as a good solution to save store room and reduce the cost of having too many mannequins of different body sizes. Between 1880s to

present, designers have new designs. Table 2-1 shows various patented design over the period.

Period	Author(s)	Design	U.S. Patent No.
1880-1890	J. Hall	Adjustable Dress Form	269,851
	A Tuck & H. A. Smith	Dress Form	393,799
	W. A. Johnson	Dress Form	397,986
1890-1900	W. Vogler	Dress Form	479,232
	J. R. Hebert	Dress Form	427,510
	H. A. Brown	Dress Waist Form	468,308
1900-1910	C. A. Ufford	Dress Form	913,329
1910-1920	F. B. Granger	Adjustable Dress Form	1,153,218
	C. A. Ufford	Adjustable Dress Form	1,259,808
	C. A. Ufford	Dress Form	1,267,937
	C. A. Ufford	Expansible Dress Form	1,165,045
	J. A. Kubal	Dress Form	1,168,653
	R. Rubin	Dress Form	963,724
	I. M. Bond	Garment Fitter	986,041
	E. Van Dusen	Model form for garment fitting	974,936
	C. W. Farquharson	Adjustable Dress Form	1,221,522
1930-1940	I. Rosenfeld	Flexible Model Form	2,056,740
1940-1950	J. Kroll	Collapsible Model Form	2,367,171
	J. L. Ray ET Al	Stand for dress-forms and the like	2,284,967

1950-1960	F. Crohn	Buckle-type Adjusting Devices For Dress Forms	2,817,469
	B. Wecler ET AL	Collapsible Dress Form	2,666,559
	A. Laikauf	Collapsible Shoulder Wing For Dress Forms	2,620,099
	J. S. Stoddard	Dress Form	2,879,928
1960-1970	E. E. Ronell	Adjustable Dress Form	3,096,916
	H. Levin ET AL	Dress Form	3,191,821
1990-2000	Jiang	Mannequin With Adjustable Parts	5,265,779
	J. L. Ray ET AL	Stand For Dress-Forms and The like	2,284,967
2000-2010	Martin Bentham, Geoffrey Bingham, David Bruner, Michelle Demers	Configurable Mannequin Form	2004/0222249 A1
	Massion Barra, Jill Ralston	Adjustable Dress Form System	2007/0275632 A1

Table 2-1. Flexible mannequins' designs

From this review, 29 different designs dated from 1880s to the present time have been carefully studied and they can be categorised into 4 major types of adjustable mannequin design as follows,

1. Belt type - This type of adjustable mannequin used soft metal belts to form the shape. It supported the clothing by the elasticity of the strips. The shape could change by adjusting the length of strips. Figure 2-6 shows one of the belt type of adjustable mannequins for fitting the ladies' skirts. The adjustable belts were rigidly connected to the collars or runners, which hold the belts in position. The belt type adjustable mannequin could provide a smooth surface because the belts were in smooth curves, and both of the longitudinal and girth dimensions could be modified. However it was very difficult to have an accurate shape control as the shapes of belts were dependent on the elasticity and toughness. After some uses, there would be permanent deformations, making the belt hard to change the shape according to the design. It was not user-friendly as well. It took times for trying to set the collars or runners in different positions before the desired shape could be obtained. This kind of designs only appeared in the first half of the 20th century, so it is not considered to be a good method of constructing the adjustable mannequins by the present standard.

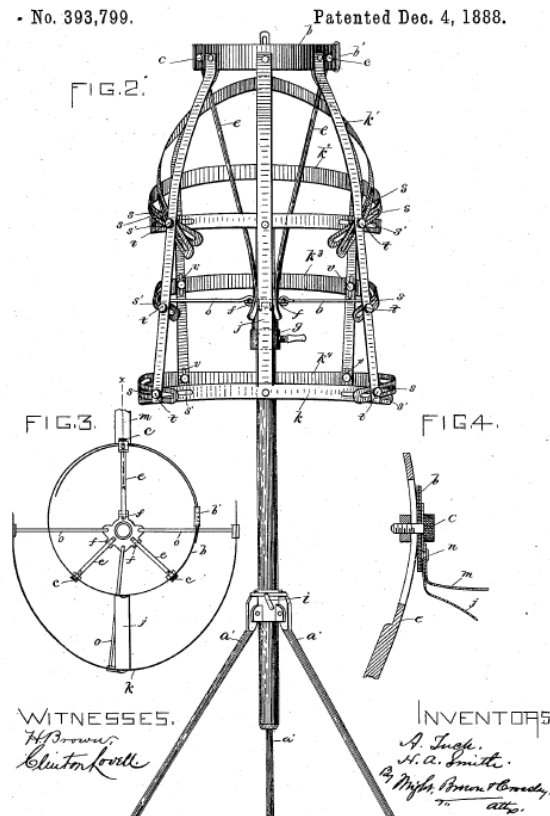


Figure 2-6. A belt type adjustable mannequin

Source: A Tuck & H. A. Smith, Dress Form, US patent 393,799, 1888.

2. Panels type - Figure 2-7 shows another example of the most common type of adjustable mannequins. The sections were assembled edge-to-edge and adjustable to vary their spacing from each other according to the size of garment of which the form is used. The sections were fastened by buckles on the surface. There were also other mannequins of this type, which used fastening devices for the form panels housed on the inside of the mannequins. They all changed their shapes by adjusting the spacing between the panels. The panels afforded a good support for draping clothing. The shape change could be tightly controlled by the drive mechanism.

There were some drawbacks of this kind of mannequin as well. Firstly, its weight was relatively heavier. Secondly, the cost was usually higher than the common mannequin because of the complex mechanism inside. Thirdly, it was not user-friendly enough. Multiple panels were needed to be set one by one manually to get the desired shape.

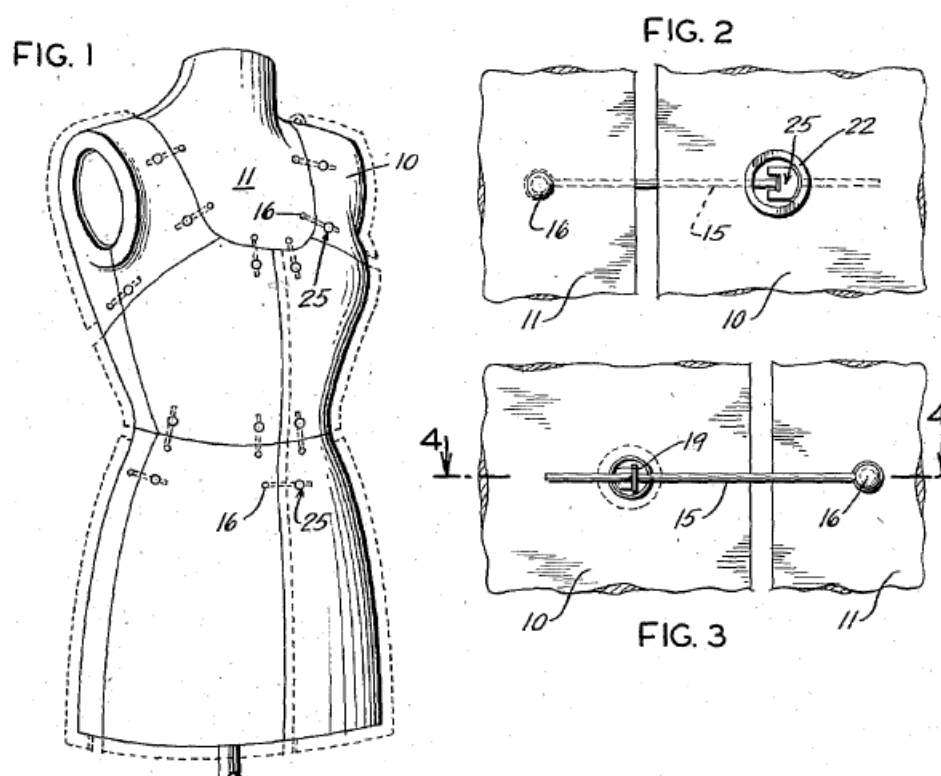


Figure 2-7. A panel type adjustable mannequin

Source: F. Crohn, Buckle-type Adjusting Devices for Dress Forms, US patent 2,817,469, 1957.

3. Flexible type - This was related to that type of adjustable dress form which was made of a material which was sufficiently non-resilient so that the dress form will retain whatever shape it is bent to by the operator. Such dress form could be

re-shaped to different figures repeatedly. Figure 2-8 shows one of the flexible type mannequins, whose surface is connected by wire mesh. The wire mesh is processed by a spraying process to a smooth plastic surface, which is incapable of scratching to prevent the user from injury. The major limitation of this kind of adjustable mannequin is that it needs an experienced operator to shape the form and the process is complex and difficult.

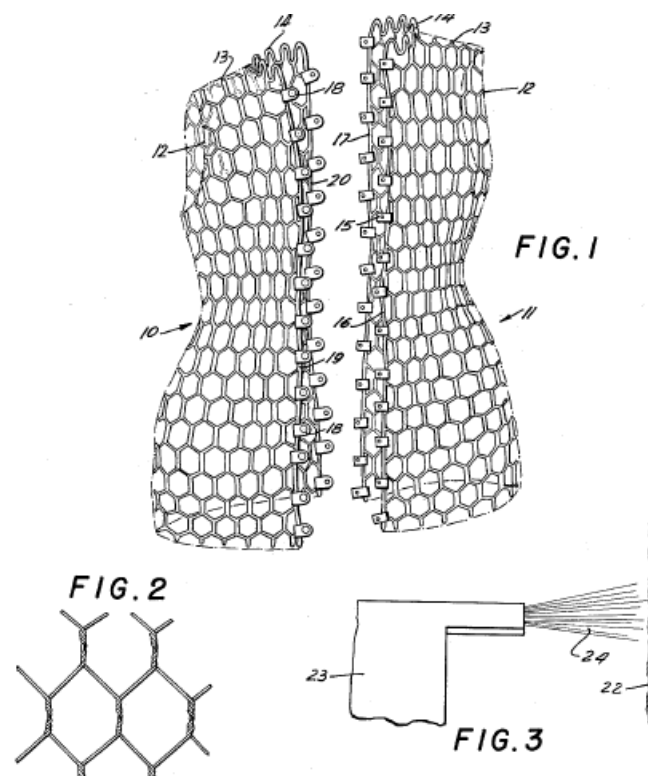


Figure 2-8. A flexible type adjustable mannequin

Source: E. E. Ronell, Adjustable Dress Form, US patent 3,096,916, 1963.

4. Simple type - It relates to the adjustable mannequins with limited adjustable measurements or the mechanism is very simple. Figure 2-9 shows a

simple type of adjustable mannequin which can change its body thickness by inserting or removing a middle piece. Figure 2-10 demonstrates a mannequin which can adjust the shape of bust and hip. The design of this type is very simple and straight forward, thus, its price is usually much cheaper than the other adjustable mannequins and very easy to use. But it has very limited adjustable measurements and the shape is usually not perfect.

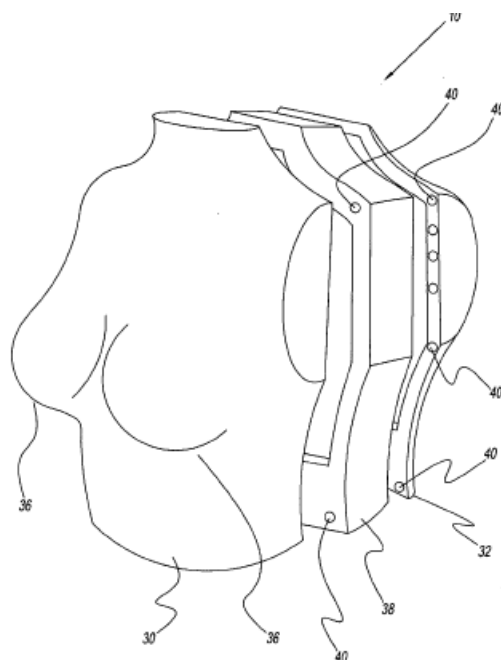


Figure 2-9. The first example of the simple type adjustable mannequins
Source: M. Bentham, G. Bingham, ant etc., Configurable Mannequin
Form, US patent 2004/0222249 A1, 2004.

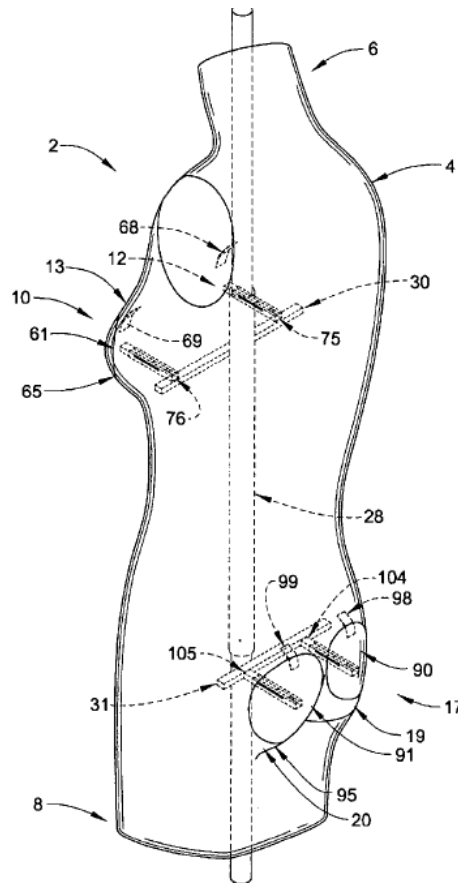


Figure 2-10. The second example of the simple type adjustable mannequins
 Source: M. Barra and J. Ralston, Adjustable Dress Form System,
 2007/0275632 A1, 2007.

From the review of the history of mannequins, it is obvious that they have always been an indispensable part of the fashion industry from the day of its appearance. New techniques and new designs were produced to satisfy the needs of the market. The users who buy a mannequin always look for one that is competitive priced, of better shape, easier storage and user-friendly. Thus, the robotic mannequin can be a feasible and efficient way to improve the mannequins' quality and user experience as it is designed to be automatic, precise, and user-friendly.

2.2. Recent technique in mannequin development

In the last 20 years, new techniques were developed that have affected the development of mannequins, examples, 3-D scanning, 3-D modelling, rapid prototyping, robotics techniques and actuators techniques have all brought about new development into mannequin design and development. In this section, the following techniques in these areas: 3-D scanning technology in fashion industry, fixed dress form manufacturing, and virtual mannequin are discussed.

2.2.1. 3-D scanning technology in fashion industry

3-D scanning technology is used to collect the data of shape or appearance from an object or environment. The collected data can be used to construct 3-D digital objects for various application, such as cultural heritage (M. Andreetto, N. Brusco and G.M. Cortelazzo, 2004; G. Guidi, J.A. Beraldin and C. Atzeni, 2004; S. Hu, H. Zha and A. Zhang, 2006; M. Pieraccini, G. Guidi and C. Atzeni, 2001), reverse engineering (V. Carbone, M. Carocci et al., 2001; K.H. Lee, H. Woo and T. Suk, 2001; M. Sokovic and J. Kopac, 2006; S. Son, H. Park and K.H. Lee, 2002; H.T. Yau, C.Y. Chen and R.G. Wilhelm, 2000), civil engineering (C. Brenneke, O. Wulf and B. Wagner, 2003; X. Dong and R. Huang, 2006; N.J. Shih, H.J. Wang et al., 2007; S. Slob and R. Hack, 2004), CAD (F. Bernardini, L.B. Chandrajit et al., 1999; G.J.

Jense, 1989; W.Y. Kim, M. Stuber et al., 2002; N. Rout, Y.F. Zhang et al., 2010), entertainment (J.A. Beraldin, M. Picard et al., 2005; Y. Gao, Q. Zhao et al., 2010; A. Golovinskiy, V.G. Kim and T. Funkhouser, 2009; H. Seo, Y. Yeo and K. Wohn, 2006; N. Werghi and Y. Xiao, 2002), etc. Besides, it is also playing an important role in the textile industry. During the development of 3-D scanning technology, it gradually shows its advantage for use in the fashion industry. With the use of 3-D body scanners, body measurements can be non-contact, instant and accurate, although there are still no standard for the 3-D scanning measurement terms for the fashion industry (K.P. Simmons and C.L. Istook, 2003). The applications of scanning technology in the fashion industry is discussed herewith:

Firstly, 3-D scanning technology has been adopted in custom apparel design. Back in the 1990s, Michael Potel (S. Paquette, 1996) has already asserted that the custom apparel design would be one of the first commercial user for 3-D scanning technology. He believed that it would bring in better fitting garment, reduced cost in terms of manufacturing and overheads and rapid response. B. Xu, Y. Huang and T. Chen (B. Xu, Y. Huang et al., 2002) developed a body scanning and 3-D garment design technology for small apparel business. They employed the 3-D scanning technology for a rapid, non-contact scanning of a whole or partial body to obtain the

size information for apparel design.

Secondly, it was also adopted in mass apparel production. 3-D scanning technology also increases the accuracy and diversity of the body measurement data in traditional mass production (M.E. Faust and S. Carrier, 2009). On the other hand, it can assist the company to improve the apparel fit through adjusting ready-to-wear sizing (S. Loker, S. Ashdown and K. Schoenfelder, 2005).

Thirdly, the 3-D scanning technology is wildly used in body digitization, which is an essential part in virtual try-on. The users are able to create a digitized 3-D body model to virtually try on a garment or involve in the design procedure as a reference. D'Apuzzo (N. D'Apuzzo, 2006) reviewed the various usage of body digitization in fashion industry as shown in Figure 2-11. On the left shows the software Digital Fashion from Japan. In the centre shows the digital customer card with stored body sizes, from e-Tailor project (EU). On the right is shown a 3-D virtual-try-on solution from Optitex (Israel). He stated that the interests in commercial applications of human body digitization were increasing, because companies want to show their customers how they would look like before they buy the clothes. On the other hand, Vassilev (T.I. Vassilev, 2000) described a fast technique for dressing virtual humans

with different pieces of clothing. The system used 3-D scanner to create body file and then produced a new body dressed with virtual garment. The results showed the system was able to sew a garment around a virtual human body in several seconds. Besides, Kakinuma and et al. (Y Kakinuma, E Tsutsumi et al., 2008) developed a customized garment design supporting system (CGDSS) for individual older aged person using a digital dress form model. They applied 3-D scanning technology to create a digital dress form based on elderly persons. Then the system developed garment patterns semi-automatically on the digital dress form.



Figure 2-11. Examples of exploitation of human body digitization for styling applications. Source: "3-D body scanning technology for fashion and fashion industry"(N. D'Apuzzo, 2006).

After reviewing the 3-D scanning technology application, the technologies of the current 3-D scanners in the fashion industry will be further discussed. As the 3-D scanners currently used in fashion industry are all optically based and non-contact, researchers classified the 3-D scanners by the type of the light used in preview

studies.

In 1995, Michael Potel reviewed the 3-D scanners in the United States (S. Paquette, 1996). He pointed out that the two primary technologies that emerged are the Laser-based scanning systems developed by Cyberware in Monterey, California, and a light-projection system known as Phase Measuring Profilometry (PMP) developed by the Textile and Clothing Technology Corporation (TC²) in Cary, North Carolina.

In 2001 Wolfgang Boehler and Andreas Marbs classified the 3-D scanners into two types: laser and light (C.L. Istook and S.J. Hwang, 2001). They said that there were other systems but not used for capture human shape yet. Table 2-2 shows the 3-D scanner classification by them. Karla Peavy Simmons also classified using the same criteria (K.P. Simmons, 2001).

Light-based		Laser-based		Other	
Company	Product	Company	Product	Company	Product
Hamamatsu	Body lines scanner	Cyberware	WBX, WB4	Immersion	Micro Scribe series
Loughborough University	The Loughborough Anthropometric Shadow Scanner	TecMath	Vitus Pro		
TC2	2T4, 3T6	Vitronic	Viro-3D series		
Wicks and Wilson Ltd.	TriForm series	Hamano	VOXELAN		
Telmat	SYMCAD 3D Virtual model	Polhemus	FASTSCAN		
Turing	Turing C3D	3D scanners	REPLICA, REVERSA, Re Mesh, PROFA		
Puls Scanning System GmbH	Puls scanning system				
CogniTens	Optigo 100 system				

Table 2-2. 3-D scanners classified by Wolfgang Boehler and Andreas Marbs (C.L. Istook and S.J. Hwang, 2001).

In 2006 Nicola D'Apuzzo summarized the 3-D scanning technologies in Europe (N. D'Apuzzo, 2006). He gave a special weight to the body scanners in his review and explored the commercial 3-D scanners worldwide, rather than limited to Europe.

He divided the 3-D scanners into 3 types: (a) laser scanning, (b) projection of light patterns and (c) combination modelling and image processing. In 2007, he published another paper focusing on the 3-D scanning technology in fashion and fashion industry (N. D'Apuzzo, 2007a), where he classified the 3-D scanners into 3 types: (a) laser scanning, (b) projection of light patterns, (c) other. Compared to the previous classification, he expanded the type C by adding scanners using digital manual measurement and technologies based on other active sensors. A distribution of the 3-D scanner companies were summarized as Table 2-3.

	Number of different Laser scanning systems	Number of different white light projection systems	Number of other Types of systems	Total
North America	7	7	5	19
Europe	0	22	7	29
Asia	4	3	0	7
Total	11	32	12	55

Table 2-3. 3-D scanners classified by Nicola D'Apuzzo (N. D'Apuzzo, 2007a)

From the table, it is obvious that the laser-based scanner and light-based scanner are major types of the commercial 3-D body scanner used in the fashion industry,

2.2.1. Laser-based scanner. A common method using laser to detect the object surface is the triangulation method which is accurate in short distance. This device project a laser beam onto the object, and a CCD camera at the other end of this base which detects the laser spot (or line) on the object. The 3-D position of the reflecting object surface can be derived from the resulting triangle as shown in the Figure 2-12. The devices are usually mounted on a movable base, in order to project the laser to different parts of the object. Also multiple devices may be mounted in one 3-D scanner, depending on the body part to be measured. For safety issue, only eye-safe lasers are adopted. There are two major disadvantages (N. D'Apuzzo, 2007a), firstly the cost is high, the system consist laser projectors, sensors, optical system, and precise motors, and secondly, it is time-consuming, as the movable base need to travel at least the length of the object to cover its entire surface.

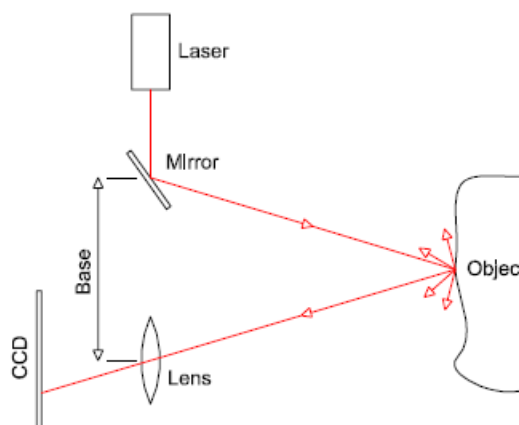


Figure 2-12. An example of the laser-based unit using triangulation method.

Source: “3-D scanning instruments” (W. Böhler and A. Marbs, 2002)

2.2.2. Light-based scanner. This type of 3-D scanner for human body measurement is based on the projection of constructed light patterns as shown in Figure 2-13. It also uses the triangulation method. Instead of moving the scanner unit, a light pattern is projected onto the object surface. The type of projection is varied, it can be a moving light spot or line, a moving stripe patterns, or a static arbitrary pattern (W. Böhler and A. Marbs, 2002). Then the light sensor receives the reflected light from the object surface. The same geometric solution is adopted to calculate the distance between the object and scanner unit from the triangle, resulting in same accuracy as the laser-based method. Multiple of scanner units are mounted on a complex body scanner. Compared to the laser method, it takes less time to complete the scanning process, i.e., it only takes several seconds to scan a whole human body. But it demand a more reflective surface than the laser method, in another word, surface in light color is preferred.

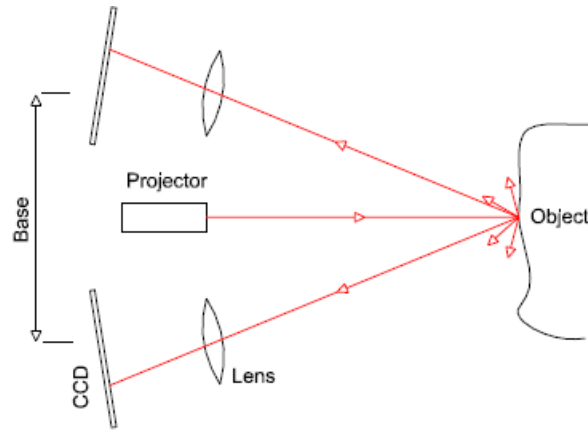


Figure 2-13. An example of the light-based unit using triangulation method.
Source: “3-D scanning instruments”(W. Böhler and A. Marbs, 2002)

2.2.2. Fixed dress form manufacture process and company currently

A dress form is a three dimensional model of the torso used to solve fitting problem in the garment production processes. When making clothing, one can fit the garment on the dress form to visualize the appearance as on a body and make adjustments or alterations. The fixed dress form is made in a series of sizes or according to one specific individual measurements, so we normally call the first type “standard dress form” and the second type “customized dress form” respectively.

Nowadays, the dress form is usually made of card boards and covered with cloth. To make a dress form, it starts with the mould, which is made of plaster. Usually, it is created by designers according to the client’s demands as shown in

Figure 2-14. Recently, with the aid of 3-D scanning technique, its shape can sometimes be even custom-made exactly as the actual human body profile. Visit was made to the Avalon mannequin factory located in Dong Guang, China, in 2011. They made the moulds using the 3-D scanner and computer numerical control (CNC) machine. They used a 3-D body scanner to acquired the body profile information, then put the data to the CNC machine to let it cut a body model from one large piece of polystyrene foam. Next spread the plaster evenly on the body model, and wait for it to dry out. This procedure is repeated until the thickness of the plaster model is reached. Lastly, split the plaster model into two halves and the mould is obtained.



Figure 2-14. Moulds used to make dress form.

Source: How it's made: Dress Forms, the Science Channel Videos,
Accessed 2010:

<http://science.discovery.com/videos/how-its-made-dress-form.html>

A video recorded media shows the following procedures to make a dress form (T.S.C.V., 2008). After the mould is ready, the next step is to soak the card boards in

water, so they are softened but not falling apart. Then they are coated with paste which is a combination of plaster and glue shown as Figure 2-15.



Figure 2-15. Coat the wet card boards with plaster and glue.

Source: How it's made: Dress Forms, the Science Channel Videos,
Accessed 2010:

<http://science.discovery.com/videos/how-its-made-dress-form.html>

Then, in a process called “feathering”, the edge of the card board is torn into a series of tails (see Figure 2-16) to let them be able to fit various curves easily.



Figure 2-16. Feathering process.

Source: How it's made: Dress Forms, the Science Channel Videos,
Accessed 2010:

<http://science.discovery.com/videos/how-its-made-dress-form.html>

Next, the card boards are pressed into the shape of the body mould, building up several layers, shown as in Figure 2-17.



Figure 2-17. Press the card boards into the mould.

Source: How it's made: Dress Forms, the Science Channel Videos,
Accessed 2010:

<http://science.discovery.com/videos/how-its-made-dress-form.html>

Overlap the feather edges, help to lock the card boards as shown in Figure 2-18.

Then join the front and back mould together and sealed the card boards inside the mould with more paste.



Figure 2-18 Overlap the card board edges.

Source: How it's made: Dress Forms, the Science Channel Videos,
Accessed 2010:

<http://science.discovery.com/videos/how-its-made-dress-form.html>

Finally, open the mould to review the shape. After about 34 hours drying in open air, they go into an oven of 350 °c for 8 hours to harden the dress form. After smoothen, the form is covered with fabric usually made of cotton canvas. Pins and tapes are used to fix the cover and served as body reference points. It is then washed with water to shrink the fabric to the form. After labelling and covering the holes on the surface (such as top and bottom), the dress form is ready for sale.



Figure 2-19. Review the dress form when opening the moulds.

Source: How it's made: Dress Forms, the Science Channel Videos,
Accessed 2010:

<http://science.discovery.com/videos/how-its-made-dress-form.html>

2.2.3. Virtual mannequins in fashion industry

Besides the various physical mannequins, virtual human models are rapidly becoming common place in many fields of industry with 3-D scanning technology and computer technology. Back to 1998, Hardaker and Fozzard (C.H.M Hardaker and G.J.W Fozzard, 1998) stated the point that 3-D simulation technology could benefited the garment design. The virtual mannequin provides garment designers with a virtual three-dimensional body model for them to refer their designs to, for try-on, to observe the body shape and to demonstrate their products in virtual environment. Virtual mannequin can be classified into two kinds; static and changeable (parametric) virtual mannequins. To construct a static mannequin, there are usually three steps. First, use 3-D scanner to obtain the body information which

is stored as point cloud data. Second, process the point cloud data to fill the holes which are caused by the blind spot of the scanner, filter the noise which are generated during the scanning process and so on. Third, generate the surface based on the points. The static mannequin can well represent the human body shape so it is useful in the fashion industry. For example, Ben Azouz, et al. used static mannequin to characterise the variation of human body shape (Z. Ben Azouz, M. Rioux et al., 2005). They created a series of mannequin based on the 3-D scanning data for visualizing the human shape variation. Simmons, Istook and et al. used it for female figure identification (Karla Simmons, Cynthia L. Istook et al., 2004). Similarly, they used the 3-D scanner to obtain the body information based on which the body types were classified.

Compared with static body model, the parametric mannequin is more efficient and has better performance in body shape variation. The static body model can represent the body shape well, but whenever a different size body is required, a real human body of that specific size has to be scanned and the whole body model building process has to start over again (C. Carrere, C. Istook et al., 2000; S. Kim and C.K. Park, 2004). It is relatively costly too. A further consideration is that the 3-D body model data size can reach more than 10 MB, bringing inconvenience in

data storage. Another point is that, online visual merchandising is showing a very promising future. A study (L. Khakimdjanova and J. Park, 2005) shows that in the past few years, e-commerce has seen growth. In 2008, online buying has reached an estimated 63 million US households, while the reported apparel sales were higher than other products.

Virtual mannequins are widely used in virtual garment design. Wang (CCL Wang, 2005) developed a parametric mannequin for automatic virtual garment design. He first obtained the point cloud data of a human body using a 3-D scanner and located all the feature points. After that a feature wireframe was constructed by connecting all the feature points into curves using the 4th-order Be'zier implementation method, which defined the each curve by 4 control points. Finally a mesh surface was added to the wireframe. The parameterization was realized by relocated these control points which will affect the shape of the curve, further reshape the surface. Figure 2-20 shows all the three steps.

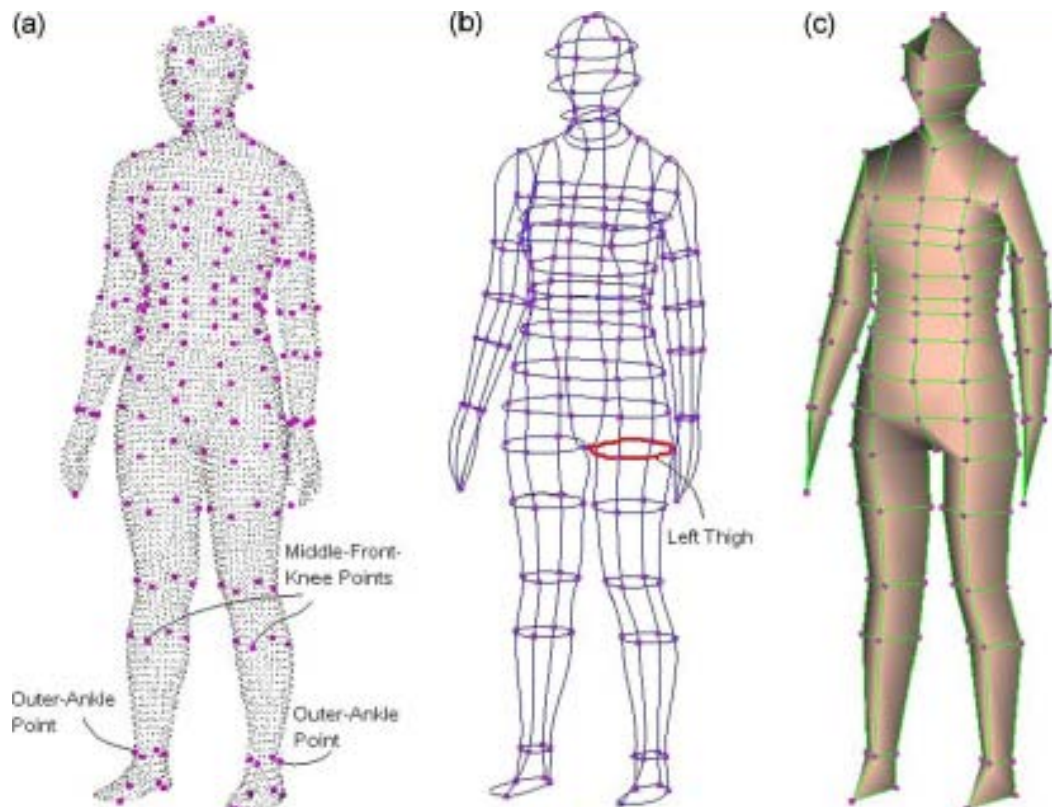


Figure 2-20. Parametric mannequin development procedures: (a) obtain the point cloud data and locate the mark points; (b) construct the wireframe; (c) generate the surface. Source: "Parameterization and parametric design of mannequins"(CCL Wang, 2005)

Another case is that, Kim and Park (S Kim and CK Park, 2004) use it for garment drape simulation. They obtained the profile of a mannequin using 3-D scanner. Then, based on the 3-D point cloud data which is the output from the 3-D scanner, they selected the cross sections at neck top, neck bottom, shoulder, armhole, armpit, bust point, waist, abdomen, hip, and applied the Graham convex hull generation method to them and generated the cross-section profiles shown as Figure 2-21. These cross-section profiles were used to define a parametric body model and

the shape and size of it could be changed by resizing and relocating every cross-section profile. The body surface was then generated by sweeping those cross-sections.

Related to the parameterization of unorganized cloud points, there are other methods beside the above two. Ma and He(W. Ma and P. He, 1998) presented an approach to use B-spline surface to generate the object surface from the unorganized cloud of points; Barhak and Fischer(J. Barhak and A. Fischer, 2001) also presented a partial differential equation based method to parameterize for the 3-D freeform objects from laser-scanned data.

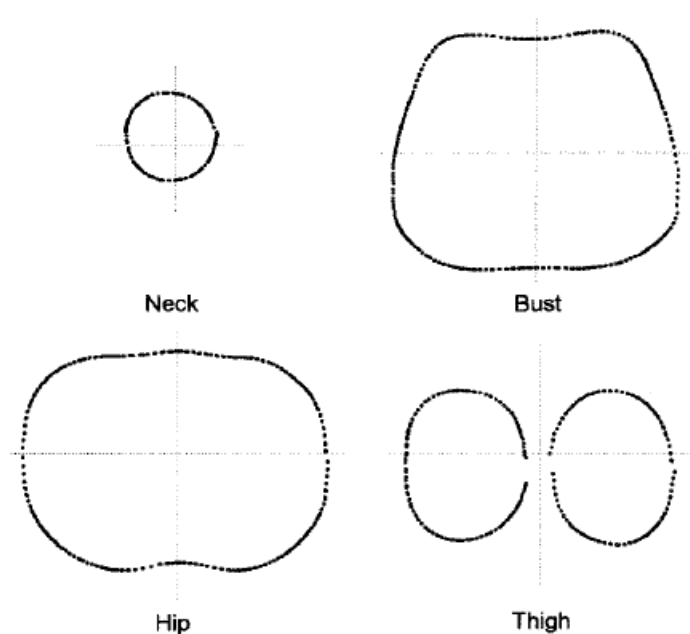


Figure 2-21. Cross-section profiles generated using Graham convex hull generation method. Source: “Parametric body model generation for garment drape simulation”(S Kim and CK Park, 2004)

Others applications can also be found. Commercial systems like Gerber, Lectra, and Pattern-aided design (PAD) system are some of the widely-used garment design computer aided design (CAD) software which relies on the virtual human models to visualize the garment design. From these cases, we found that there are three general steps to construct a parametric body model, firstly, obtain a basic mannequin shape with the adoption of 3-D scanner, secondly, parameterize the mannequin using controllable wires or points, and thirdly, generate the surface based on these controllable wires or points.

From this part of the review, one can see that the physical fixed mannequin/dress form and virtual mannequin are both important to the fashion industry, but they both have some significant drawbacks. The fixed mannequin/dress form is expensive and cannot change its shape according to the user's desire. The virtual mannequin is able to change its shape and ideal to integrate into garment design software and online shopping. But it can only "visualize" and "simulate" the body shape, so it was reported that 85 percent of the women online purchasers avoided buying apparel because of the inability to try an item on for size or fitting (R Greenspan, 2003). The mechanical adjustable mannequin/dress form described in section 2.1.2 was designed to solve these problem, but according to the poor market

performance, its popularization is facing obstacle mainly because of the lack of user-friendliness.

2.3. Robotic mannequin background and prospect

2.3.1. Robot development

Mankind always has a vision of an artificial intelligent life in the form of a machine which can behave like people to help them with various tasks. The effort and attempt for developing such a system can be traced back to ancient China (C.A. Ronan and J. Needham, 1978), where a story about a "robot" was recorded. In the 3rd century BC, a mechanical engineer known as Yan Shi, demonstrated a life-size humanoid mechanical figure to the king of Zhou dynasty. His masterpiece was able to walk, posture, and sing, and was made of feather, wood, glue and lacquer. A more realistic origin of robot was considered to be the water clocks construct in China in the 6th century BC. Similarly, in ancient Greece, Ctesibius (M.E. Rosheim, 1994) also built a water clock with moving figures in 3rd century BC. Both of these inventions reflected the commonality of designing some kinds of mechanisms to serve human, which is also the core purpose of a robot. Another important feature of the robot is automation technology. Back to ancient China again, Su Song (Physics

Laboratory of NIST, 1995) designed an astronomical clock tower featured mechanical figurines that chimed the hours as shown in Figure 2-22.

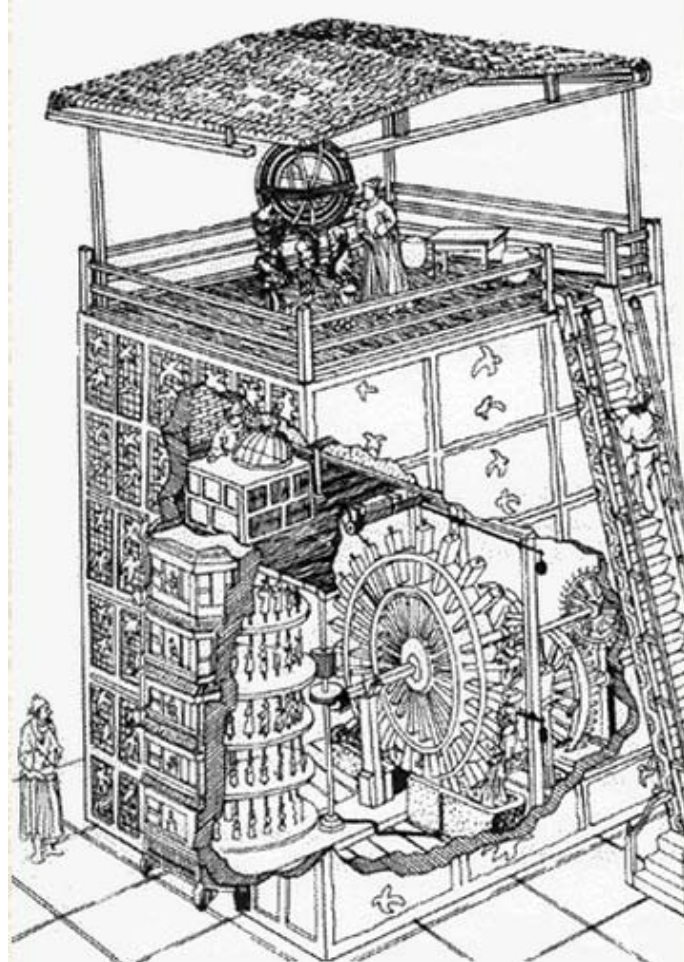


Figure 2-22. Water clock built by Su Song.

Source: <http://physics.nist.gov/GenInt/Time/early.html>

As time goes by, the robot design becomes more complex. Leonardo da Vinci (1452–1519) was well known as an artist, but he also showed great interest in automated devices. Among his numerous mechanical devices, carts, and even plane design, the “mechanical knight” is a humanoid robot (F.C. Moon, 2007). According

to the design, the robot is able to do several human-like movements. It can sit, move its arms and neck.

In Japan, puppets were used in religious festivals, performing the characters in the fairy stories. Karakuri ningyō (J.M. Law, 1997) was one of them. It was a mechanical device which appeared between the 17th to 19th century and designed to automatically carried out some preset movements. For instance, Figure 2-23 shows a Karakuri which can be triggered to walk for a set distance when a cup of tea is placed in his hand.



Figure 2-23. A tea-serving Karakuri.

Source: <http://www.allonrobots.com/karakuri-ningyo.html>

While the word “robot” was introduced to the world by the Czech writer Karel Čapek (K. Capek, 1920). He described the robot as a kind of manufactured living machine designed to work for human in his play Rossum’s Universal Robots in 1920. The Industrial Revolution stimulated various appearances of complex machines between the late 18th and early 19th centuries. The steam powered machine started to be used in manufacturing, primarily in the textile industry (J.A. Angelo, 2007). People demanded a machine that could handle multiple tasks. The discovery of electricity was an important factor for the driving power for robot. In 1948, the first electronic autonomous robot was created by William Grey Walter in England. It was three-wheeled and moved very slowly, however, it was able to find the light source with its light sensor. The world's first humanoid robot, Televox, operated through the telephone system, was constructed in the United States in 1927. In the late 1940s, the digital computer and microprocessors was in rapid change with the use of microelectronic instruments such as transistor. All these new technologies and the need from automobile industry promoted the rise of modern robot systems. The first industry robot is Unimate (S.Y. Nof, 1999). It is a programmable robotic hand for lifting and stacking hot metal in a General Motors’ assembly line in New Jersey, 1961.

Nowadays, with the great achievements in the fields of computer hardware, control, automation, material, actuator, communication and relative technologies, the robot has become quicker and nimbler in motion; lighter and stronger in structure; smarter and faster in judgement. Robots are no longer in fiction or movies, but involve in many aspect of our society. Examples are,

1. Military use. The need from military is an important stimulation for the rise of modern robot systems. During World War II, space technology, tele-operated system, advanced micro electronics chips technology all contributed to robot development. The Talon 3B robot (Figure 2-24a) is designed for searching and destructing explosive devices. It allows the technicians to carry out the operation in a safe location with the use of the monitors and manipulator mounted on the robot. The U.S. Air Force MQ-1 Predator (Figure 2-24b) is an unmanned aerial vehicle robot. It took part in the Iraqi war for investigation and assassination tasks. With the help of robots, the military can reduce casualties and improve action's concealment and 24-hour strike capability.



Figure 2-24. Left: A Talon 3B robot unit removes a mine. Right: A MQ-1 Predator equipped two laser-guided Hellfire anti-tank missiles.

Source: Photograph courtesy of U.S. Navy and Air Force.

2. Industry use. The manufacturing industry is one of the main fields adopting robots. These industrial robots can come in a variety of shapes, sizes, and configurations. The most common type is stable and equipped a precise manipulator which can be Cartesian, cylindrical, spherical, SCARA (selective compliant assembly robot arm), articulated and parallel. They are usually designed for handling, assembling, packing, spraying and dispensing task and are used in vehicle manufacturing (J.A. Angelo, 2007). Figure 2-25 shows a typical industrial robot which is an articulated robot for use in welding. It has 6 axes and repeatability of ± 0.05 mm. Its flexibility and precise manipulator design makes it capable for complex and fine welding tasks. The manipulator is also designed for surgery which can help to eliminate the shaking of the doctor's hand and improve on the accuracy.



Figure 2-25. A KR 16 ARC HW robot.

Source: http://www.kuka-robotics.com/en/products/industrial_robots/special/arc_welding_robots/kr16_arc_hw/

3. Research robot. This kind of robot is mainly used in the laboratories. They are rather designed for specific research use, for example, the Curiosity Mars Rover is a part of the Mars Science Laboratory launched by NASA on November 26, 2011(Allard Beutel, 2011). Its mission is to improving the knowledge of Mars on the habitability, climate, and geology.

The humanoid robot is a robot with the human shape. It can be in the form of the whole human body, from the waist up, or even a single part of the body. These robots are designed to help people improve their understanding of the human facts, such as movements, the way of thinking and body structures. For example, ASIMO (shown as Figure 2-27a) is a robot made which is able to perform multiple

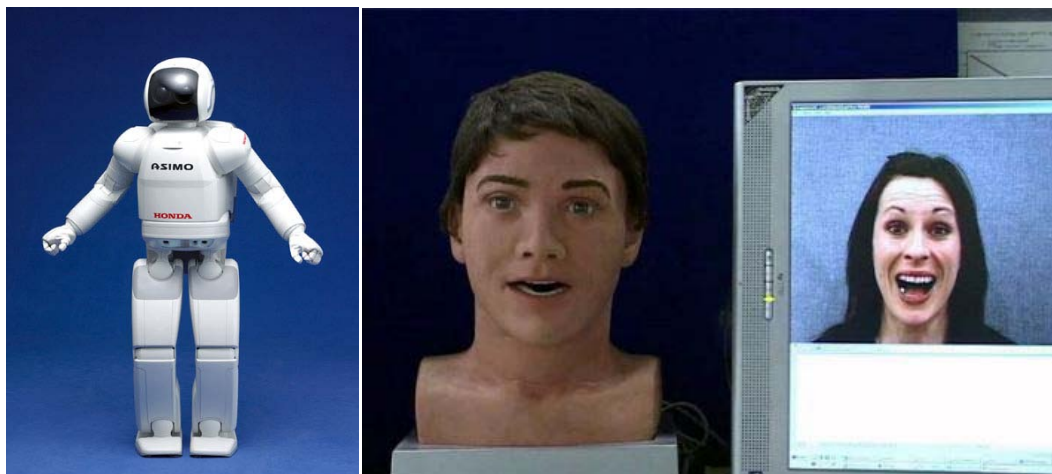
movements such as walking and grabbing, as well as making movement planning. The

Jules robot can mimic the human facial expression as shown in Figure 2-27b.



Figure 2-26. Curiosity Mars Rover relies on the radioisotope power system and numerous tools equipped to access the habitability of Mars.

Source: Photograph courtesy of NASA website.



a

b

Figure 2-27. a: The ASIMO robot (Y. Sakagami, R. Watanabe et al., 2002). b: The Jules robot. Source: a: Photo courtesy of Honda Motor Co., Ltd. b: Photo courtesy of Daily Mail Co. UK, Ltd.

4. Other applications. Robots are also designed for mining, healthcare, cleaning and so forth. These tasks are normally either dangerous, repeatable, long-term, dirty, or dull for people. For example, they can be used to humanitarian mine detection and removal (K. Kato and S. Hirose, 2001), mining coal (K. Kato and S. Hirose, 2001), for robot-assisted surgery (D. Gerhardus, 2003), etc.

2.3.2. Robotic mannequin

The idea of the robotic mannequin mainly generates from six aspects. First, the robotic mannequin has advantages over the existing ones, such as, more options in shape than the fixed type, easier to use than the flexible type, and more visual than the virtual type. Second, it can be adopted in on-line shopping to let the customers be more confident about the chosen clothes' fit. It can also assist the remote teamwork between design studios and manufacturing factories by providing the dress forms of identical body shape for their fashion design process. Third, as robot technology develops, the robot has been adopted in industry and research areas as mentioned in the previous part. Fourth, as space becomes costlier in Hong Kong, and the robotic mannequin can help the factories to reduce the storage space by replacing multiple mannequins. Fifth, the robotic mannequin can be used in retail application to attract the customers. Sixth, good in providing for education and training in sizing pattern

design and garment fitting.

During the development of this project, the Fits.me Company launched a male robotic mannequin which could mimic the customer's shape in June 2010 (C. Boyd, 2010) as shown in Figure 2-28. They described their robotic mannequin system includes a 3-D scanning device, computer, network and a robotic mannequin (M. Kruusmaa, A. Aabloo et al., 2010). The user obtained their body dimensions with the use of a 3-D scanner and input to the robotic mannequin via the network as shown in Figure 2-29. The robotic mannequin was able to change the shoulder width, neck girth and partial front chest shape. The surface of the robotic mannequin was made of a flexible material which was attached to some extendable links in the shoulder. These links were driven by motors to change the surface shape. However the method of mimicking the profile of whole body or the trunk was not covered. This system was designed and developed for improving on-line purchasing.

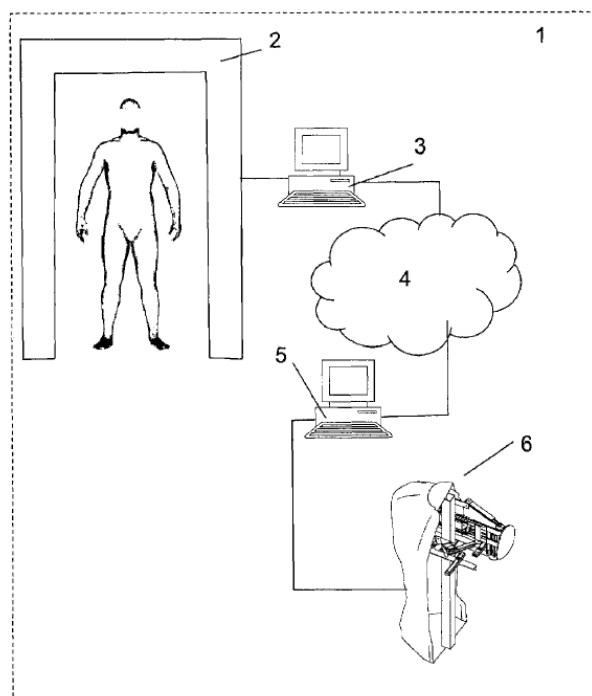


Figure 2-28. A robotic mannequin system for online shopping.

Source: Kruusmaa, M. et al. US patent 2010/0070384 A1

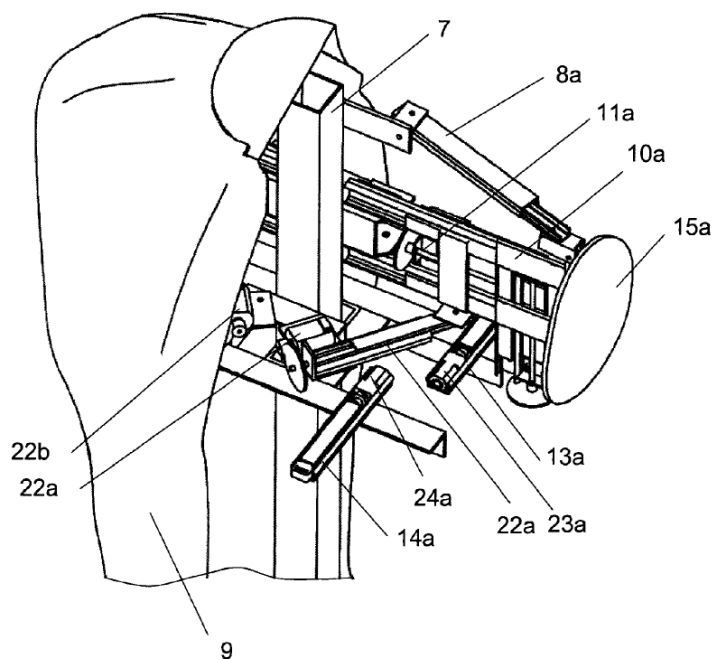


Figure 2-29. Male robotic mannequin from Fits.me can shift between small and extra large

Source: <http://www.bbc.com/news/technology-10687701>

Chapter 3 Research Methodology

3.1 Introduction

As described in the last chapter, there were market need for a better mannequin for fashion design, garment display and online shopping. The entire research project process followed the stages of innovative product design, to develop an idea into a realistic and workable product. Such process requires robot design consideration too as the project is to develop a humanoid robotic system. The research generally followed the product design stages, and within these stages, the robot design stages were integrated and relative methodologies adopted. Due to the limitation of time, manpower and budget, the final objective is to build a prototype which is fully workable to demonstrate its ability forwards commercialization.

3.2 Research Framework

The innovative product design stages and methods have evolved since the middle of the last century, brought about by new technique, market demands, economic environment, etc. There are some common principles, for example, that always begin with the enthusiastic satisfaction of human needs (M. Asimow, 1962; R. Black, 1996;

K.N. Otto and K.L. Wood, 2000). The process follows a feasibility study, the definition of specifications and solution design, and eventually the implementation of concept. As shown in Figure 3-1, the left column represents the innovative product procedures. For a robot prototype design and development project, it generally follows the product design phases but specification sub-stages must be considered to handle the inevitable technical issues such as kinematic and mechanisms design, control, programming, interface, and etc (T.M. Sobh and X. Xiong, 2012; C.J. Spiteri, 1990; R. Vepa, 2009). Furthermore, as it is a humanoid robot which mimics the body shapes of human, anthropometric analysis is also needed as shown in the right column of Figure 3-1. A detailed description will be given in the following sections together with the methodologies used in each stage.

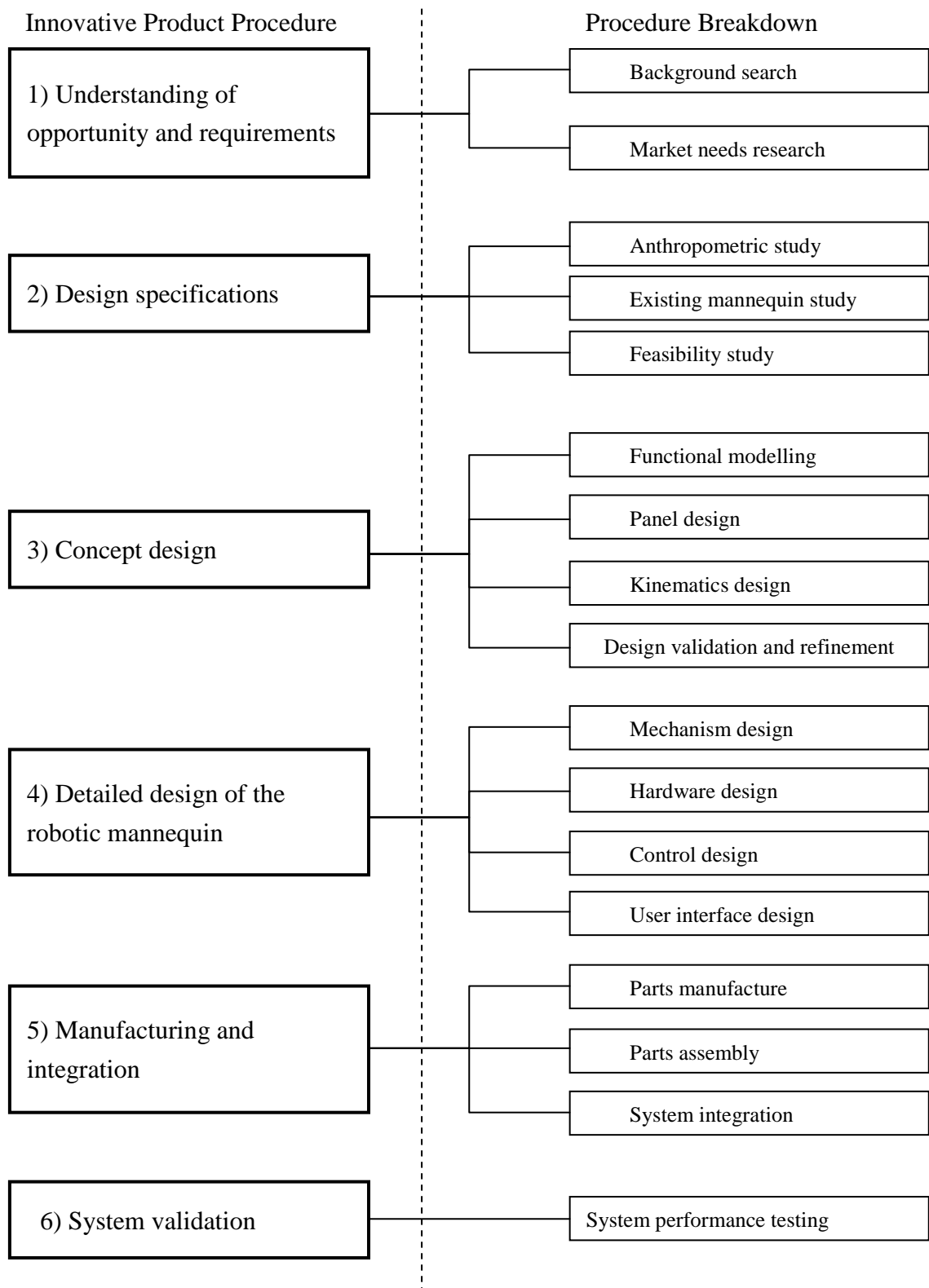


Figure 3-1. Frame work of project

3.3 Research methodology

3.3.1 Understanding of opportunity and requirements

In the beginning of the project, a literature review was done on the background, for example, the mannequin history of development, and robotic technique that is applicable to the project. In order to understand the role of the mannequin in the fashion industry; the current mannequin and its drawbacks; the needs of the market for mannequin improvement and feasible innovative solution for mannequin improvement were discussed.

3.3.2 Design specifications

In this section, the size and the function specifications of the robotic mannequin system were determined according to the market requirements, feasibility of human body shape variation. For investigating the human body shape variation, a data base of 130 Chinese female profiles was built using a 3-D body scanner. Statistic analyses were performed to analyze the length, girth, variation of different body parts of the trunk quantitatively. For a more comprehensive understanding of regularities of the body variation, the anthropometric surveys of other population were also studied where similar regularities of body shape variation were found, which indicates the feasibility

for covering body shapes across various races using one robotic mannequin. As it is developed for garment design and retail, the configurations of existing mannequins were studied, to obtain the understanding of the major body size range for the garment design and fitting, ensuring the final robotic mannequin to be practical for use in the fashion industry.

3.3.3 Concept design

According to the design specifications, a virtual mannequin which is able to decrease/increase its body size for simulating the appearance and function of the real robotic mannequin was developed. The surface was generated with B-spline technique and based on the 3-D scanned samples. The panels of the robotic mannequin were designed by separating the surface of the virtual mannequin. Then kinematic design were conducted to determine the movements of these shells. By moving the shells to different positions, the robotic mannequin changes into various types of body, thus the virtual mannequin became parametric. The design of the movement mechanism should realize the major body shape variation. To validate the concept design, an expert in garment design was invited to validate the virtual parametric mannequin performance and the design was improved in the light of the feedback before moving into next stage.

3.3.4 Robotic mannequin system detailed design

The "robotic mannequin system detailed design stage" involved an in-depth discussion and design of the physical robotic mannequin based on the virtual parametric mannequin. Firstly, the mechanical parts are designed using CAD software, which covered the design of support module, neck module, chest module, waist module, and hip module. Finite element analysis were applied to the critical parts to ensure the construction is safe. The actuators were selected according to the precession requirement and for cost performance. Then force analyses were applied to ensure the proposed actuators were able to drive the robotic mannequin smoothly. The control units and driving units were selected according to the actuators used and system requirements. They should be replaceable for easy maintenance and extensible for further improvement. A body cladding which contains a cover and soft films were developed to cover the gap between shells. At last, a user-friendly graphical user interface (GUI) was developed to control the robotic mannequin system. During these design sections, considerations were given to the manufacture, parts, material purchasing, costs, maintenance, and expandability issues by adopting the standardized design and modular design to eliminate the iteration in the design phase for large production.

3.3.5 Manufacturing and integration

Parts of the robotic mannequin were produced by the Industrial Centre in The Hong Kong Polytechnic University. The material, dimension, tolerance, surface and roughness of every parts are specified and checked for quality control. Then the processes of integration of mechanical parts, driving units, control units, software and body cladding were described.

3.3.6 System validation

The main concern about performance of the robotic mannequin system is the variation range of the robotic mannequin and the precision. As a result the system validation of the robotic mannequin is about the actual variation range, precision, operating time and repeatability. The identifications of precession and repeatability are specified by the ISO 9283:1998 manipulating industrial robots - performance criteria and related test methods. According to this standard, the dynamic performance of the robotic mannequin was tested.

Chapter 4 Design Specifications

4.1 Introduction

This chapter focuses on the main specifications of the robotic mannequin design.

The specifications state the major features and functions for the design of the robotic mannequin. In order to mimic the body shape change, the human body profiles of various sizes, and shape profile change were studied. The understanding from the study can be used to guide the design of robotic mannequin's features and functions which are used as guidance in the following design stages.

1. To obtain the anthropometric data, first 130 Chinese females were scanned using a 3-D scanner and performed the statistical analyses to understand the size and body shape variation across these samples.

2. The widely used mannequins in the market were studied to understand the major size range for fashion industry.

3. For a more comprehensive understanding of the body shape variation in other population, the anthropometric surveys in other countries, such as U.S. and Japan were studied.

4. Based on the information for the existing mannequins size charts and

anthropometric surveys, the variation range for robotic mannequin is determined, with the purpose to cover the most common female body shapes for fashion industry use.

4.2 Body morphological variation analysis

The robotic mannequin is designed to change into desired body dimensions and shapes accurately, so it is essential to develop a comprehensive understanding of body morphological variation. A body profile data base was built from the 3-D scanning body data. From the analyses of the body data base, the regularities of shape variation were found, as the support information for the design of the surface panels and kinematics of the robotic mannequin.

4.2.1 Anthropometric survey of Chinese female

130 Chinese females aged between 17-22 years old were scanned using the TC² NX-16 body scanner. The samples were extracted from the anthropometric data base built by the Institute of Textiles and Clothing of The Hong Kong Polytechnic University. In the recruitment process, participants must have reasonably symmetrical body proportions without any obvious deformities or postural problems caused by neurological or musculoskeletal diseases. This was done to limit the study

to females who could be well-fitted in ready-to-wear clothing. Participants were scanned in a light colour close-fitting undergarment, which allowed the 3-D body scanner to capture the body shape while avoiding deforming it. Participants were positioned in an erect but relaxed posture, with arms and legs abducted slightly so that the cameras in the scanner could capture the full torso. The scanning process finished in 10 seconds, and then the raw data were processed into the .rbd file format by the 3-D body scanner software as the output. In the final step, the critical measurements for garment construction were extracted and analyzed to support the following research stages.

4.2.2 Anthropometric analysis result

The anthropometric measurements of the 130 subjects is shown in Appendix I. Table 4-1 shows the mean, standard deviation and range of body measurements, which were used as reference for the initial body shape of the robotic mannequin. The body shape dimensions which are used in the garment construction dimensions, according to the ISO8559 (garment construction and anthropometric surveys-body dimensions), are selected and applied statistical analysis is made. As these dimensions are critical dimensions for garment design and fitting, the major robotic mannequin shape variation will take place at these areas. The selected dimensions

include: neck girth, bust girth, waist girth, abdomen girth, hip girth, shoulder length, bust width, and neck to bust length. Table 4-1 shows the distribution of the selected dimensions. It shows the average value (μ) of the important dimensions for the garment and robotic mannequin design. As the robotic mannequin prototype is first targeting to mimic the Chinese females with common body type, we use the 85% of the body size range a bench mark for the interested range.²³

Dimensions	Mean (cm)	Standard deviation (cm)	Interested Range (cm)
Neck girth	33.6	2.0	30.7 to 36.5
Bust girth	83.5	6.6	72.7 to 94.3
Waist girth	70.0	5.7	60.7 to 79.3
Abdomen girth	80.2	7.6	69.3 to 91.4
Hip girth	93.0	5.9	86.1 to 113.1
Shoulder length	11.2	1.6	8.9 to 13.5
Bust width	17.1	1.8	14.5 to 19.7
Neck to bust length	24.8	2.0	21.9 to 27.7

Table 4-1. Mean, standard deviation, and range of the anthropometric measurements of 130 female subjects

Researchers indicated that when the size of human body is increasing, the front part of the body and back part of the body is not growing at the same rate (P.J. Taylor and M.M. Shoben, 1993). This consideration is of concern because when designing the movement of the robotic mannequin, we need to decide whether to use one driving unit to drive the front body and back body to simplify the construction or use

two independent driving units to enable the back body and the front body to move independently. To measure the dimensions, the 3-D body was split into the front part and back part using a plane which is from the left and right waist points intersecting the crotch point as shown in .

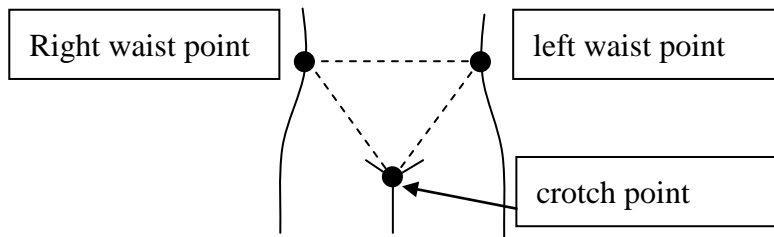


Figure 4-1. A plane determined by the left, right waist point and crotch point.

The front half waist and hip girth were compared to the back part respectively. For a clear demonstration, the samples were grouped by the full girth. For example, all the samples with hip girth within 84 to 86 cm will be put into group 1 and labelled as 84, all the samples with hip girth within 86 to 88 cm will be put into group 2 and labelled as 86, and so on. The average values of the proportion of the waist and hip girth which are calculated by dividing the front girth by the back girth are then shown in Figure 4-3. The reason why the bust and neck girth is not compared is that the cup size will affect the bust result greatly and not able to show the proportion significantly, on the other hand, the neck posture cannot be set to a standard thus it is

not able to be compared. The result reveals that: when body size increases, the increasing rate of the front part of the waist is larger than the back part of the waist as shown in Figure 4-2; while increasing rate of the front part of the hip is smaller than the back part of the hip as shown in Figure 4-3. These findings is in conformance with the previous research result (P.J. Taylor and M.M. Shoben, 1993). So the robotic mannequin will be divided into the front and back part to realize the quantum of variation.

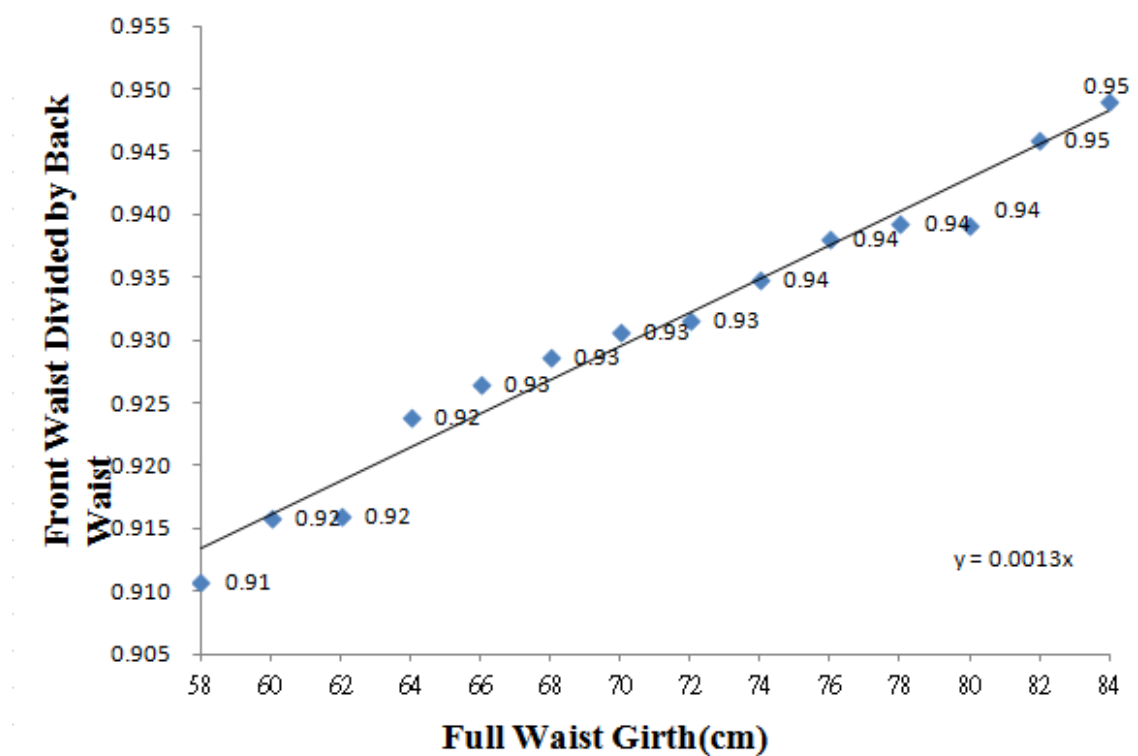


Figure 4-2. Comparison of the increasing rate between the front part and back part of the waist girth.

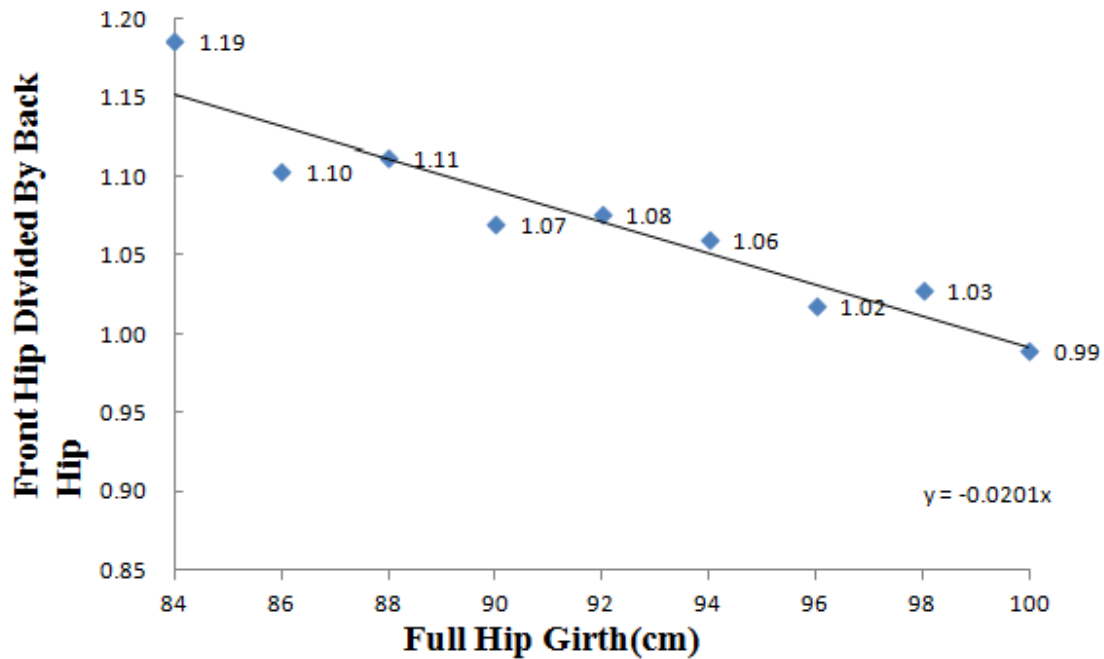


Figure 4-3. Comparison of the increasing rate between the front part and back part of the hip girth.

When the human body size is increased, some parts of the human body will change accordingly, for example when the hip girth becomes larger, the abdomen girth will increase as well. To gain a further understanding of the relationship between these critical dimensions during size change, the correlation relationships between several critical dimensions are figured out to assist in mannequin panel design. A sample correlation coefficient (r), sometimes referred to as a Pearson Product-moment correlation, is a measure of the strength of the linear relationship between two variables. If we have a series of n measurements of x and y written as x_i and y_i where $i = 1, 2, \dots, n$, r is rewritten as (4.1)

$$r_{xy} = \frac{n \sum x_i y_i - \sum x_i \sum y_i}{\sqrt{n \sum x_i^2 - (\sum x_i)^2} \sqrt{n \sum y_i^2 - (\sum y_i)^2}} \quad (4.1)$$

Its value ranges from -1.00 to + 1.00, with -1.00 representing a perfect negative linear relationship, 0.00 representing a total non-linear relationship, and + 1.0 representing a perfect positive linear relationship between the variables. Table 4-2 shows the correlation relationships among the listed body dimensions. The correlation between bust girth and shoulder length, bust girth and neck girth, as well as neck girth and shoulder length are relatively low which are indicating the linear relationship between them are relatively weak. The correlation coefficient analyses results of anthropometric survey of U.S. army (female) in 1988 (J Cheverud, CC Gordon et al., 1988), where the ethnic range has significant difference, is shown in bracket in Table 4-2 for comparison. Similar values can be seen, indicating this relationship are not only appropriate for Hong Kong females but also American counterparts. So following these regularities of shape variation, the robotic mannequin is possible to simulate not only the Asian but also other ethnic groups.

	Neck girth	Shoulder length	Scye circumference	Bust girth	Under bust girth	Waist girth	Hip girth
Neck girth	-	0.105 (0.080)	-	0.457 (0.645)	-	-	-
Shoulder length	0.105 (0.080)	-	-	0.118 (0.074)	-	-	-
Scye circumference	-	-	-	0.708 (0.768)	-	-	-
Bust girth	0.457 (0.645)	0.118 (0.074)	0.708 (0.768)		0.907 (0.875)	0.706 (0.863)	-
Under bust girth	-	-	-	0.907 (0.875)	-	-	-
Waist girth	-	-	-	0.706 (0.863)	-	-	0.774 (0.740)
Hip girth	-	-	-	-	-	0.774 (0.740)	-

Table 4-2 Correlation coefficients between critical body dimensions. The correlation relationship for 130 Chinese female is shown as the value without brackets. The correlation relationship of U.S. females is shown as the value with brackets (J Cheverud, CC Gordon et al., 1988). "-" means the two part of body are irrelevant in robotic mannequin panel design.

Next, bust size is an important and essential dimension for the women's foundation garments, anthropometric and figure classification. Bust and bra

classification follows the ISO DIS 4416 standard as shown in Table 4-3, and the bust size distribution analyses results of the 130 Chinese subjects are shown in Table 4-4.

As the cup shape various according to the difference between the under-bust girth and bust girth, the bust panels will be designed to be separate parts, able to move independently from the chest panel.

Under-bust Girth(cm)	64	68	72	76	80	84	88	92
Bust Girth(cm)-Cup A	76	80	84	88	92	96	100	104
Bust Girth(cm)-Cup B	80	84	88	92	96	100	104	108
Bust Girth(cm)-Cup C	84	88	92	96	100	104	108	112
Bust Girth(cm)-Cup D	88	92	96	100	104	108	112	116
Bust Girth(cm)-Cup E	92	96	100	104	108	112	116	120
Bust Girth(cm)-Cup F	96	100	104	108	112	116	120	124

Table 4-3. ISO DIS 4416 standard bra cup size specification

Underbust Girth(cm)	64	68	72	76	80	84	88	92	Percentage
Cup A	14%	18%	17%	6%	1%	1%	0%	0%	57%
Cup B	8%	12%	7%	3%	0%	1%	2%	1%	34%
Cup C	2%	5%	1%	1%	0%	0%	0%	0%	8%
Cup D	0%	0%	0%	0%	0%	1%	0%	0%	1%

Table 4-4. Bust size distribution of the 130 Chinese females

4.3 Variation range definition

The analysed results of the database provided useful and valuable information to the design specification of the robotic mannequin in terms of the morphological variation. It is used for panel design and kinematic of the robotic mannequin. Besides the morphological variation, the variation range of the robotic mannequin must be next determined. The size range is determined according to most common body size range, which is the global existing mannequin series of widely used mannequin manufacturers in the market. The variation range can then be modified according to the anthropometric survey for a more comprehensive range besides the existing mannequin range.

4.3.1. Mannequin size

The popular mannequins on the market represent the major body size range for the fashion industry. Thus the mannequin products from two most popular manufacturers (Avalon and K&L) are studied. Various models and sizes technical measurements of the mannequins provided the useful information and identify the mannequin's shape. As these dimensions have such importance, they are used as reference when designing the adjustable measurements of the robotic mannequin.

The robotic mannequin is designed to cover the full range of sizes that covers the

present mannequins found in the market.

1. Alvanon (Alvanon website). Alvanon is a major mannequin manufacturer and supplier of a wide range of mannequins for the fashion industry. Their products are well used in the market among which names like Gap, Anne Klein, and Li Fung are their customers. They adopt the 3-D scanning technology in the design stage of their products. Alvanon's Missy Miss (shown as Figure 4-4) series are a full body female mannequins with general body types designed based on their global body data base. Size 2 to 12 is the major range of this series.

2. Kennet & Lindsell Ltd (K&L website). It is a British company established in 1877. They insist making their entire products by hand with traditional skills and with British sizing chart standard. The WED series is the first and widely accepted series as shown in Figure 4-5. Size 8 to 18 is the major range of this series.

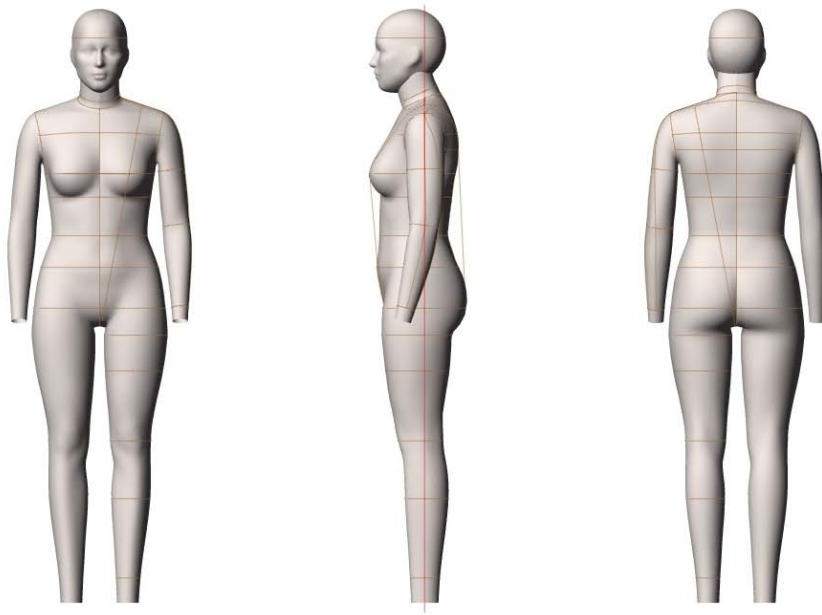


Figure 4-4. Alvanon's Missy Miss series full body mannequin.
Source: Alvanon product catalogue.



Figure 4-5. K&L's WED series dress form.
Source: K&L product catalogue

These two companies mannequin series are selected to represent a wide range of female body shapes. By covering their major range (listed in Table 4-5), the robotic mannequin's size variation is able to meet the requirements of the body shape size

range for the fashion industry.

	Alvalon Missy Miss (size 2 to 14)		K&L WED (size 8 to 18)	
All length unit is cm	min	max	min	max
Neck Base Girth	33.0	38.1	N.A.	N.A.
Bust Girth	84.7	100.0	82.0	100.0
Waist Girth	63.5	79.3	64.0	82.0
Hip Girth	89.5	105.4	89.0	105.0

Table 4-5. Major size range for existing mannequins. The neck base girth measurements are not available on the K&L website.

Source: Alvanon website: http://www.alvanon.com/M01_S03.html; K&L website: <http://www.kennettlindsell.com/>

4.3.2. Anthropometric data of Japanese and American studies

The body size range of the Japanese and American anthropometric surveys were used as a reference data base for the present study,

1. Japanese female data base (Makiko Kouchi and Masaaki Mochimaru, 2002). It consists of 107 Japanese adult females age from 19 to 26.
2. U.S. army females (M. Handbook, 1991). The U.S. military anthropometry has been in use for more than 100 years in order to provide body size information in military research and development. The survey was done in 1988 covering 2208

women in military age from 18 to 50, from different places of U.S. and of different ethnic background.

Table 4-6 shows the relative measurements to the robotic mannequin design. As the robotic mannequin prototype is targeted to mimic the females with common body type, our interested range is the 85% of the body size range of the anthropometric survey.

		Japanese study	U.S. study
Sample size		107	2208
Age	Min	19.0	18.0
	Max	26.0	50.0
Bust circumference(cm)	Mean	83.0	90.7
	σ	6.2	6.4
	Interested range (85%)	77.4 to 99.8	81.5 to 99.9
Waist circumference(cm)	Mean	65.9	72.5
	σ	5.9	6.3
	Interested range (85%)	60.0 to 80.0	63.4 to 81.6
Hip circumference(cm)	Mean	91.7	96.7
	σ	5.3	6.0
	Interested range (85%)	87.0 to 105.6	88.1 to 105.3
Shoulder length (cm)	Mean	N.A.	14.5
	σ	N.A.	1.1
	Interested range (85%)	N.A.	12.9 to 16.1

Table 4-6. Body measurements of Japanese (Makiko Kouchi and Masaaki Mochimaru, 2002) and U.S. (M. Handbook, 1991) anthropometric surveys. N.A. means the values are not available in the result of the study.

4.3.3. Robotic mannequin size variation range

Based on the commercial mannequin size range and anthropometric surveys data, the robotic mannequin size variation range is tabulated in Table 4-7. The variation range of the robotic mannequin should be able to cover the range of the existing commercial mannequins, to represent the major body size range used in the

fashion industry. The lower bounds of the neck, bust, waist and hip girth of Chinese and Japan female is smaller than the existing mannequins, as they are thinner than the average body size normally. To cover this part of subjects, the lower bounds of the neck, bust, waist and hip girth of robotic mannequin are adjusted lower correspondingly. The designed range of dimensional variation is able to cover the standard series of the mannequin from two popular mannequin manufacturers and 85% of the subjects of the Chinese, Japanese and U.S. anthropometric survey, which is sufficient for general use in the fashion industry.

	Robotic mannequin variation range	Size range of mannequins (Avalon and K&L)	Interested range of Chinese females (85%)	Interested range of adult Japanese females (85%)	Interested range of U.S. women (85%)
Neck girth	30.3 to 38.1	33.0 to 38.1	30.3 to 36.9	N.A.	N.A.
Bust girth	75.7 to 100.0	82.0 to 100.0	75.7 to 94.3	77.4 to 99.8	81.5 to 99.9
Waist girth	60.0 to 82.0	63.5 to 82.0	62.8 to 78.9	60.0 to 80.0	63.4 to 81.6
Hip girth	87.0 to 111.1	89.0 to 105.4	87.6 to 111.1	87.0 to 105.6	88.1 to 105.3
Bust to waist vertical length	15.5 to 17.5	15.5 to 17.5	N.A.	N.A.	N.A.
Waist to hip vertical length	18.4 to 21.6	18.4 to 21.6	N.A.	N.A.	N.A.

Table 4-7. Variation range the robotic mannequin compared to existing mannequin and anthropometric survey of Chinese, Japanese and U.S. female. All units are in cm. "N.A." means the value is not available in the original source.

Chapter 5 Concept design

5.1 Introduction

This chapter describes the concept design stage which focuses on generation of the profile of the robotic mannequin, the panels and the kinematic design. According to the design specification in Chapter 4, the morphological variation and variation range have been defined. To develop the robotic mannequin, it starts with designing the initial shape. The initial shape is the original shape of the mannequin, from which various shapes can be generated. Next, the parametric mannequin is divided into pieces of panels to realize the shape variation. Last, the movements of the panels are defined with the use of kinematic design.

5.2 Initial shape design

The initial shape is extracted from the database of the anthropometric study. Referring to the methodology of virtual body model construction in Section 2.2.3, the initial shape can be built by generating a loft surface fitting through the body cross-section (Kim et al., 2004) outlines which are presented in the form of B-spline (W. Ma and P. He, 1998). The configurations of the cross-section are designed based

on the scanning data of females and mannequin profiles. The first step is preparing the body profile data for shape extraction, where an alignment process is implemented. The second step is cross-section level design to define the layout of the cross-sections. The final step is generating the B-spline curves according to the anthropometric data using an average algorithm.

5.2.1 3-D scanning body profile data preparation

Figure 5-1 shows a sample of the 3-D body scan data which is the output of the 3-D body scanner. It is constructed by parallel slices of points from the neck to the feet. TC² body scanner software processed the raw scan data, filled the holes, filtered the noise, and then saved the 3-D body model data in an .rbd format file which contained the vertices and triangle mesh information. After that, the .rbd file was processed and split into a .vrt file which contained the vertices coordinates' information and a .tri file which contained the triangle mesh information. The y direction is the front direction of body as shown in Figure 5-4. The x direction is perpendicular to the y direction and pointing to the left hand side of the body. The z coordinate is perpendicular to the ground pointing upwards.

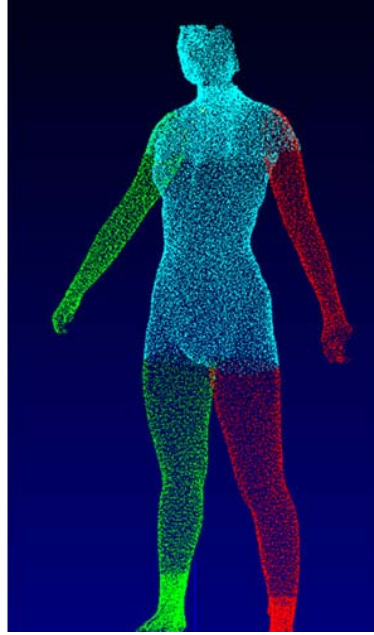


Figure 5-1. 3-D body scan data

A trunk section points' filter was used to preserve only the trunk points within the height from the armpit level to the hip level. Firstly, it loaded all of the body points $P_{all}(x,y,z)$ then filtered to obtain only the body points $P_b(x,y,z)$ with the mid-neck level $P_{mid_neck}(z)$ and crotch level $P_{crotch}(z)$:

$$P_b = P_{all} \cap [P_{crotch}(z), P_{mid_neck}] \quad (5.1)$$

Secondly, the hands points were screened out according to the points' y-coordinate locations, in order to obtain only the trunk points $P_{trunk}(x,y,z)$. During the scanning process, the subject would hold the handle which was located on the left and right side of the body respectively. The y-coordinate of the armpit, $P_{armpit_left}(y)$ and $P_{armpit_right}(y)$, can be measured by the scanner. The points of the hand parts can be filter by the value of y-coordinate. Thirdly, all the points between

the middle neck level and armpit level were added in to form the completed part of body for shape extraction.

$$P_{\text{trunk}}(x, y, z) = P_b(x, y, z) \cap [P_{\text{armpit_right}}(y), P_{\text{armpit_left}}(y)] \cap [0, P_{\text{armpit}}(z)] + P_b(x, y, z) \cap [P_{\text{armpit}}(z), +\infty] \quad (5.2)$$

All of the subjects were scanned in an identical standing posture, with two arms straight and holding two handles. In this way, the trunk was stretched straight so there was an assumption that the body was not bending forward or backward, in another word, no alignment was needed for the frontal trunk bending. However, there were still some variations in posture, bringing in shape measure errors which were non-ignorable. Three main uncontrollable influence factors were shift left/right, rotation, and incline. The first two were variation problem at slice level, while the third was an inter-slice problem.

Shift left/right problem was arisen because the centre of subject was not located at the centre between two feet during the scanning process or her chronic standing posture. Take one slice of the cross-sections which is shown as Figure 5-2 for example. The red points are the original slice points which shift to the left base of body, and the blue points show the correction result that the original slice points are shifted back. This is done by shifting the centre point of the slice, marked as asterisk,

back to the x-axis. The centre point is defined as the centre point of the left point (red circle near the top) and the right point (red circle near the bottom). The left/right point is located at the centre point of the most outer 2-3 points at left body side and right body side respectively in order to eliminate the noise error.

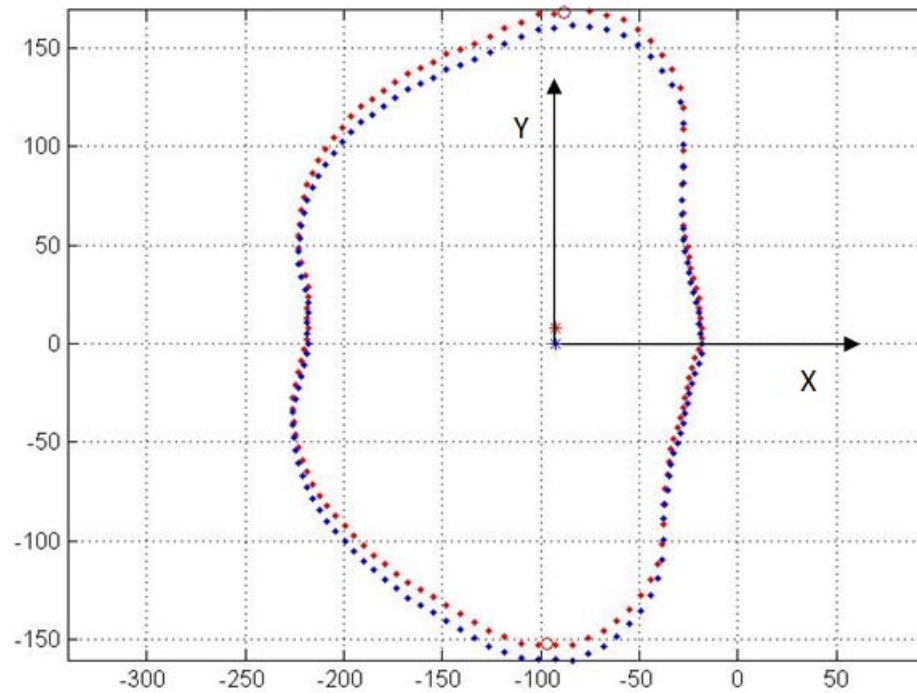


Figure 5-2. Comparison of one slice before and after the alignment process.

After the shift left/right problem was fixed, variation caused by rotation problem needed to be eliminated. Rotation problem was caused by the rotation of the trunk. For instance, the rotate angle is the angle θ between the line linking the left/right point and the Y axis direction in Figure 5-2. The maximum rotation angle of the slice among all the subjects was 6.91° and the mean rotation angle was 1.41° . The problem can be fixed by rotating back every slice round the centre point of the slice

by θ degree, making the line linking the left /right points parallel to the Y axis. If the slice points $P_{\text{slice}}(x,y,z)$ need to be rotated by θ , we have,

$$P_{\text{SF}}(x, y, z) = P_{\text{slice}}(x, y, z) \begin{bmatrix} 1 & 0 & 0 \\ 0 & 1 & 0 \\ P_{\text{SC}}(x) & P_{\text{SC}}(y) & 1 \end{bmatrix} \begin{bmatrix} \cos \theta & \sin \theta & 0 \\ -\sin \theta & \cos \theta & 0 \\ 0 & 0 & 1 \end{bmatrix} \quad (5.3)$$

$P_{\text{SF}}(x,y,z)$ are the points rotated to the desired position.

$P_{\text{SC}}(x)$, $P_{\text{SC}}(y)$ are the X and Y coordinates of the center of the slice. As the shift left/right problem has been solved, the $P_{\text{SC}}(y)$ will always be 0.

At this stage, all of the variation problems in slice level have been solved. The last one variation in posture was the incline problem. Although the participants were guided to position in an erect but relaxed posture, their trunk inclined forward or backward slightly as shown in Figure 5-3.

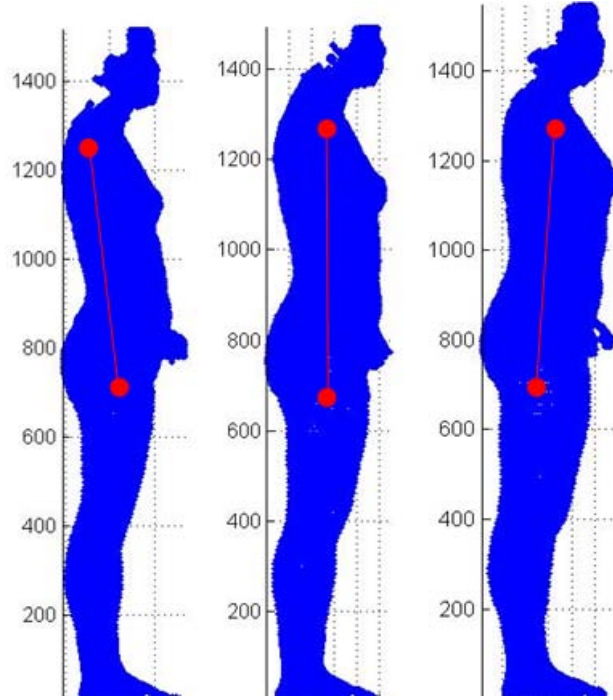


Figure 5-3. From left to right, three different subjects with a slightly backward, straight, slightly forward posture. The two points are the shoulder point and crotch point.

The trunk incline degree could be represented by the body angle, which was the angle between the plane defined by two shoulder points, the crotch point and the horizontal plane as shown in Figure 5-4. The 130 subjects' body angles had a range $[84.9^\circ, 95.9^\circ]$ with an average value of 91.1° . To fix the incline problem, the body angle were modify to the average angle $\alpha=91.1^\circ$ by rotating all the points $P_{SF}(x,y,z)$ around the Y axis at the crotch point. Suppose the body angle of a subject was β ,

$$\begin{aligned}
 &P_{SF_{fixed}}(x,y,z) \\
 &= P_{SF}(x,y,z) \begin{bmatrix} 1 & 0 & 0 \\ 0 & 1 & 0 \\ P_{crotch}(x) & P_{SF}(y) & 1 \end{bmatrix} \begin{bmatrix} \cos(\beta - \alpha) & \sin(\beta - \alpha) & 0 \\ -\sin(\beta - \alpha) & \cos(\beta - \alpha) & 0 \\ 0 & 0 & 1 \end{bmatrix} \quad (5.4)
 \end{aligned}$$

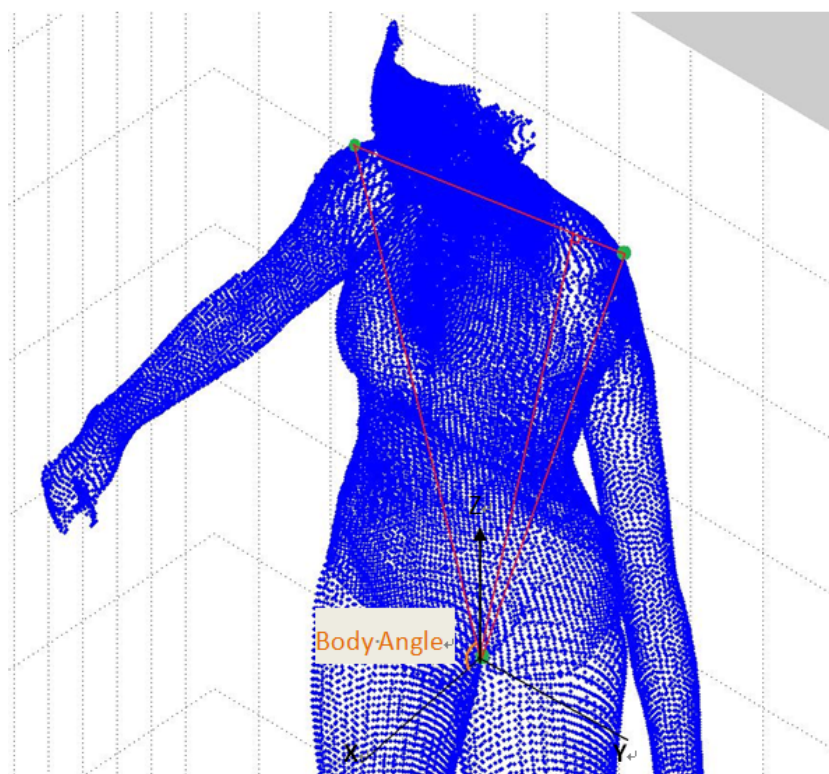


Figure 5-4. A plane is defined by the two shoulder points and crotch point. The body angle is the angle between the x axial and the plane.

5.2.2 Cross-section level design

There are two main concerns about the layout design of cross-sections. Firstly, the initial shape is designed mainly based on the 3-D scanning body profile data base. However, the age range of the body data base is narrow, result in a bias to the initial body shape, especially the size. In order to compensate the limitation, a widely recognized mannequin (Alvanon size 12 mannequin) was used as a reference to set the vertical location of the cross-sections first as shown in the Figure 5-5. As a result the initial shape size will be close to size 12 as defined in design specification. The values in bracket are the relative distance to the mid neck level.

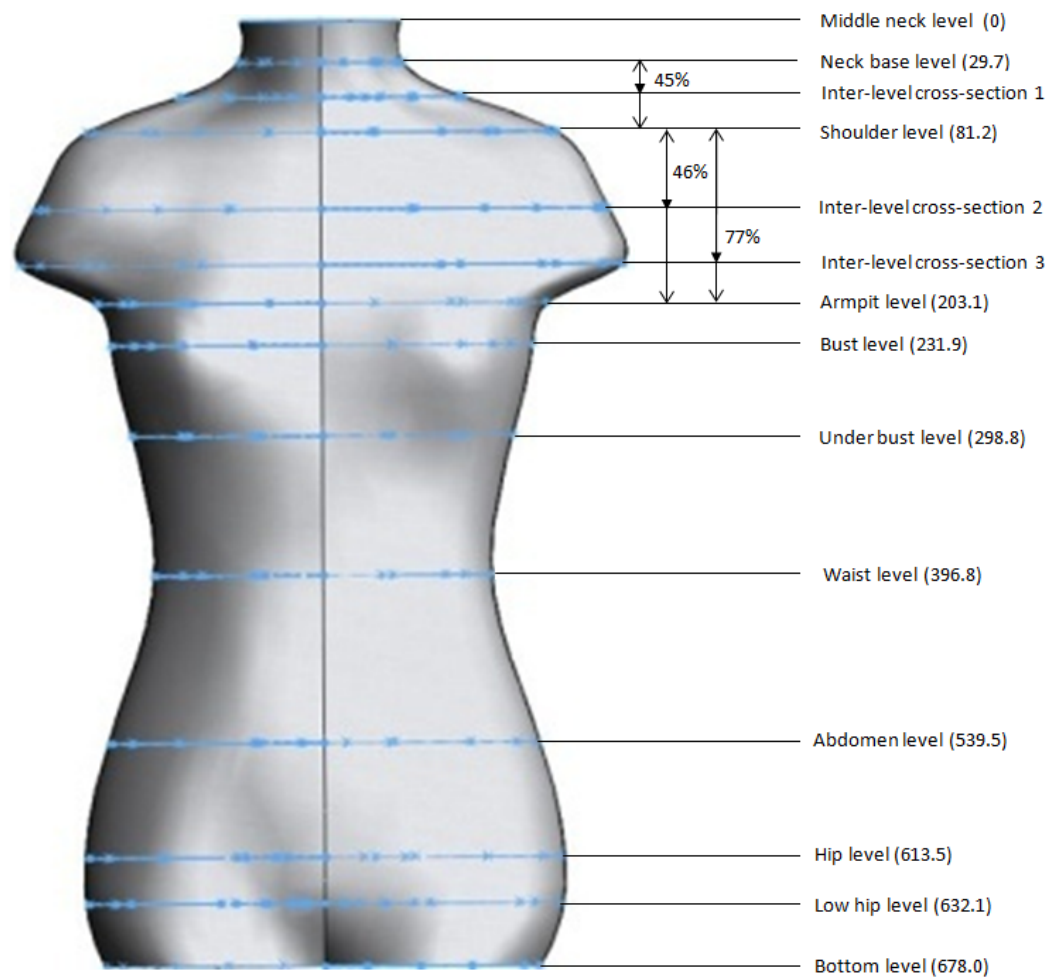


Figure 5-5. Layout of the cross-sections for the initial shape. All units are in millimetre.

Secondly, the quantity and location of the cross-section setup has a impact on the initial shape. On the one hand, the initial shape can represent more details by increasing the number of cross-sections. On the other hand, more cross-sections will result in a more concave-convex profile. As a result, the main cross-sections relative to the critical body dimensions, such as neck level, bust level, waist level, and so on, are built to ensure the important information for garment design and fitting have

been reserved. The vertical locations of these levels are determined by the relative distance to the middle neck level, which is the averages value of the corresponding values of the 130 samples measured by the 3-D body scanner. Using the relative distance to the mid neck level instead of the height relative to the floor can eliminate the error caused by the soft surface of the carpet on the floor and the thickness of sole. Then inter-level cross-sections were inserted to achieve a realistic and smooth shape as shown in Figure 5-5. The location of the inter-level cross-section is specified by the relative height between specified main levels.

5.2.3 B-spline curve construction

The generation of B-spline curve using Solidworks requires control points for segment. By adjusting the location of these points, the shape of the B-spline curve can be modified. The initial locations of these points are determined based on the responding points of the 130 3-D body scanning profiles and a size 12 mannequin. Figure 5-6 shows an example of the construction of the B-spline curve at bust level, which is identified by 8 points. To construct such a curve, first, search the level of points with the height value proximate to its bust height from one aligned 3-D body scanning data. Then, find the two points whose angular values are the two closest to

0° and average their locations to obtain the first points for B-spline curve. Similarly, the points on the B-spline curve at the angle 23° , 45° , 66° , 90° , 120° , 137° , and 180° can be obtained. Repeat this procedure on all the 130 profile data to obtain the 8 points for each one. Last, all the 8 points of the bust level are averaged respectively to obtain the final 8 points which identify the lower segment of the B-spline curve. As the left and right side of human body are assumed to be symmetric, the upper segment of the B-spline curve can be obtained by mirroring the lower segment as shown in the right side of Figure 5-6. Thus, the B-spline curve of bust level is obtained.

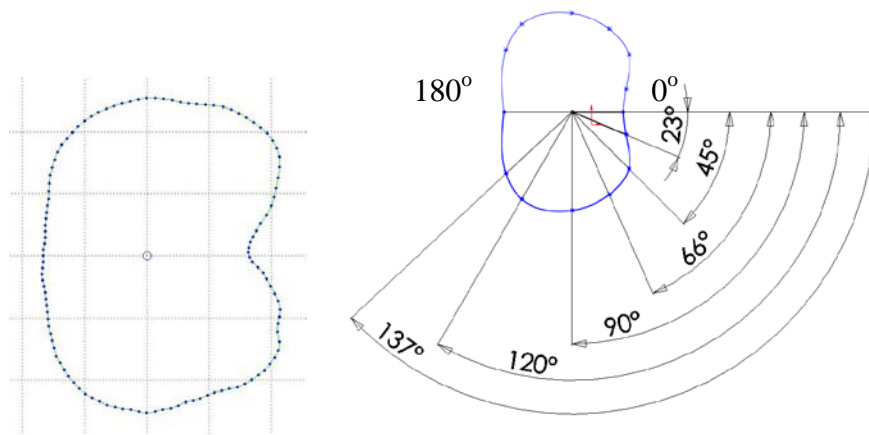


Figure 5-6. The cross-section at the bust level constructed by the points and B-spline curve. Left shows the proximate level to the bust level. Right shows the average shape represented by B-spline curve.

According to the design specification, the variation range of the robotic mannequin is listed as Table 5-1. The dimensions of the initial shape are set to the

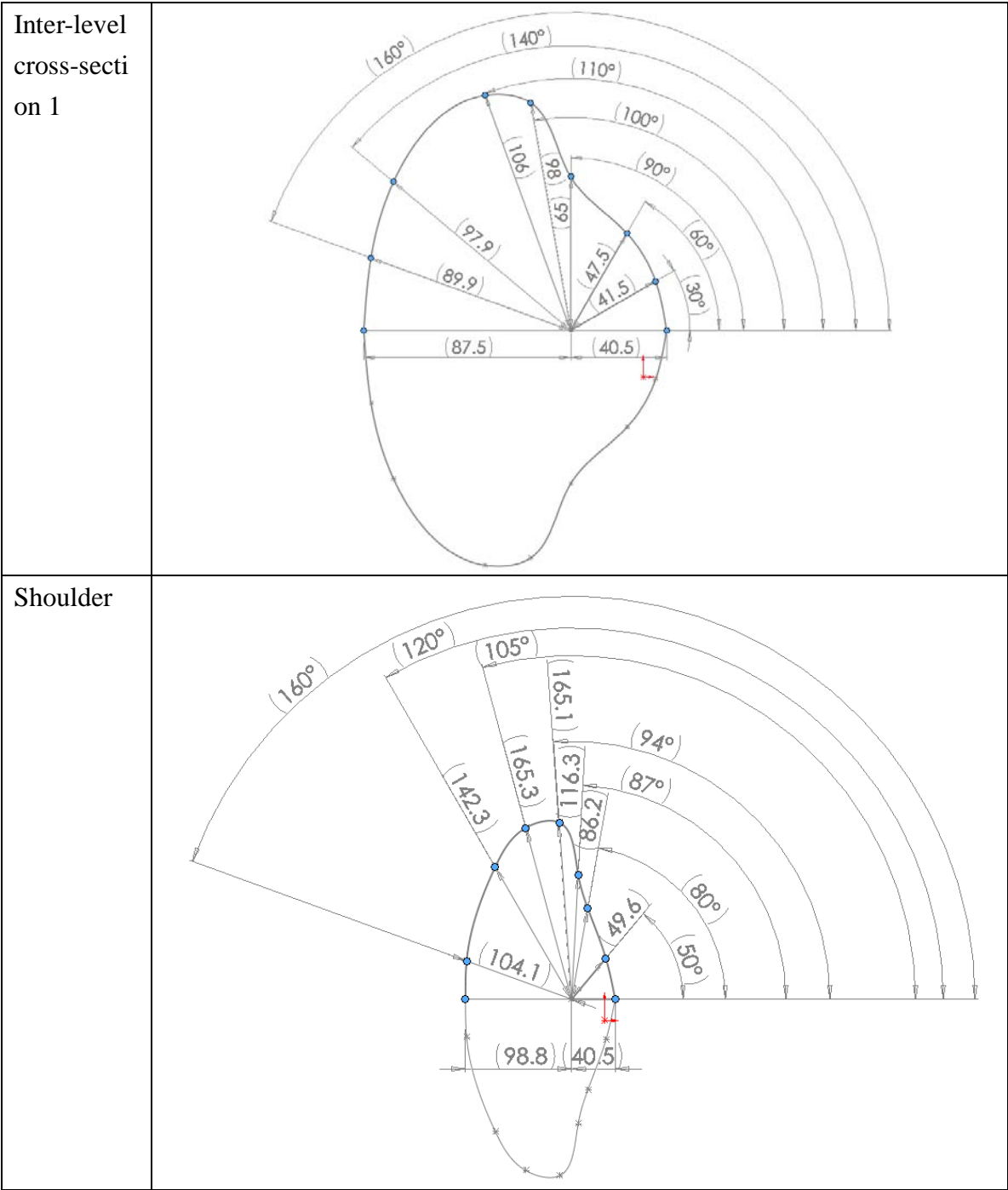
average values of the variation ranges, which is close to Asian size 12 mannequin's measurements

	Robotic mannequin variation range	Dimensions of initial shape
Neck girth	30.0 to 38.5	34.3
Bust girth	78.0 to 100.0	89.0
Waist girth	61.5 to 83.0	72.25
Hip girth	87.0 to 112.0	99.5
Bust to waist vertical length	15.5 to 17.5	16.5
Waist to hip vertical length	18.4 to 21.6	20.0

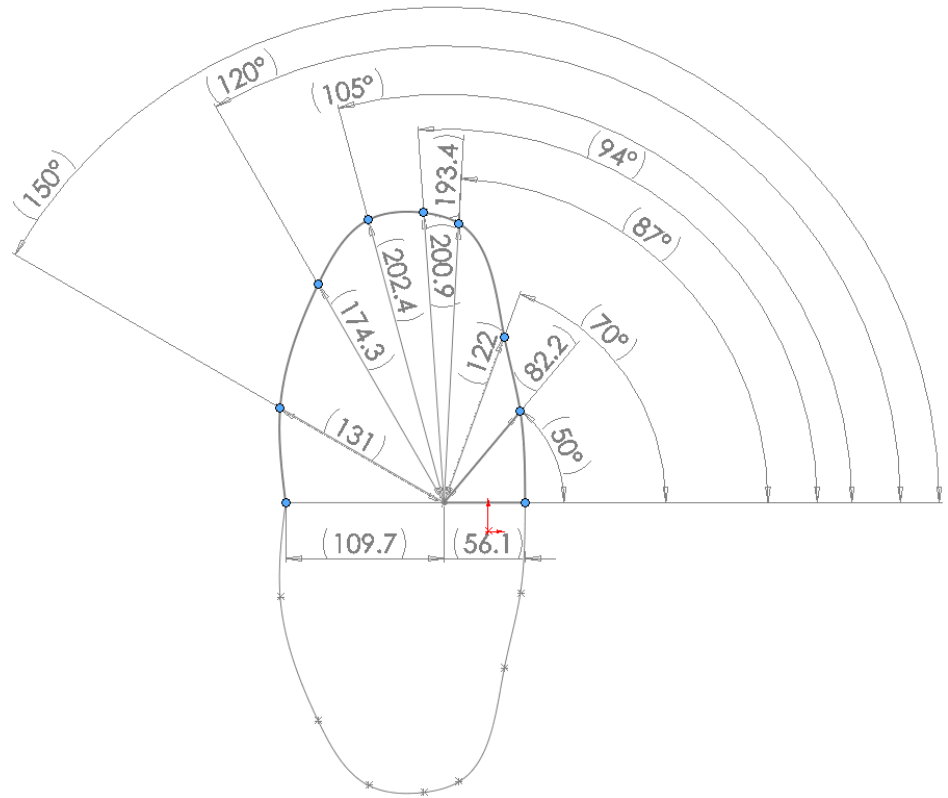
Table 5-1. Robotic mannequin variation range and dimension for initial shape

The B-spline curves were modified proportionally until the measurements meet the defined dimensions of initial shape in Table 5-1. Table 5-2 shows the B-spline curve of the average shape on all the 14 cross-sections. The location of the points on curve was identified by the angular value and the relative distance to the centre point of the slice.

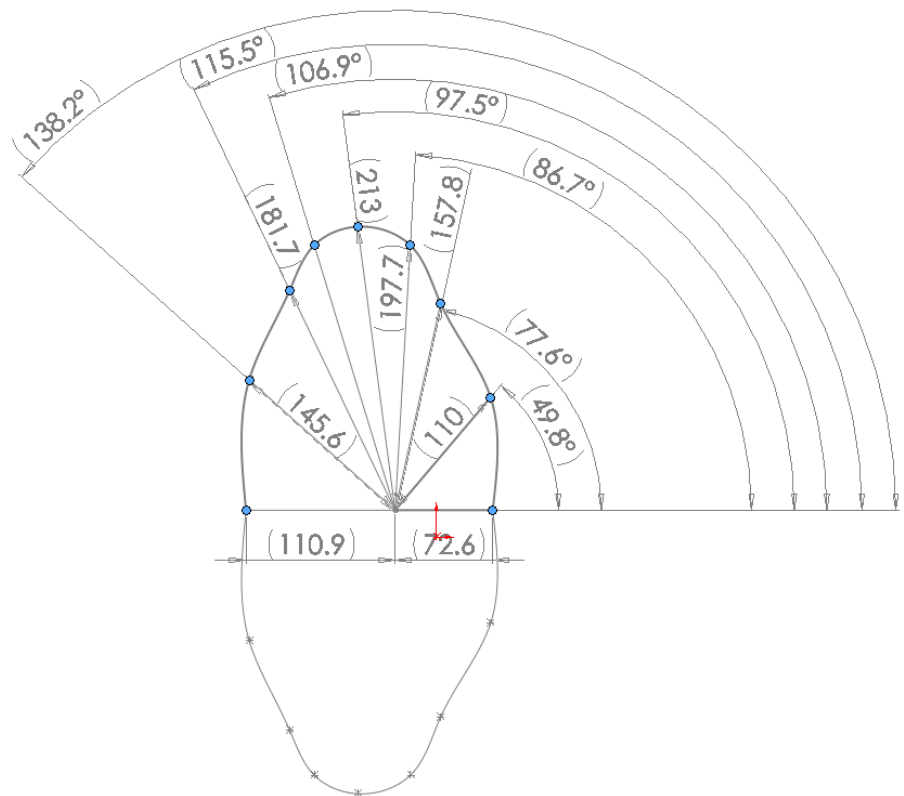
Level name	Cross-section design (not to scale)
Middle neck	
Neck base	

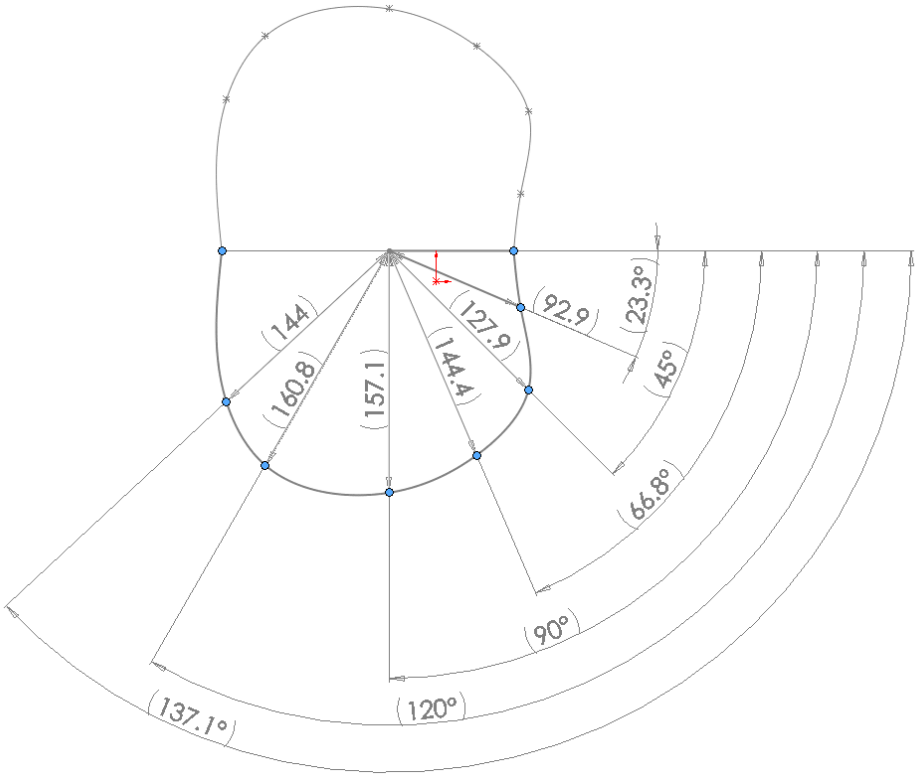
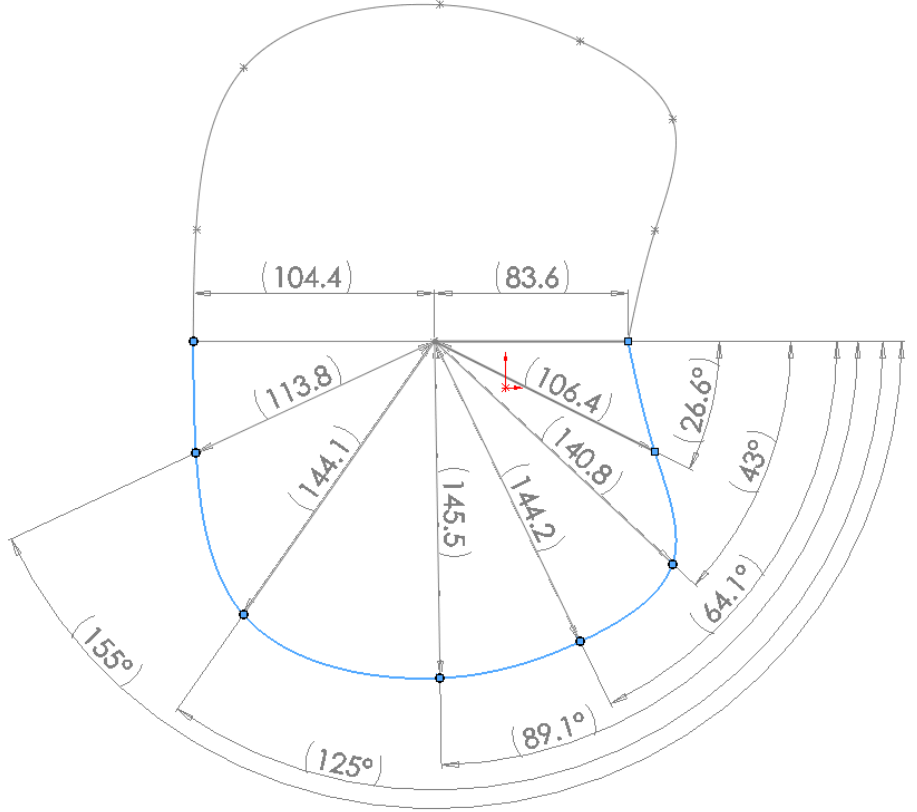


Inter-level
cross-section
on 2

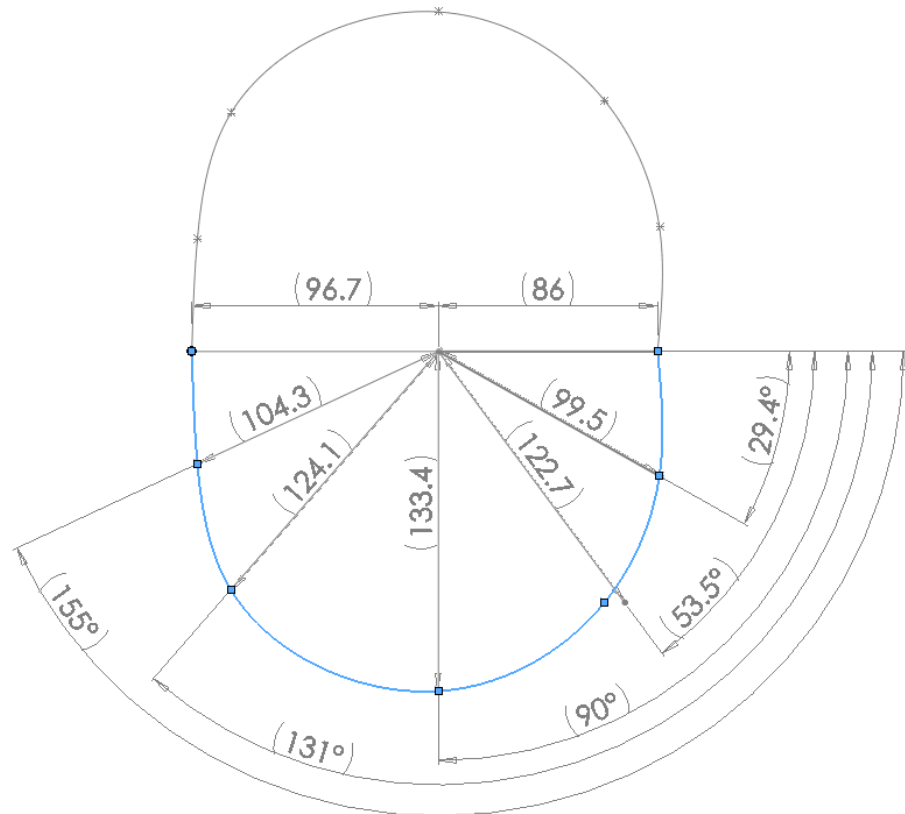


Inter-level
cross-section
on 3

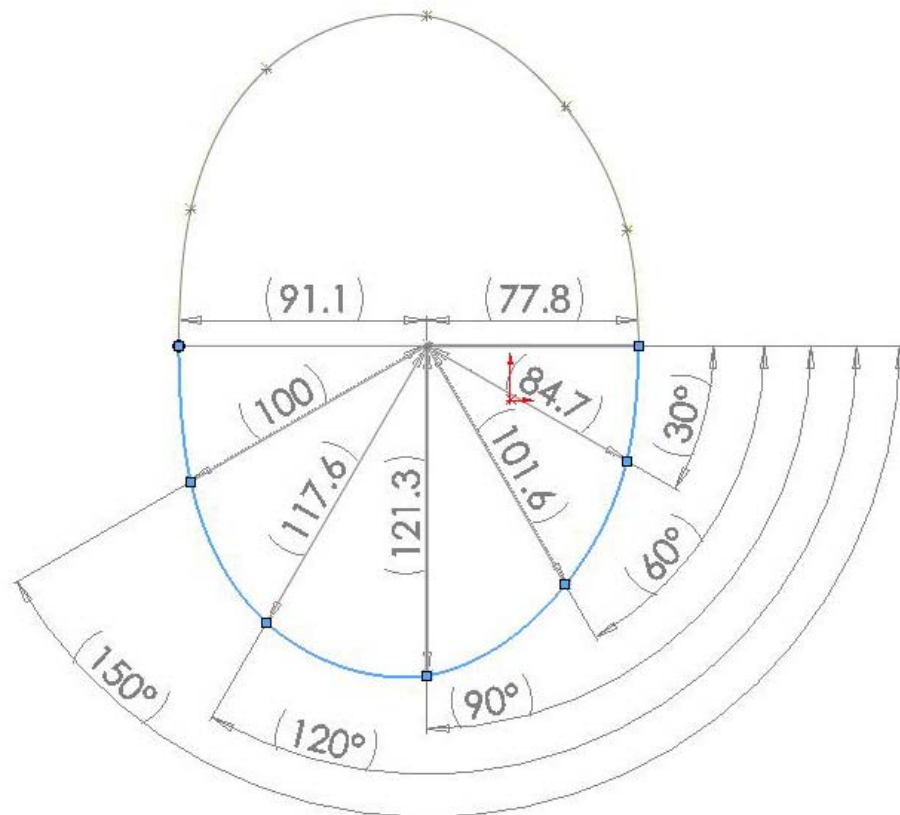


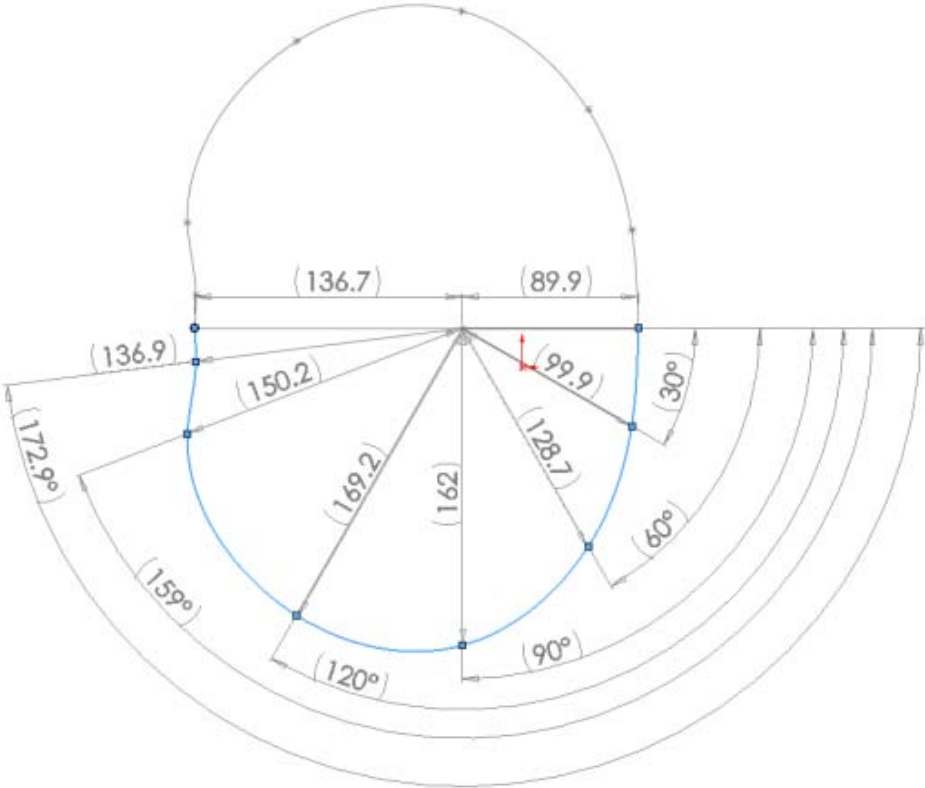
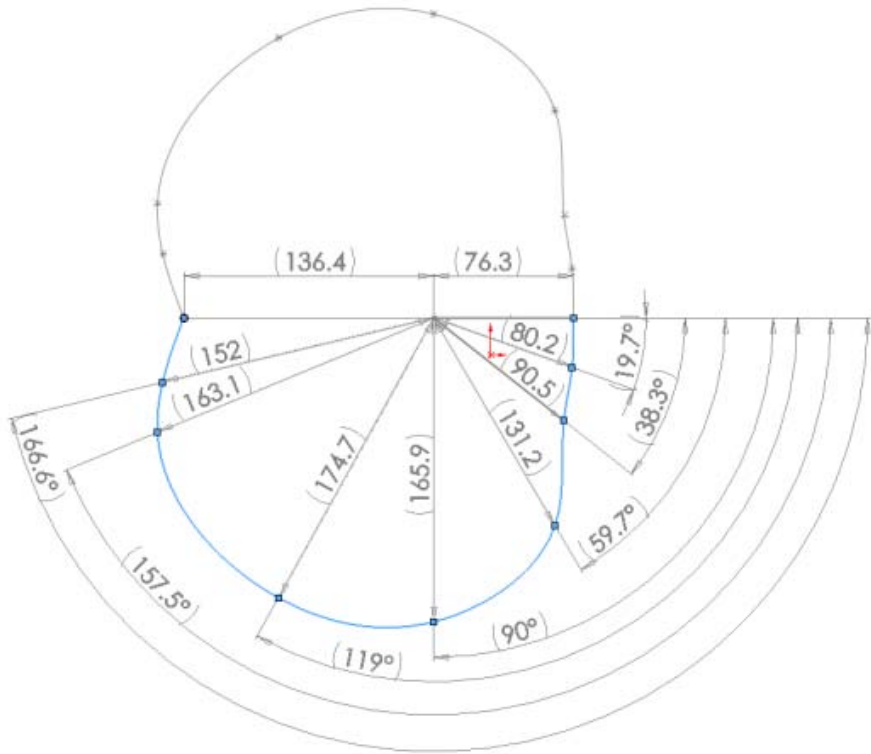
Armpit	 <p>Technical drawing of the Armpit pattern. It shows a circular sector with a central point. Radii are labeled with values in parentheses: (144), (160.8), (157.1), (144.4), (127.9), and (92.9). Angles from the horizontal line are labeled: (23.3°), (45°), (66.8°), (90°), (120°), and (137.1°). A red arrow points to the center. The pattern is divided into several curved segments.</p>
Bust	 <p>Technical drawing of the Bust pattern. It shows a circular sector with a central point. Radii are labeled with values in parentheses: (113.8), (144.1), (145.5), (144.2), (140.8), and (106.4). Angles from the horizontal line are labeled: (26.6°), (43°), (64.1°), (89.1°), (125°), and (155°). Horizontal distances from the center are labeled: (104.4) and (83.6). A red arrow points to the center. The pattern is divided into several curved segments.</p>

Under bust



Waist



Abdomen	 <p>Technical drawing of a bodice pattern for the abdomen area, showing a quarter-circle layout with various measurements and angles. The pattern is divided into several segments by radial lines. Key measurements include: horizontal distances of 136.7 and 89.9; radial distances of 136.9, 150.2, 169.2, 162, 128.7, and 99.9; and angles of 172.9°, 159°, 120°, 90°, 60°, and 30°. A blue curved line represents the side seam, and a red arrow indicates a specific direction or adjustment.</p>
Hip	 <p>Technical drawing of a bodice pattern for the hip area, showing a quarter-circle layout with various measurements and angles. The pattern is divided into several segments by radial lines. Key measurements include: horizontal distances of 136.4 and 76.3; radial distances of 152, 163.1, 174.7, 165.9, 131.2, 90.5, and 80.2; and angles of 166.6°, 157.5°, 119°, 90°, 59.7°, 38.3°, and 19.7°. A blue curved line represents the side seam, and a red arrow indicates a specific direction or adjustment.</p>

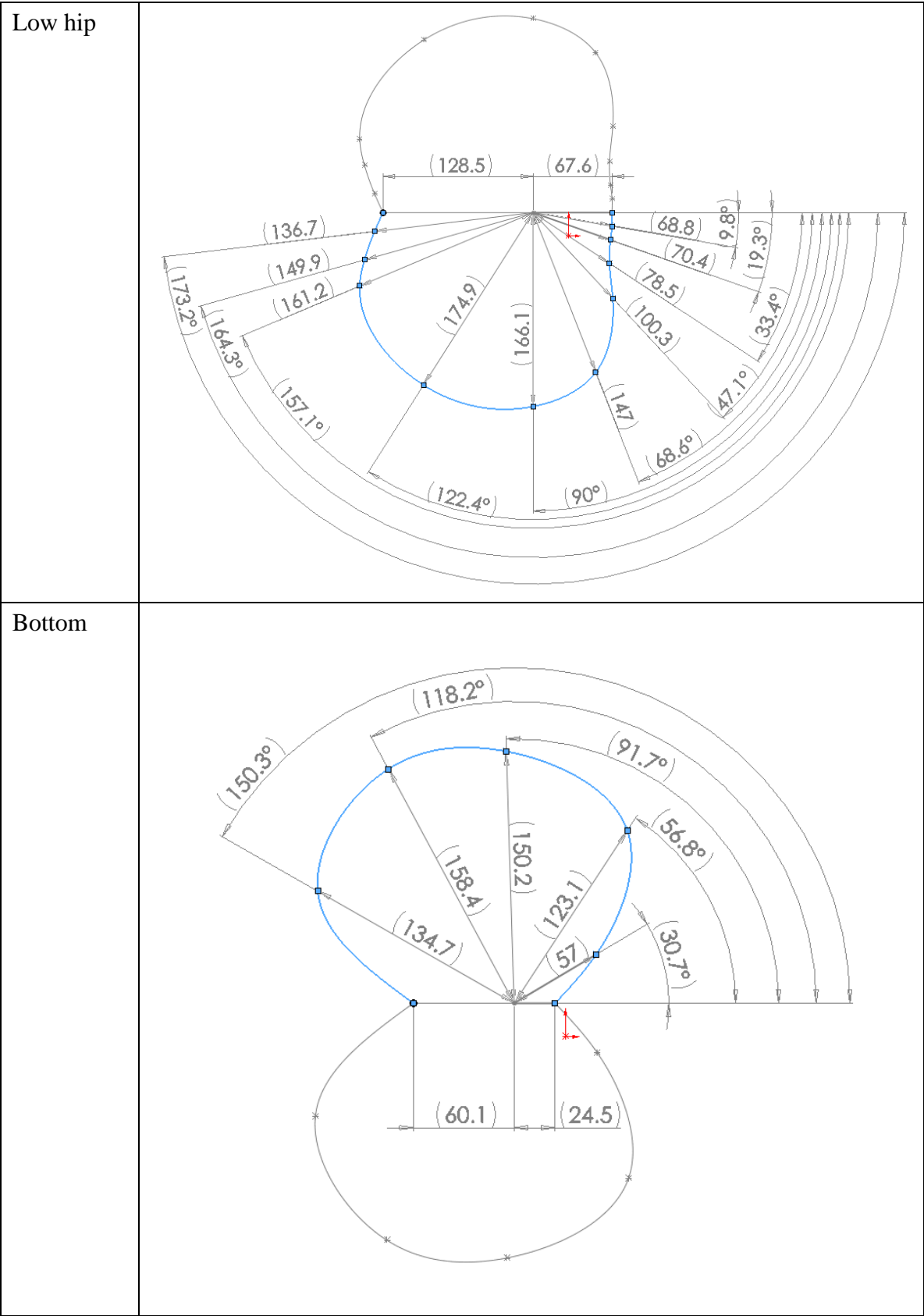


Table 5-2. Cross-section design

5.2.4 Initial shape Generation

The final profile of the initial shape is a surface created through the B-spline curves on all the cross-sections as shown in Figure 5-7 using the lofted surface function of Solidworks, which is able to generate a smooth surface.

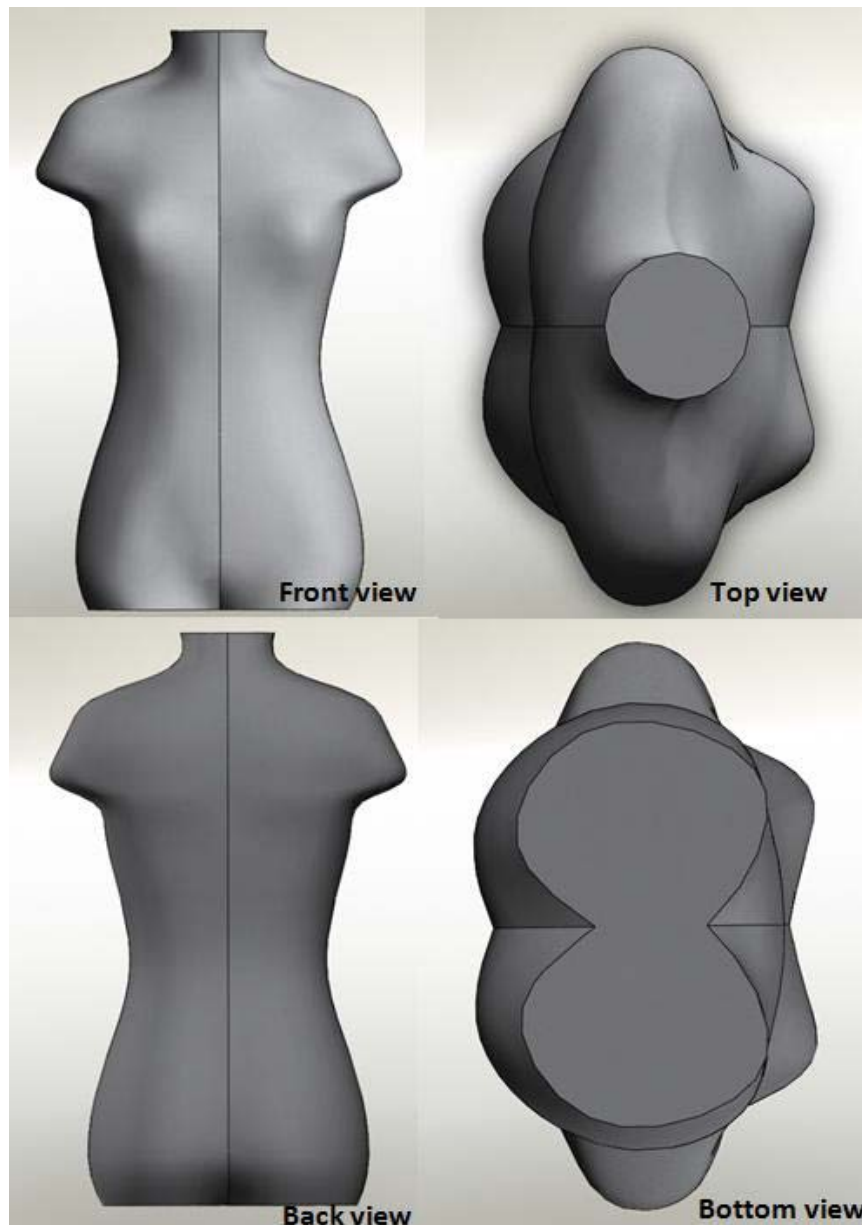


Figure 5-7. The front, top, back and bottom view of the initial shape profile

5.3 Panel and kinematics design

5.3.1. Primary panels design.

As described in section 2.1.2, there are different designs of the flexible mannequin, among which the panel type mannequin can afford a good support for donning the garment and still a good shape control. So the robotic mannequin will use panels for its surface. The parametric model surface was cut into 16 panels as described later on in the chapter. The panels will have the following important features,

1. There are gaps between the neck, the chest, the waist and the hip as these parts need to accommodate the physical change.
2. The neck consists of two panels, left and right. As the neck girth change is relatively small compared to the other panels (see Table 4-1).
3. From studying the 3-D body profile data base and research done by others (P.J. Taylor and M.M. Shoben, 1993), it is found that the grading of major body sections is in the way shown as Figure 5-8. The variation can be represented using 4 panels moving in 4 different directions as described in Figure 5-9. As a result, the chest, waist and hip parts consist of 4 panels. The gaps between them

are all 2.5cm and the gaps are designed to be able to close and expand to 5 cm. Thus the chest, waist and hip girth can reduce and increase by 10 cm which is adequate to cover the adjustable size range as listed in Table 4-7. The gap can be covered using a cladding made of highly elastic fabric.

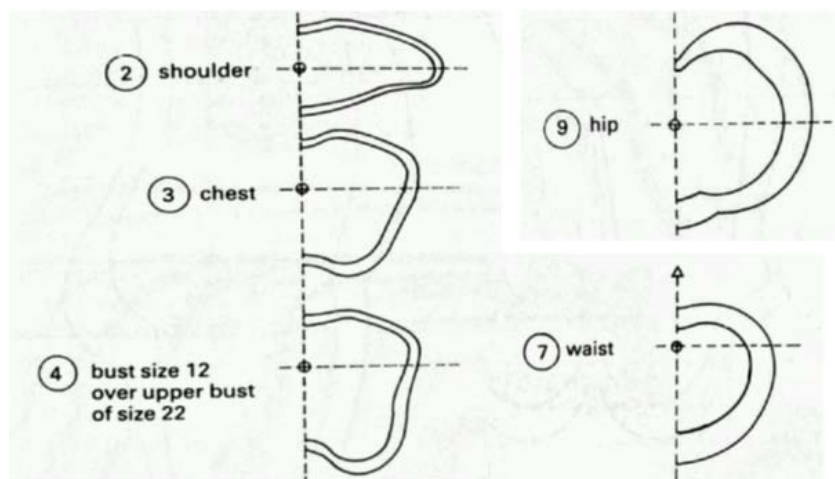


Figure 5-8. Major body sections of UK size 12 and 22 superimposed on each other (P.J. Taylor and M.M. Shoben, 1993)

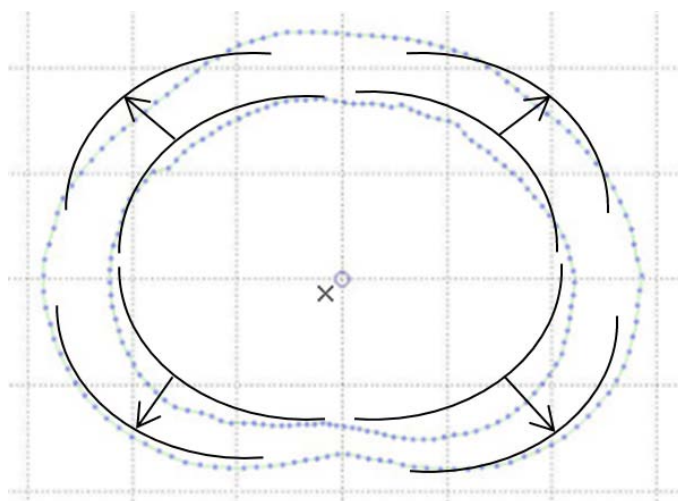


Figure 5-9. Dotted line shows waist cross-sections of 62cm and 80cm in waist girth superimposed on each other according to the center point. The curve and arrow shows that the general shape can be represented by move 4 panels in 4 different directions.

4. The gap between waist and chest section is 2 cm and the gap between waist and hip is 3 cm. In other words the length between chest and waist has a change range of 4 cm and the length between the waist to hip has a change range of 6 cm which is enough to cover the adjustable range as described in Table 4-7.
5. The bust panels are separated from the front chest panels so it can move to change the cup size.
6. The bust point's variation is shown as Figure 5-8, and the bust panels movement should design according to these findings.

The Figure 5-9 to 5-14 show the different view of the panel design.

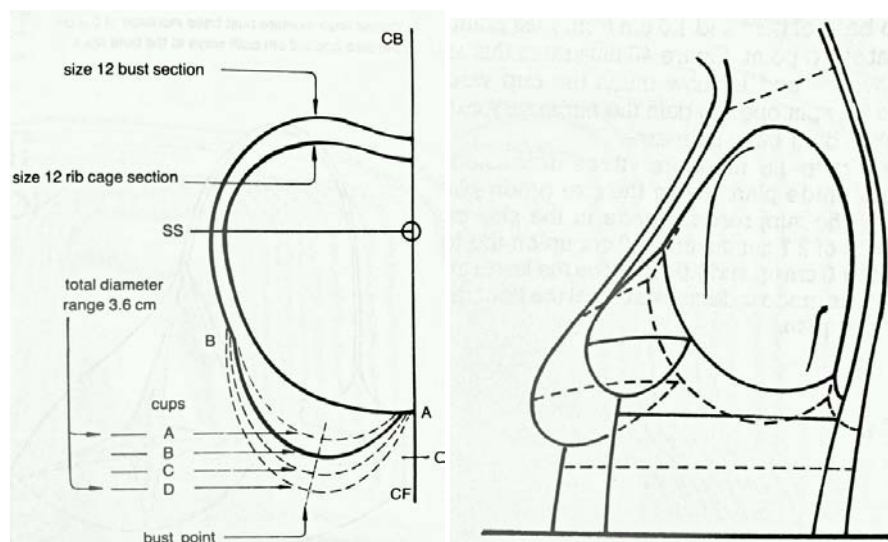


Figure 5-8. Left shows the bust point's horizontal variation. Right shows the bust point's vertical variation when the body size increases (P.J. Taylor and M.M. Shoben, 1993).



Figure 5-9. Virtual robotic mannequin shell

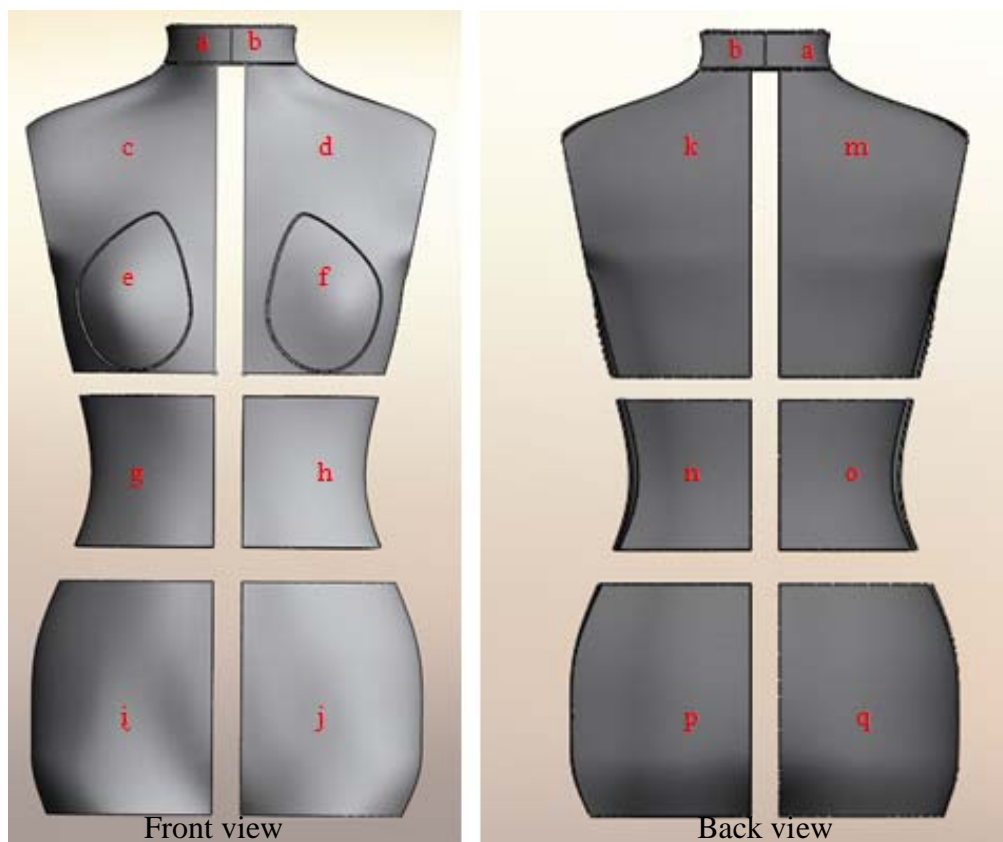


Figure 5-10. Front and back view of the virtual robotic mannequin panels.

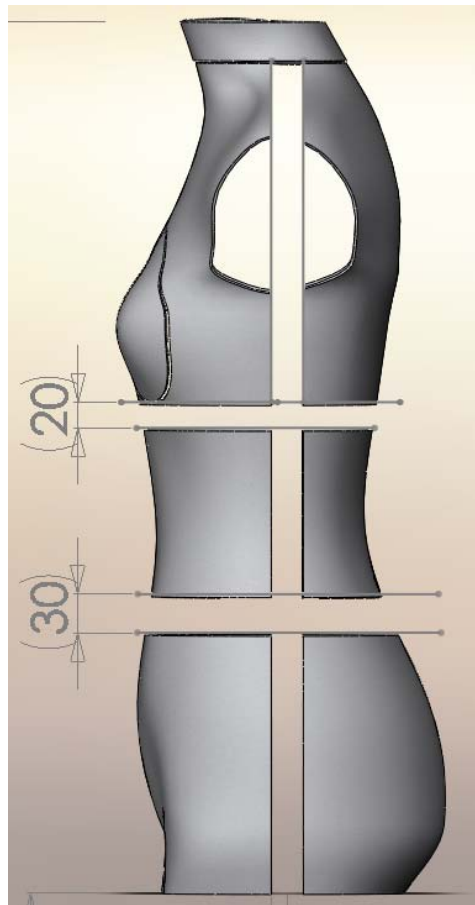


Figure 5-11. Side view of the virtual robotic mannequin panels.

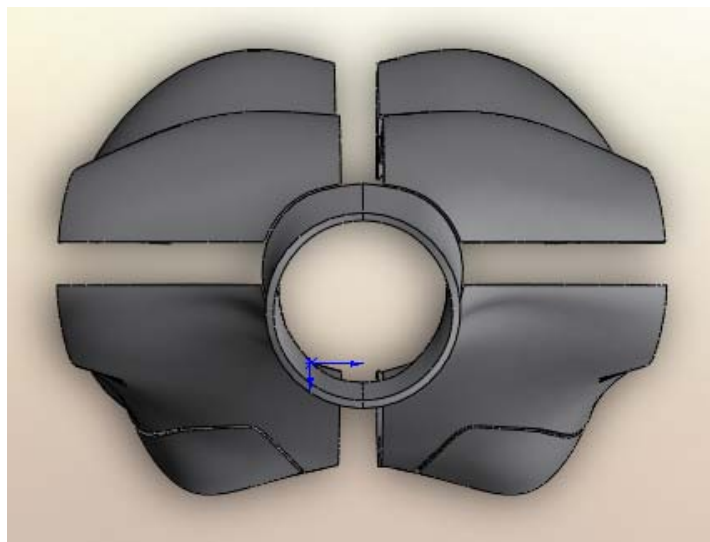

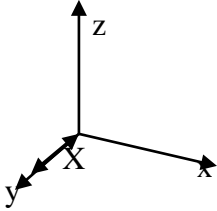
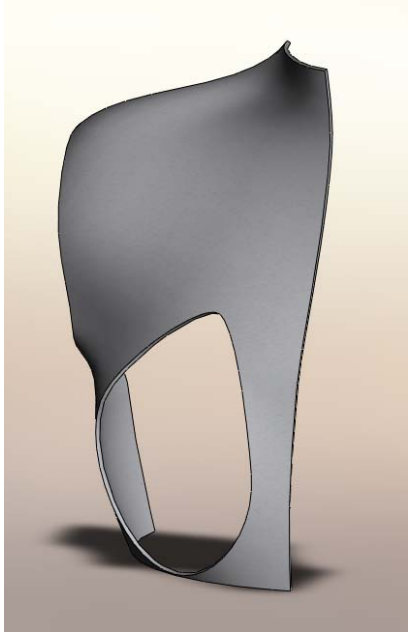
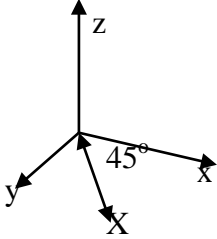



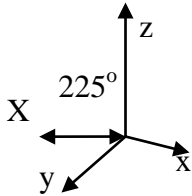
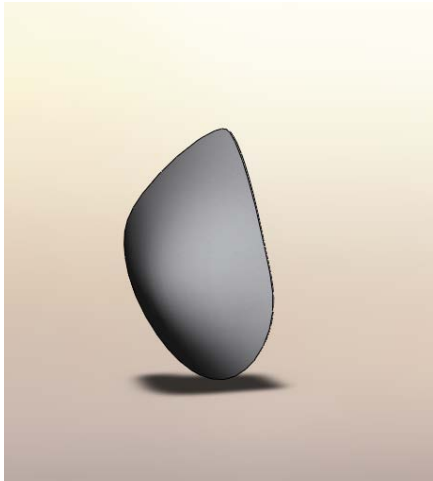
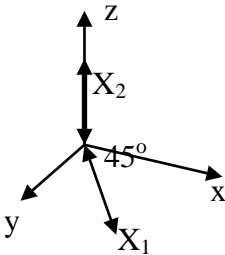
Figure 5-12. Top view of the virtual robotic mannequin panels


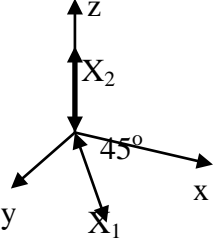

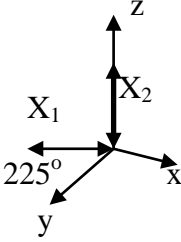

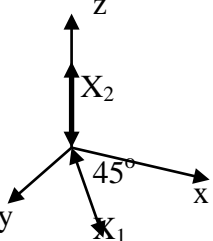
5.3.2. Major panel movement simulation and kinematic design

According to design specifications in Chapter 4 and the specifications in section 5.3.1, the direction and distance of movement of each panel is defined as Table 5-3.

Panel movement direction and distance control. As the movements of left body side and right body side panels are symmetrical, only the panels on the right body side are tabulated.

Panel	Movement direction	Movement distance control equation
<p>a. Right neck panel</p> 		<p> $X \in [-2.1 \text{ cm}, 2.1 \text{ cm}]$ $Y \in [30.0 \text{ cm}, 38.5 \text{ cm}]$ Where X is the horizontal distance of the panel's movement. Y is the neck girth. </p>
<p>c. Right front chest panel</p> 		<p> $X = [-1.7 \text{ cm}, 1.7 \text{ cm}]$ $Y \in [67.0 \text{ cm}, 85.0 \text{ cm}]$ where X is the horizontal distance of the panel's movement. Y is the under-bust girth. </p>

<div>m. Right back chest panel</div> <div></div>	<div></div>	<div>$X = [-1.7\text{ cm}, 1.7\text{ cm}]$ $Y \in [67.0\text{ cm}, 85.0\text{ cm}]$</div> <div>where X is the horizontal distance of the panel's movement. Y is the under-bust girth.</div>
<div>e. Right bust panel</div> <div></div>	<div></div>	<div>$X_1 \in [-2.1\text{ cm}, 2.1\text{ cm}]$ $X_2 \in [-0.6\text{ cm}, 0.6\text{ cm}]$ $Y \in [78.0\text{ cm}, 100.0\text{ cm}]$</div> <div>$X_1$ is the horizontal distance of the panel's movement. X_2 is the vertical distance of the panel's movement. Y is the bust girth.</div>

<p>g. Right front waist panel</p> 		<p> $X_1 \in [-1.9 \text{ cm}, 1.9 \text{ cm}]$ $X_2 \in [-1.0 \text{ cm}, 1.0 \text{ cm}]$ $Y \in [61.5 \text{ cm}, 83.0 \text{ cm}]$ </p> <p>where</p> <p>X_1 is the horizontal distance of the panel's movement.</p> <p>X_2 is the vertical distance of the panel's movement.</p> <p>Y is the waist girth.</p>
<p>o. Right back waist panel</p> 		<p> $X_1 \in [-1.7 \text{ cm}, 1.7 \text{ cm}]$ $X_2 \in [-1.0 \text{ cm}, 1.0 \text{ cm}]$ $Y \in [61.5 \text{ cm}, 83.0 \text{ cm}]$ </p> <p>where</p> <p>X_1 is the horizontal distance of the panel's movement.</p> <p>X_2 is the vertical distance of the panel's movement.</p> <p>Y is the waist girth.</p>
<p>i. Right front hip panel</p> 		<p> $X_1 \in [-1.9 \text{ cm}, 1.9 \text{ cm}]$ $X_2 \in [-1.6 \text{ cm}, 1.6 \text{ cm}]$ $Y \in [87.0 \text{ cm}, 112.0 \text{ cm}]$ </p> <p>where</p> <p>X_1 is the horizontal distance of the panel's movement.</p> <p>X_2 is the vertical distance of the panel's movement.</p> <p>Y is the hip girth.</p>


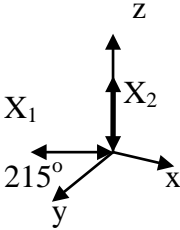
<p>p. Right back hip panel</p> 		<p>$X_1 \in [-2.0\text{ cm}, 2.0\text{ cm}]$ $X_2 \in [-1.6\text{ cm}, 1.6\text{ cm}]$ $Y \in [87.0\text{ cm}, 112.0\text{ cm}]$</p> <p>where X_1 is the horizontal distance of the panel's movement. X_2 is the vertical distance of the panel's movement. Y is the hip girth.</p>
--	---	---

Table 5-3. Panel movement direction and distance control

5.3.3. Style panel design and modification.

The movements of basic panels realize the major body shape variation and cover the size variation. Style panels are added to provide the user with customized shape for more realistic body configuration,

1. The neck panels were redesign as shown in Figure 5-13. Four panels can provide imitation of neck variation better than only left and right neck panel.
2. Two independent abdomen panels, the upper and lower abdomen panels, were added offering more variation in the front abdomen as shown in Figure 5-14.

3. The shoulder is extended towards both sides of the body, to support the sleeve design better as shown in Figure 5-15.

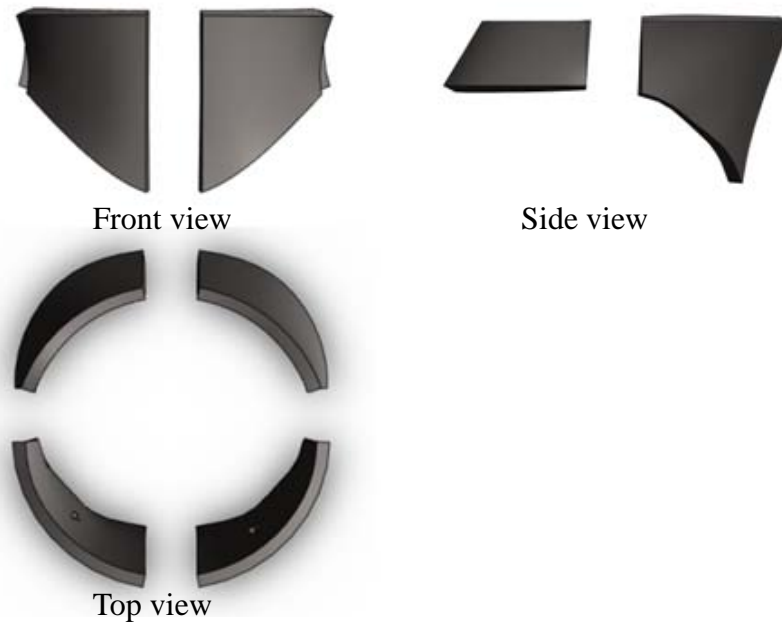


Figure 5-13. The front, side and top view of modified neck panels.

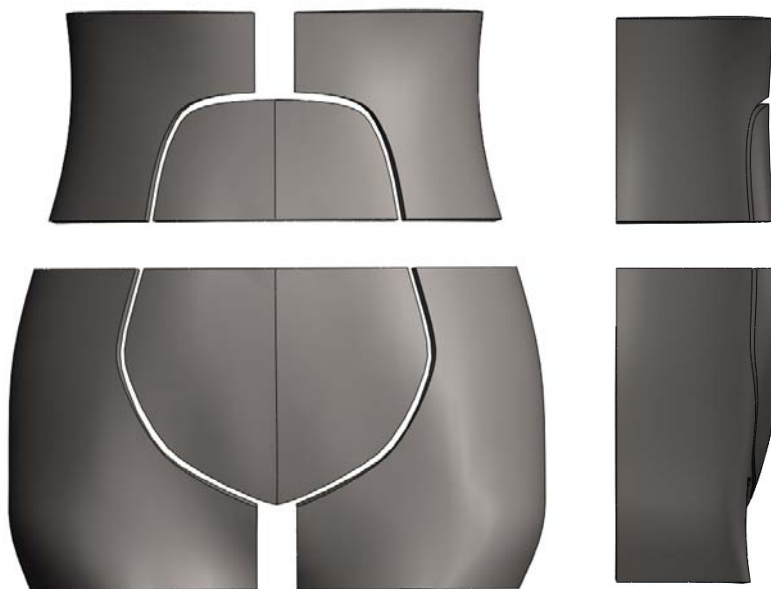


Figure 5-14. Front and side view of modified abdomen panels.

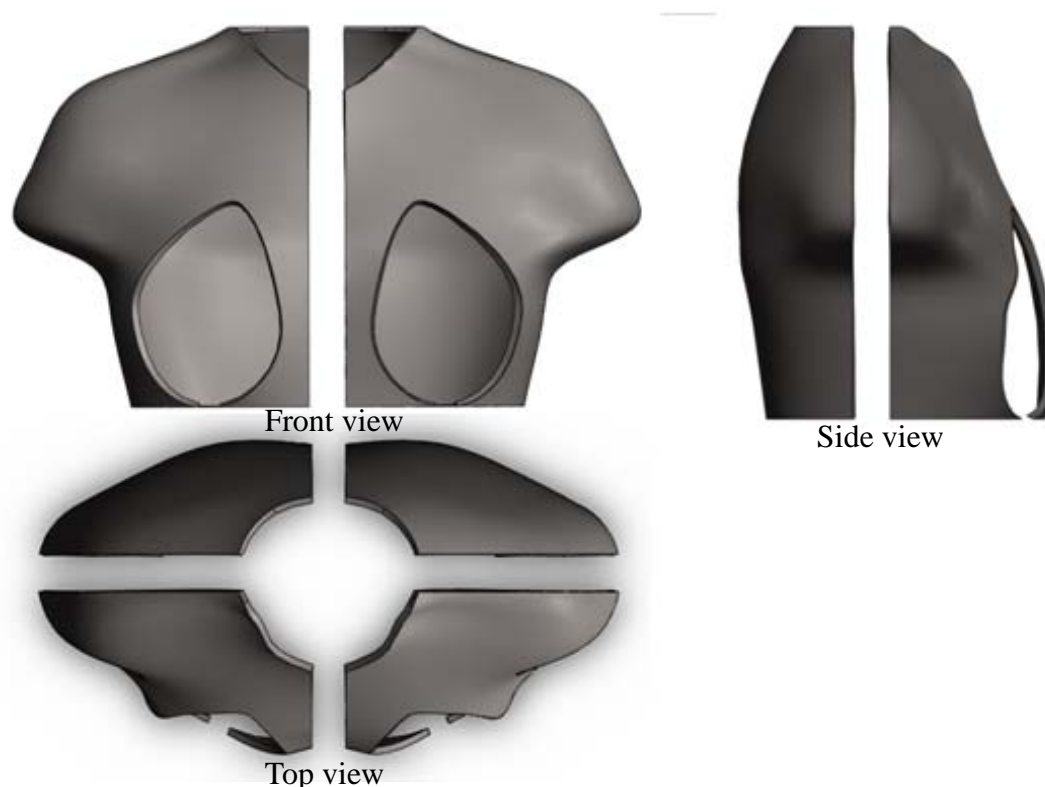


Figure 5-15. The front, side and top view of the additional part added to the shoulder.

5.3.4. Pilot validation result and comment

A pilot validation was carried out to verify the concept design of the robotic mannequin. The virtual robotic mannequin demonstrated the shape variation from the minimum size to the maximum size. And it mimicked 3 existing mannequin on the market which are Asian Size 10, 12, and US Size 8 (detailed measurements are shown in Table 5-4). These mannequins were scanned and displays in blue point cloud as shown in Figure 5-16, 5-19 and 5-20. The panels of robotic mannequin were shown in yellow colour. The red, blue and green lines indicate the bust, waist and hip

girth correspondingly.

	Asian Size 10	Asian Size 12	US Size 8
Neck base(cm)	37.0	38.0	36.8
Bust girth(cm)	82.5	86.5	92.5
Waist Girth(cm)	60.0	64.0	72.4
Hip Girth(cm)	89.0	93.0	97.8
Waist to hip(cm)	19.75	20.0	20.3
Total rise(cm)	68.5	70.0	67.6

Table 5-4. Size table for the size 10, 12 and US Size 8 mannequin

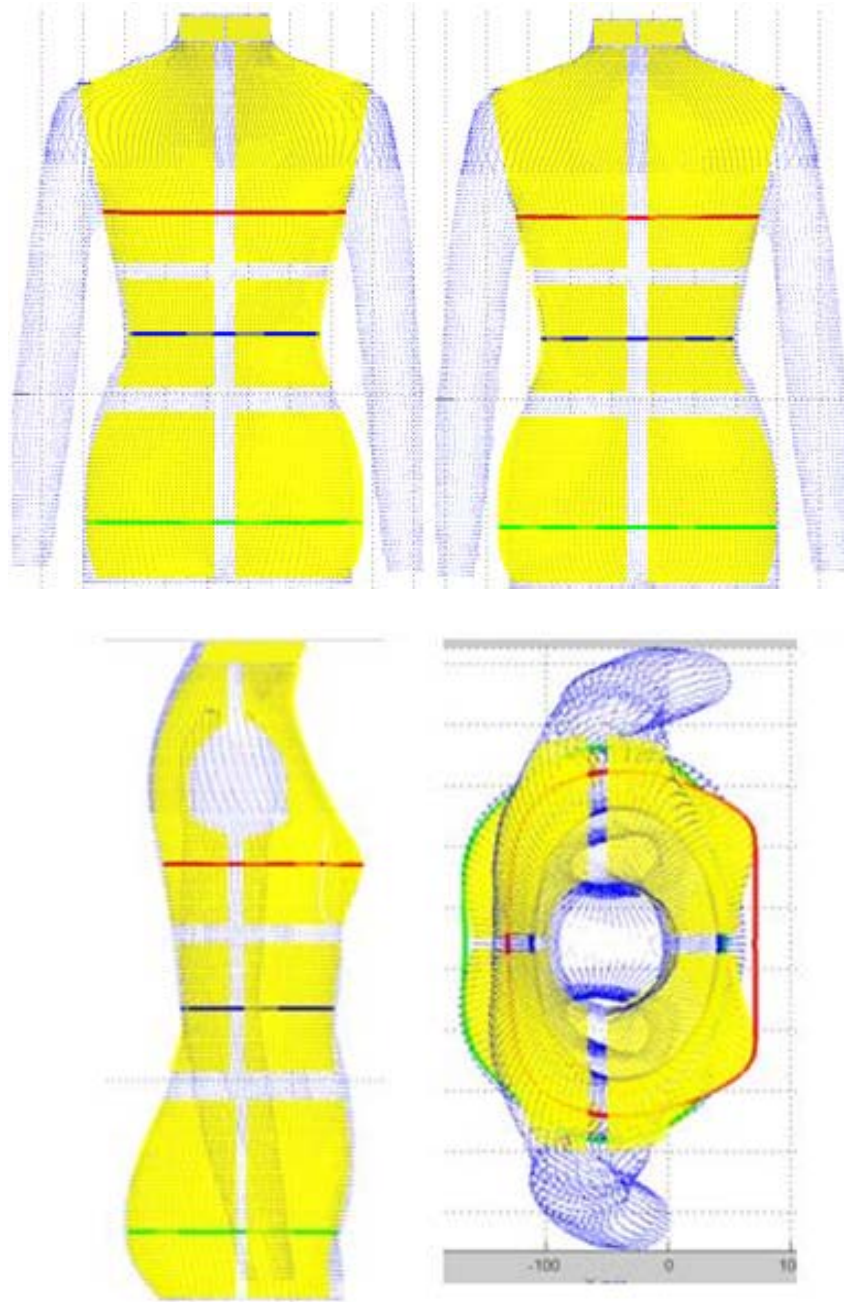


Figure 5-16. virtual robotic mannequin imitates the shape of an Asian Size 10 mannequin. Top left is the front view, top right is the back view, bottom left is the side view, and bottom right is the right view.

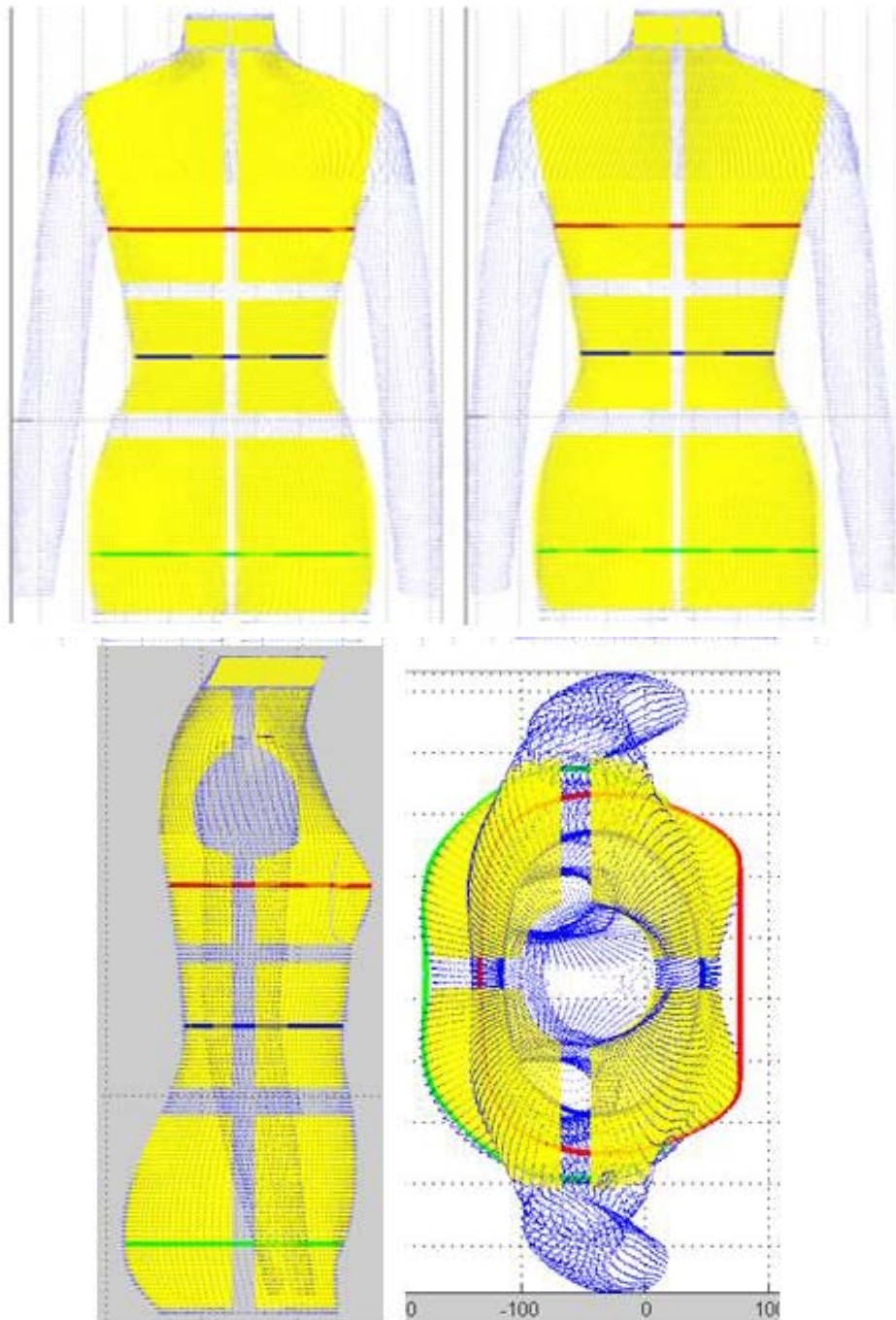


Figure 5-17. Virtual robotic mannequin imitates the shape of an Asian Size 12 mannequin. Top left is the front view, top right is the back view, bottom left is the side view, and bottom right is the right view.

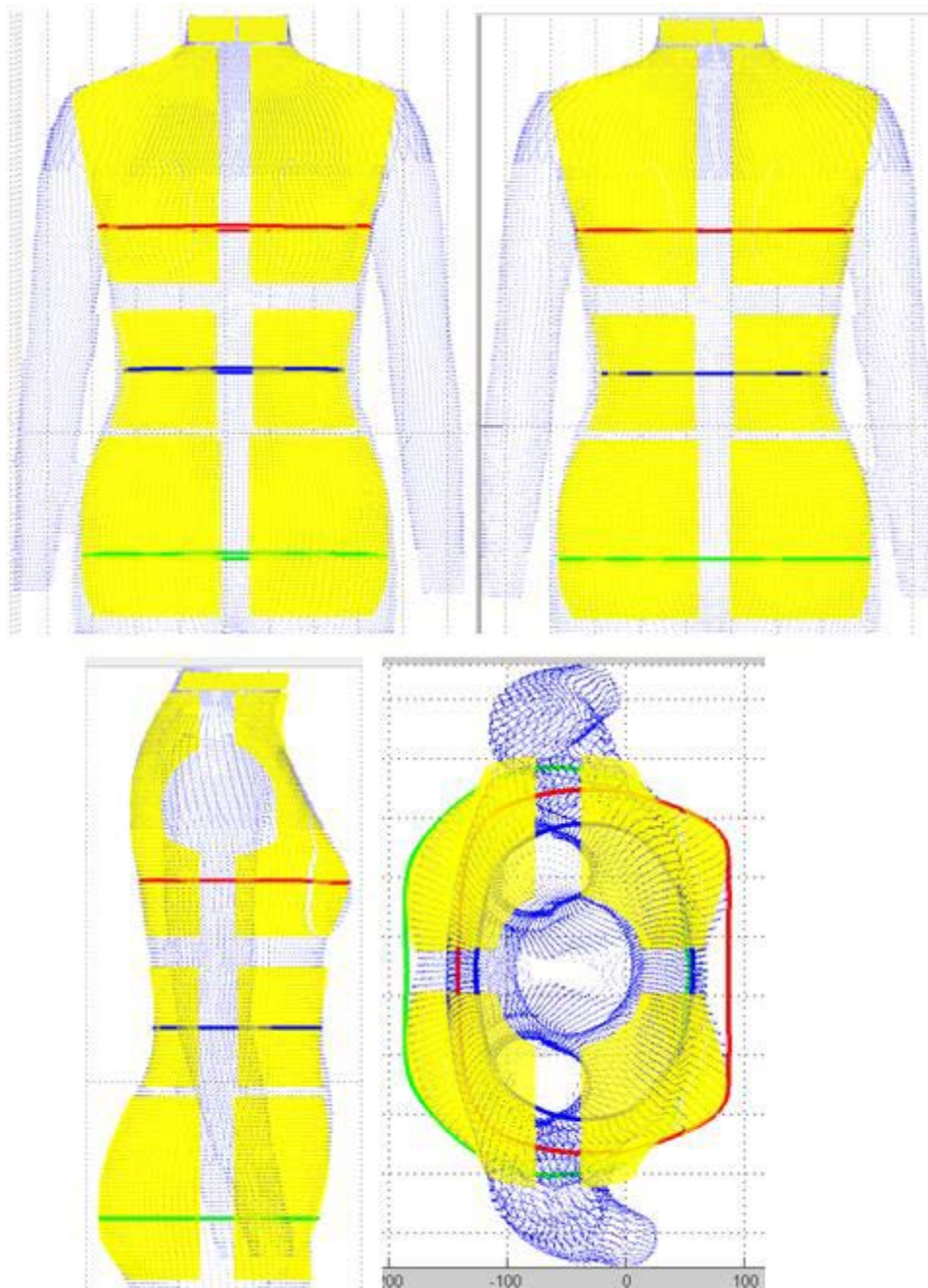


Figure 5-18: Virtual robotic mannequin imitates the shape of a US Size 8 mannequin. Top left is the front view, top right is the back view, bottom left is the side view, and bottom right is the right view.

A pilot validation (Appendix II) was completed by Mrs Cheung who is a teacher and researcher after watching the demonstration. She has over 30 years of

teaching and industrial technical experience in the fashion industry. The feedback shows that,

1. The robotic mannequin can mimic the shape of the 3 reference mannequins.
2. The shape of the robotic mannequin is close to the real human body within the design size variation range.
3. The design size variation range of the robotic mannequin is sufficient for the research and industry use.

Chapter 6 Detailed design of the robotic mannequin

6.1. Introduction

This section describes the detailed design of the development of robotic mannequin. After the concept design stage, the shell (in the form of panels) and their motion trajectories are specified, based on which, the mechanism, actuator, control system are designed to realise the desired functions. In-depth discussion starts with the mechanical design, followed by the driving module, cladding design and lastly the graphical user interface. The top-down design method is adopted, which starts from rough, overall and general design of the robot, followed by the refinement of design at the level of single component. In the area of product design, designers and engineers rely on both a bottom-up and top-down approach (M. Mantyla, 1990). The bottom-up approach is being utilized when off-the-shelf or existing components are selected and integrated into the product. The top-down approach is more suitable for a product with more specific requirements. In the field of computer-aided design (CAD), top-down method refer to designing the product in entirety first, then split it into assemble parts (H. Yoshiura, K. Fujimura and T.L. Kunii, 1984). This method

helps to create product with complex dimension and movement relationship within the components. The stages of detail design are shown as Figure 6-1. The design procedure starts from the definition of the main components and general appearance. Next, based on the desired functions, the mechanical design, driving unit design and control software are designed. Finally, the integration of the robotic mannequin system is described at the end of this chapter

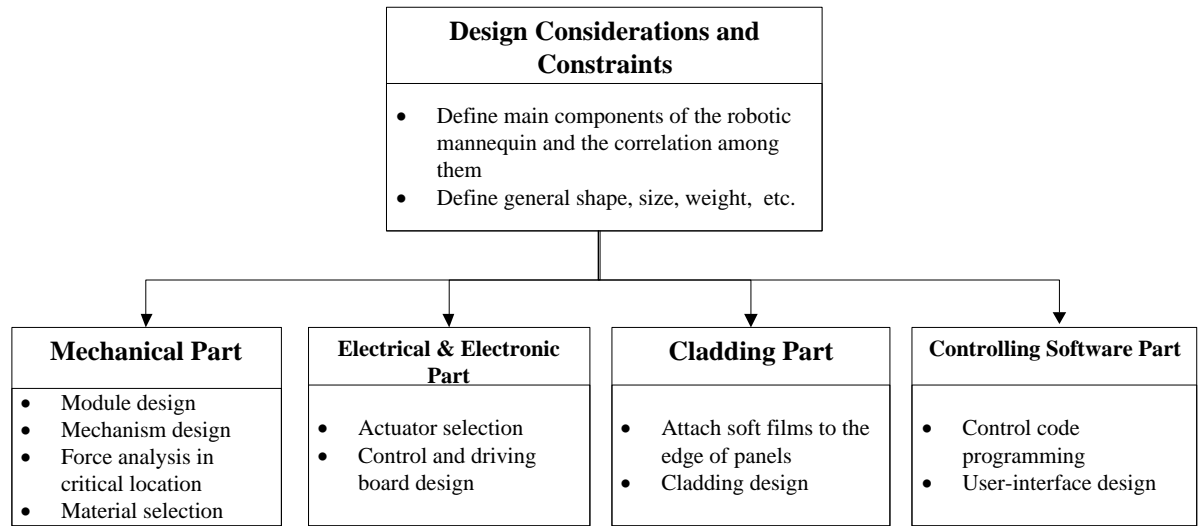


Figure 6-1. Top-down design procedure for robotic mannequin development

6.2. Mechanical part

The mechanical design covers three stages. First stage is the module design. Using a modular design method, the robotic mannequin is divided into individual modules: neck, chest, waist, hip and base module. These modules can function individually for the ease of maintenance and argumentation. It also enhances the

flexibility of the system. The second stage is mechanism design, which focuses on the mechanism design detailed to the fine level of material, size, and weight. The third stage verifies the entire mechanisms on their robustness of the design.

6.2.1. Mechanical module design

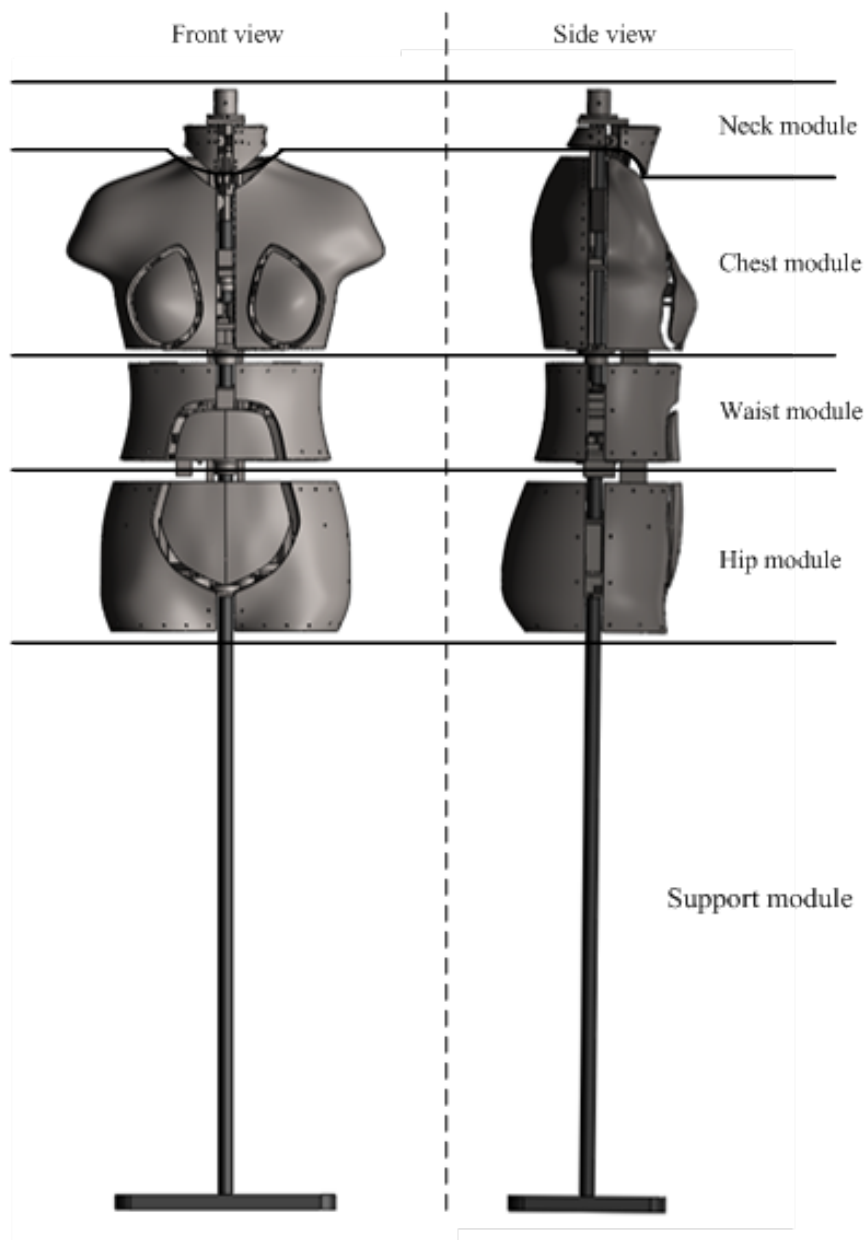


Figure 6-2. Layout of modules

Figure 6-2 shows module compositions of the robotic mannequin,

1. Neck Module. There are two main functions for this module. Firstly, it has to be fix the entire robotic mannequin frame to the stand. Secondly, it is the realization of the neck girth variation.
2. Chest module: This module is designed to realize the shape variation and dimension change in the front chest, back chest and bust. It is fixed below the neck module and provides support for the lower modules.
3. Waist module: This module is designed to realize the girth variation in the front waist, back waist. Besides, it enables the bust-to-waist length to be adjustable. It is fixed below the chest module and provides support to the lower module.
4. Hip module: This module is designed to realize the girth variation in the front hip and back hip. It also enables the waist-to-hip length to be adjustable.
5. Support module: The support module is designed to support the weight of the robotic mannequin and provide mobility.

6.2.2. Mechanism design

Solidworks is used to design the mechanism for each module. The mechanism can be classified into three types, which are the moving parts, frame and adapting pieces. In this section, the design of significant mechanism is described.

6.2.2.1. Support module design

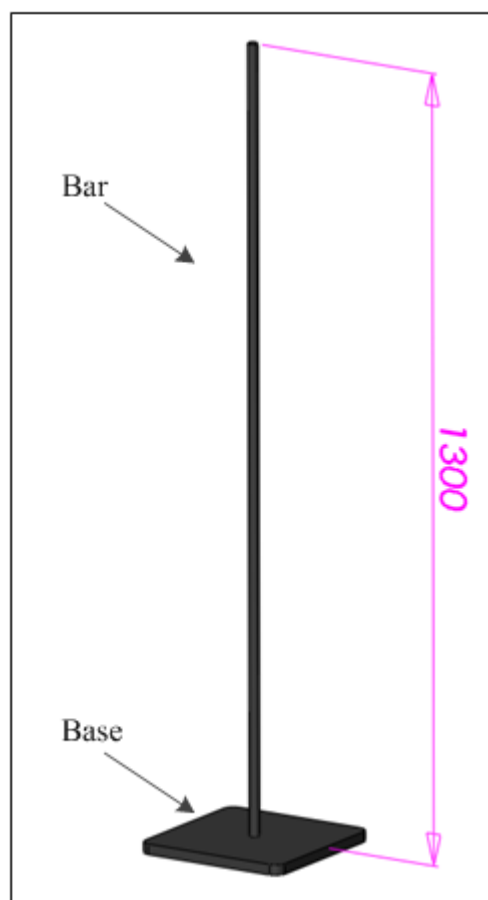


Figure 6-3. Support module overview. All units are in mm.

The support module is made up of a metal bar and a base. The bar support the weight of the entire robotic mannequin can allow the waist and hip modules to move along it. The module can be changed to portable type for mobility, fixed type for better stability, or suspension type for the design of skirt and pants. Figure 6-3 shows the support module.

The bar is made of Ductile iron which is a common material for pipes, Table 6-1

lists its mechanical properties. The main dimensions of the module is shown in the top view of the support module (Figure 6-4).

Label	Ductile iron
Elastic Modulus	$1.2\text{e}+11 \text{ N/m}^2$
Poisson's Ratio	0.31
Shear Modulus	$7.7\text{e}+10 \text{ N/m}^2$
Density	$7.1\text{e}+3 \text{ kg/m}^3$
Tensile Strength	$8.6\text{e}+8 \text{ N/m}^2$
Yield Strength	$5.5\text{e}+8 \text{ N/m}^2$

Table 6-1 Ductile iron mechanical properties

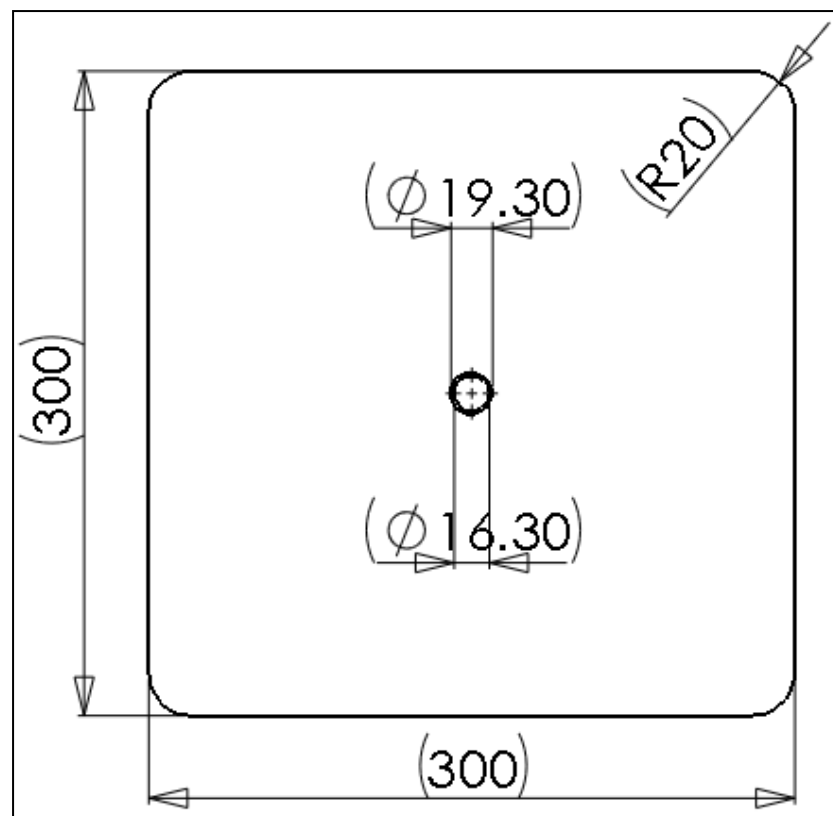


Figure 6-4. Top view of the support module (Unit: mm)

The robotic mannequin is fixed on the top of the bar, the finite element method

(FEA) is applied to ensure the structure is able to support the weight. Solidworks Simulation software is used to perform the FEA. The module is meshed using 4-point Jacobian mesh with the default setting in Solidworks Simulation. It is stated that the Jacobian mesh is able to map curved geometry much more accurately than linear elements of the same size (Solidwork 2012 online helps, 2012). The main load applied to the support module is the weight of the robotic mannequin which is located at the top surface of the bar. The total weight of the entire robotic mannequin is 10.4 kilogram (kg). For safety, other possible external loads, such as force applied by user, impact, weight of objects hung on the robotic mannequin, etc. are taken into account, result in a conservative maximum force estimation of 120N. Figure 6-5 shows the von Mosis stress distribution on the support module with a 120N force applied to the top of the bar. A maximum of 1.6 megapascal (MPa) is observed which is far less than the yield strength (551.485 MPa), with a minimum Factor of Safety (FOS) of 346.5, so the support module is able to support object about 3603.6 kg, which is strong enough for supporting the robotic mannequin.

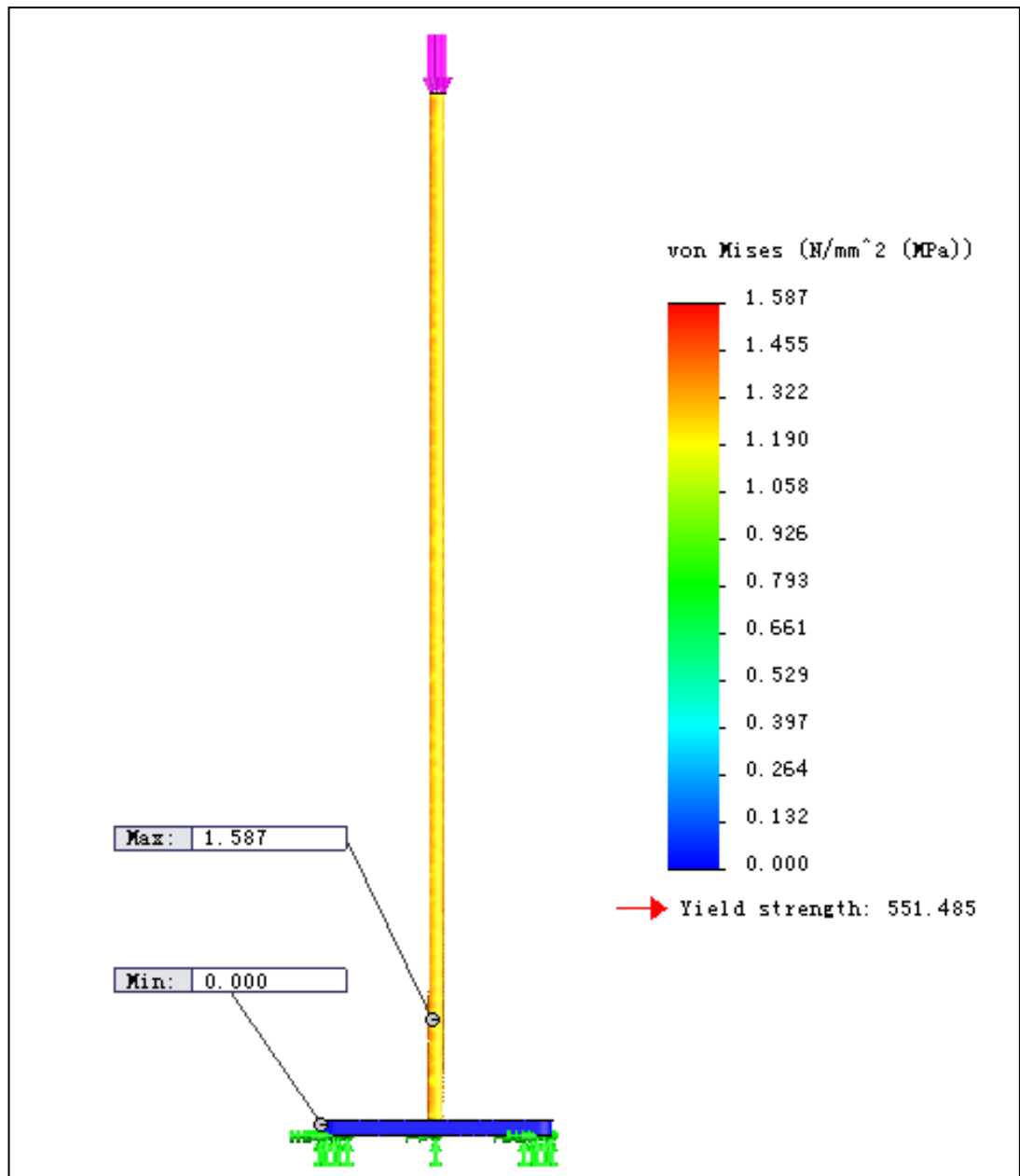


Figure 6-5. Von Mises stress distribution of the support module. The green arrow represents the fixture. The purple arrow represents the external force.

6.2.2.2. Neck module design

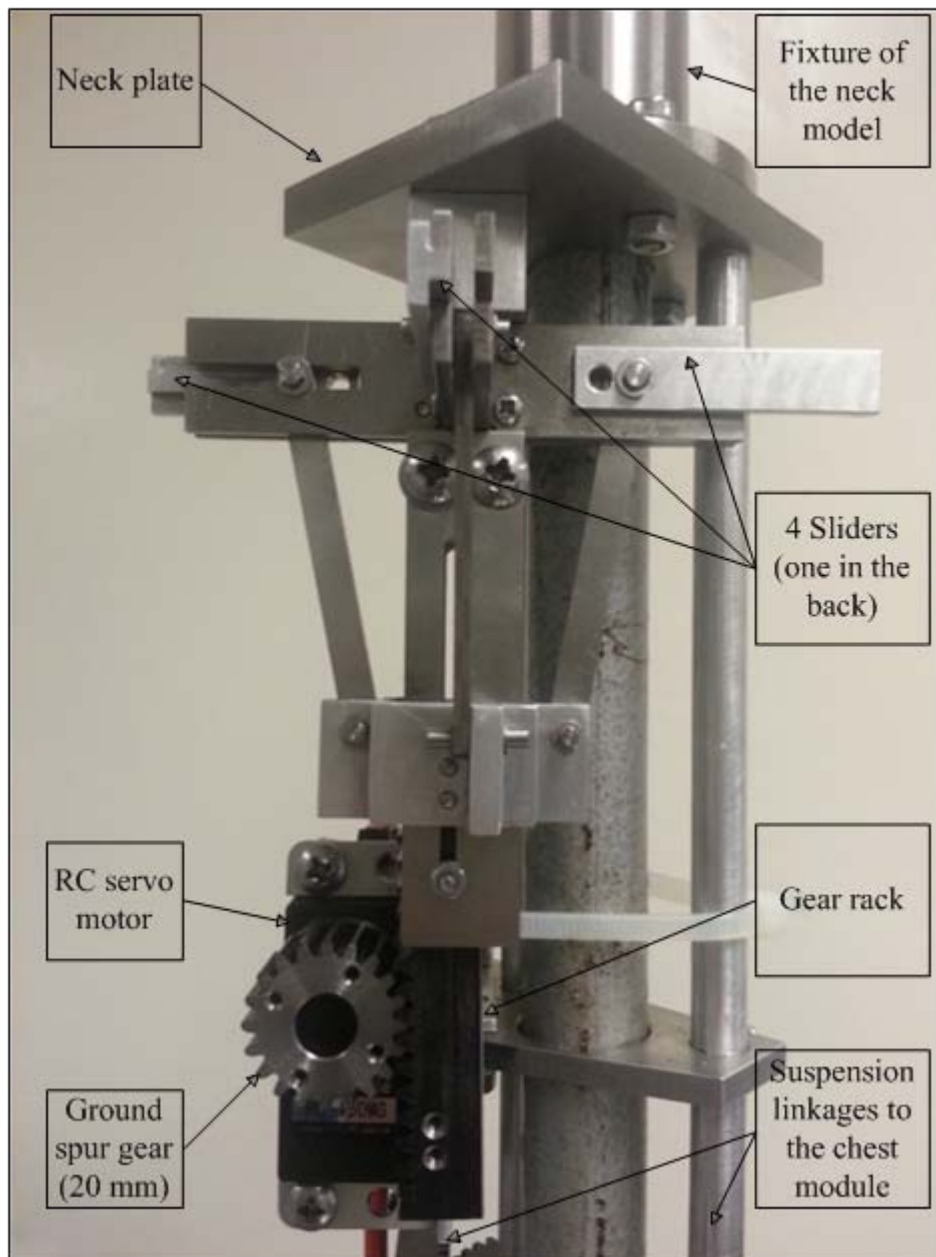


Figure 6-6. Neck model overview

Figure 6-6 shows the overview of the neck module, which consists of 2 main parts,

1. Support part. The usage of this part is to support the weight of the robotic

mannequin. It consists of 3 main components: the fixture of the neck model, the neck plate and the suspension linkages to the chest module. The fixture of the neck model. It fixes the neck module on the top of the bar by interference fit. The neck plate provides the platform for the installation for the other parts. The suspension linkages support the remains modules other than the neck module. Thus the main load on this part is the gravity of 92.3N, which is weight of the modules (9.4 kg) except the neck module. As the fixture and plate component carry the maximum stress, they are made of stainless steel, while the other parts are made of Aluminium alloy (6061 alloy) to reduce weight, and their mechanical properties are listed in Table 6-2. To ensure the support part is functional, FEA is applied. Refer to Figure 6-7, the FEA result shows the maximum Von Mises stress is 13.1, which is smaller than the yield strength, and FOS is 13.2, indicating the structure is safe.

Label	6061 Aluminium alloy	Stainless steel
Elastic Modulus	$6.9 \times 10^{10} \text{ N/m}^2$	$2 \times 10^{11} \text{ N/m}^2$
Poisson's Ratio	0.33	0.28
Shear Modulus	$2.6 \times 10^{10} \text{ N/m}^2$	$7.7 \times 10^{10} \text{ N/m}^2$
Density	$2.7 \times 10^3 \text{ kg/m}^3$	$7.8 \times 10^3 \text{ kg/m}^3$
Tensile Strength	$1.2 \times 10^8 \text{ N/m}^2$	$5.1 \times 10^8 \text{ N/m}^2$
Yield Strength	$5.5 \times 10^7 \text{ N/m}^2$	$1.7 \times 10^8 \text{ N/m}^2$

Table 6-2. Mechanical properties of 6061 Aluminium alloy and stainless steel

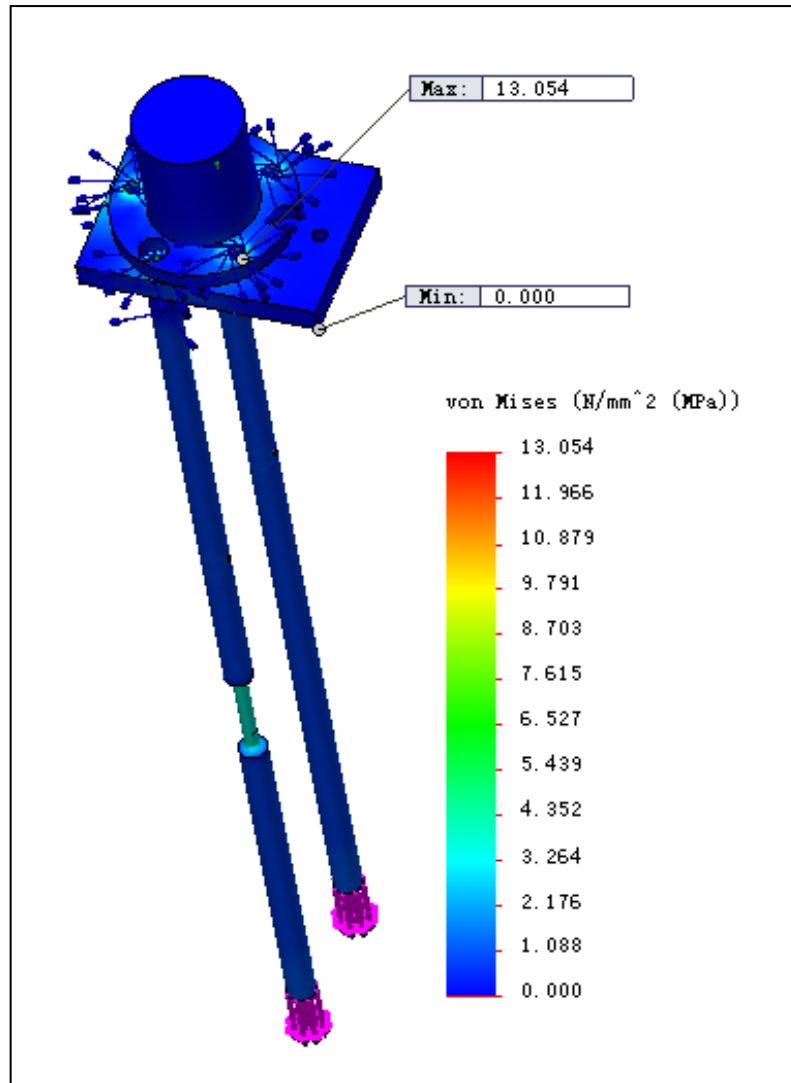


Figure 6-7. Von Mises stress distribution on the support part of the neck module. The blue line with a dot in the end represents a connector.

2. Link mechanism part. There are 4 sliders in this part as shown in Figure 6-6.

Figure 6-8 describes the kinematics of the link mechanism. As the 4 sliders is centrosymmetric, one is shown in the figure. The gear drives the gear rack to move upwards result in a extension of the slider, which will increase the neck girth from 30.0 mm to 38.0 mm. The slider force ($F_{\text{neck_slider}}$) is the force to move the neck

panels and overcome the friction and the external force applied on the neck panels which mainly are the tension of the cladding. It can be calculated as follows,

$$F_{\text{neck_slider}} = \left(\frac{T\eta_g}{4R} - G_{\text{Linkage}} \right) \times \cos(\alpha - 90^\circ) \times \cos(180^\circ - \alpha) \quad (6.1)$$

Where, $F_{\text{Neck_slider}}$ is the slider force. T is the torque of the motor which is 1.27 Nm. R is the radius of the gear which is 10 mm. η is the efficiency of mechanical transmission. It is suggested that the efficiency of cylinder gear transmission η_g is 0.90 ~ 0.93 (Wang Da Kan Wang Zhi Li, 2003), and 0.9 is adopt in this calculation. G_{Linkage} is the weight of the linkages which is 0.7 N. α is the angle between the slider and linkage with a range of $[100.8^\circ, 111.6^\circ]$. Thus the quantity of $F_{\text{Neck_slider}}$ is 5.3 N ~ 9.8 N. Mechanism of the robotic mannequin is running at low, stabilizing speed, light loaded and shock free, so the possibilities of linkage breakage, gear damage and nut failure are negligible.

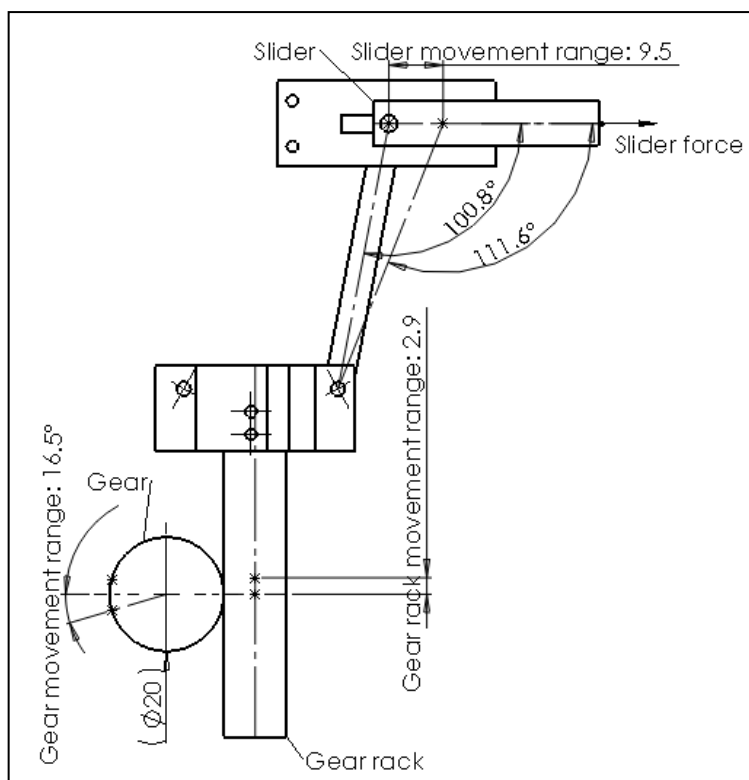


Figure 6-8. Link mechanism schematic diagram. The solid arrow shows the movement direction. The circle of the gear represents the reference circle. All the linear dimensions are in mm.

6.2.2.3. Chest module design

The chest module is designed to realize the driving dimensions variations such as under-bust girth, bust girth, and neck girth. The shapes also vary at the driven dimensions such as the length of neck-to-bust point, shoulder length, bust-to-bust point width, scye depth, etc. Figure 6-9 and Figure 6-10 show the front and back views of the chest module. The module is located between the neck module and the waist module, suspended on the neck module and providing support to the lower modules. Transmission is mainly using cylinder gearing, which is high in efficiency

and compact in structure. The module is consists of four parts as follows,

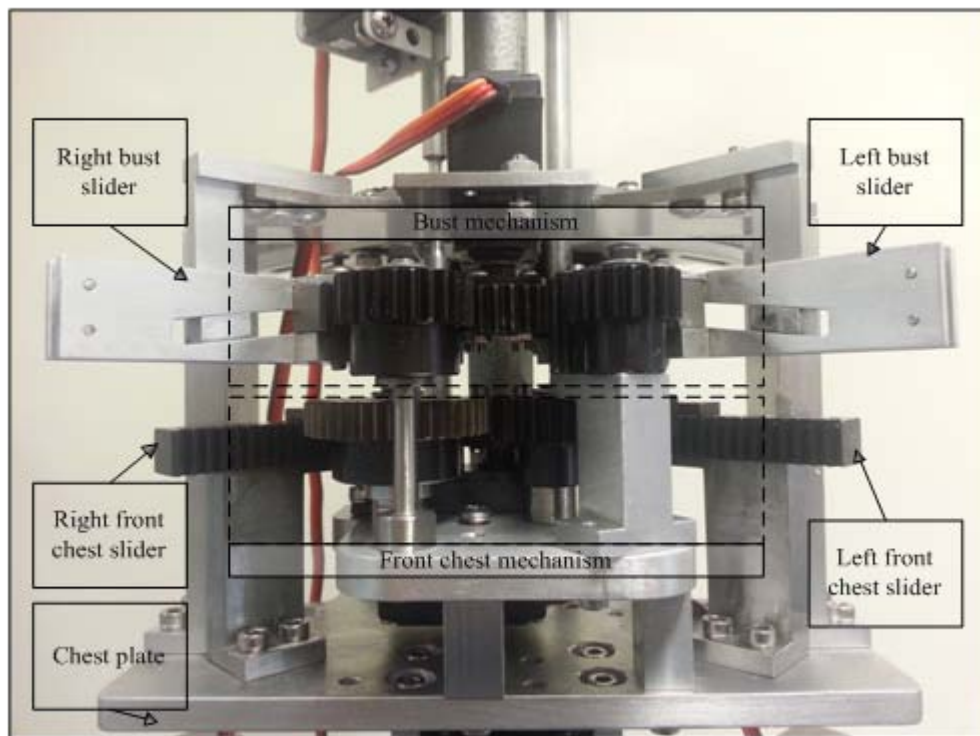


Figure 6-9. Front chest overview

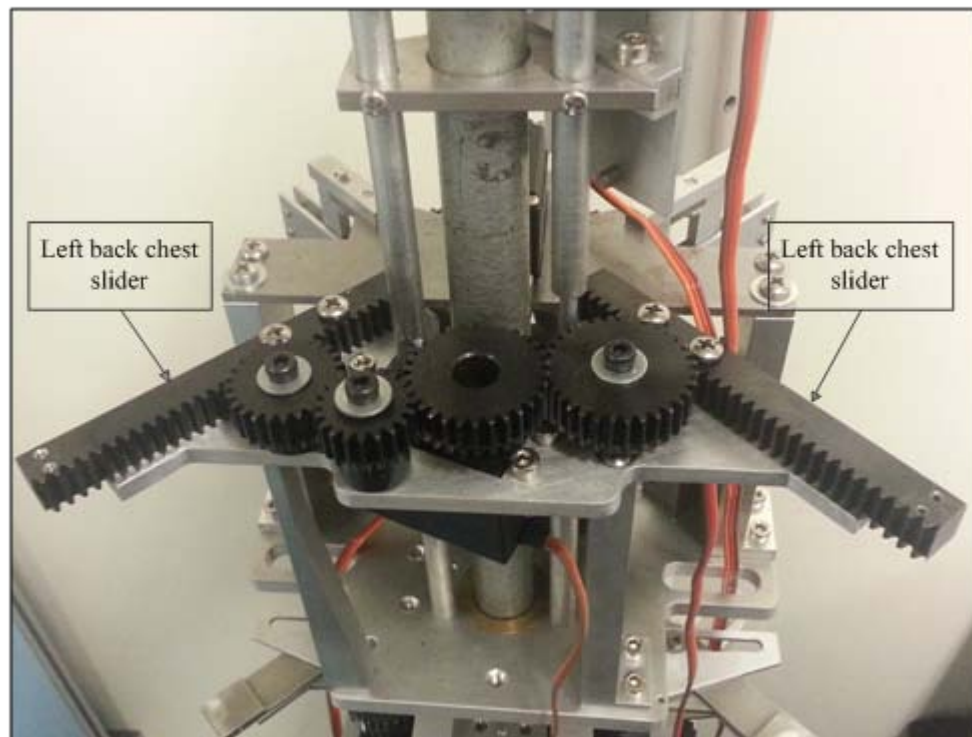


Figure 6-10. Back chest overview

1. Chest plate. The chest plate is designed to support the chest, waist, and hip module. The main external force is the weight of these modules. Figure 6-11 shows the overview of the chest plate. The chest plate is made of stainless steel as it bears the main weight, especially a bending force across its surface. The flange is made of brass to obtain a better fit with the bar going through it with its relatively low stiffness. There are a circular pattern of 3 screws on the flange, with an angle of 60° between each of them, as shown in Figure 6-12. These screws assist in fixing the chest plate to the bar, in order to eliminate the lateral oscillation due to the operation and external force. Other components are made of 6061 Aluminium alloy to reduce the weight. These components are connected with bolt. FEA is applied to ensure the chest module is able to support the weight. The result shows that the structure has a minimum FOS of 15.1, indicating the structure is safe. Figure 6-13 demonstrates the Von Mises stress distribution. It is observed that significant stress is located at the thinner part of the suspension linkage to the neck module, the middle of the chest plate and the lower part which is connected to the waist module.

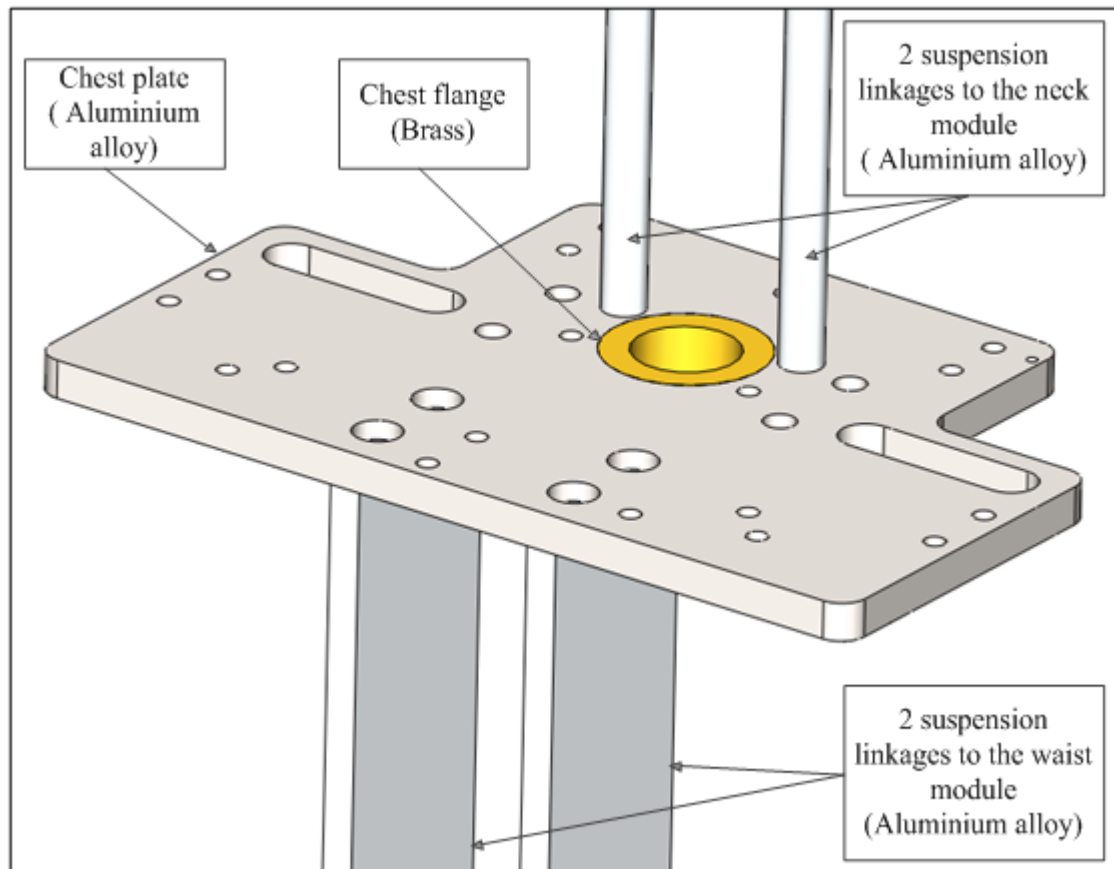


Figure 6-11. Chest plate part overview

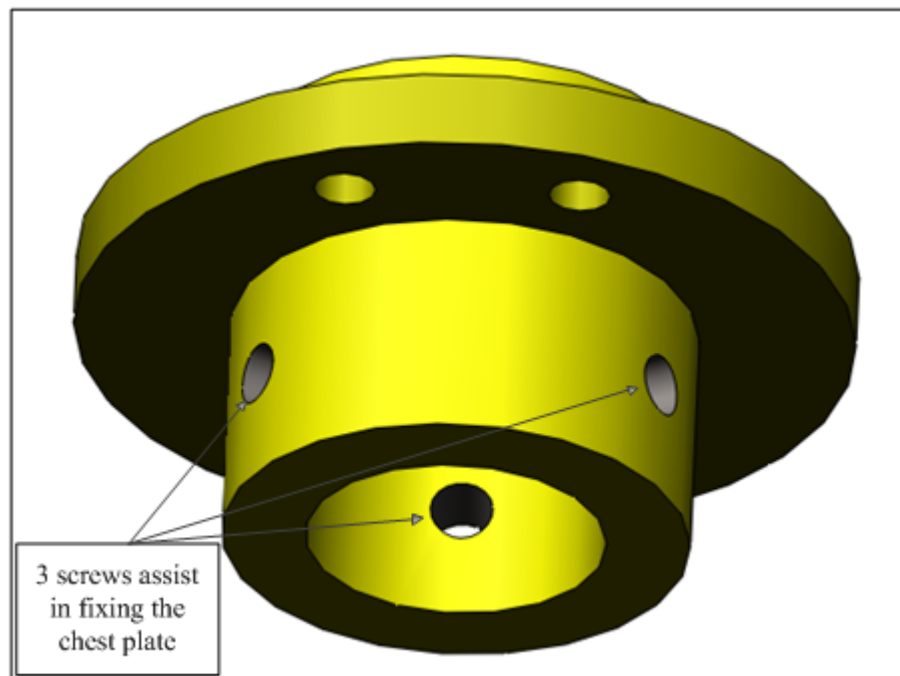


Figure 6-12. A circular pattern of screws on the flange to assist in fixing.

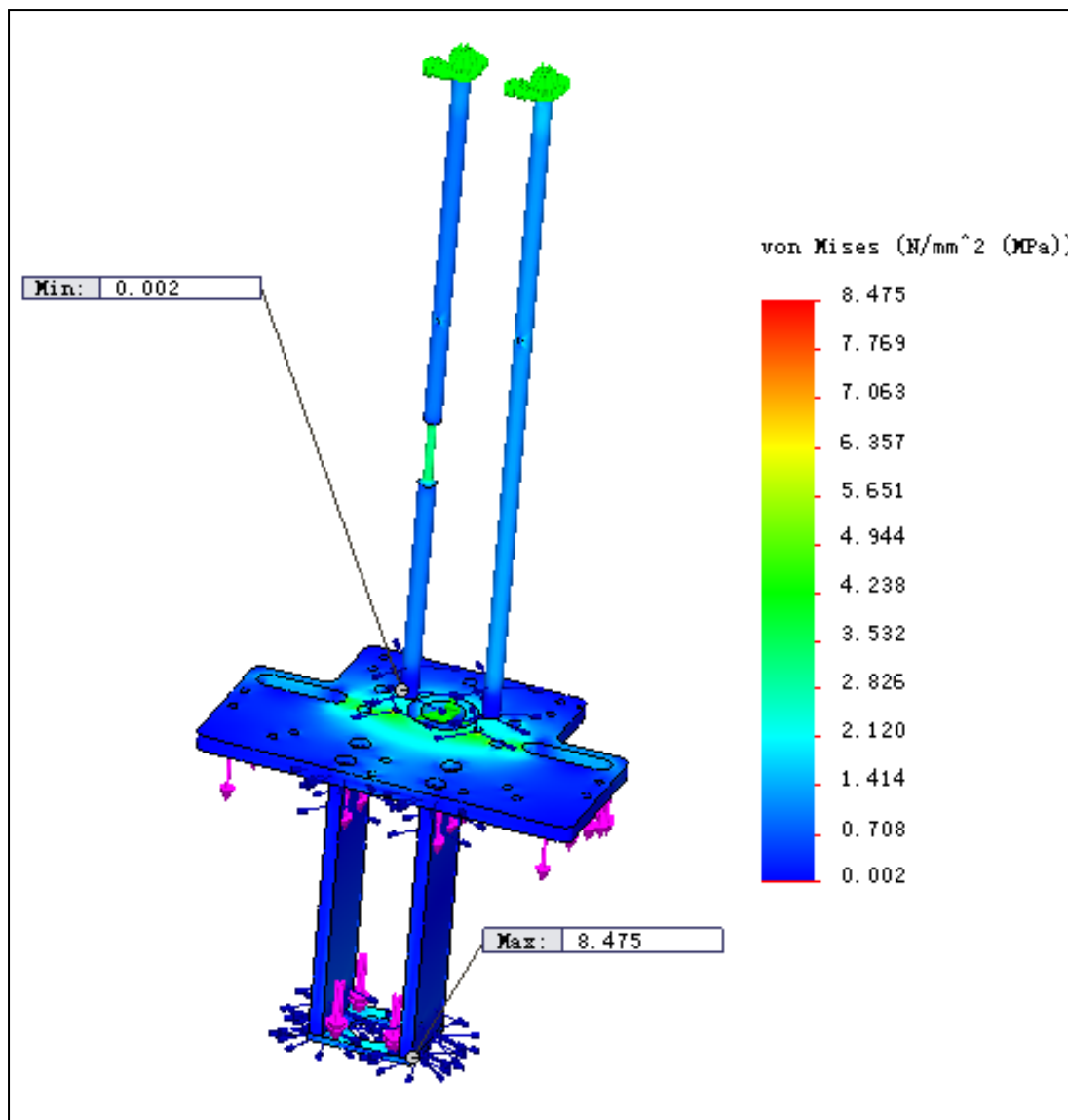


Figure 6-13. Von Mises stress distribution on the support part of the chest plate part

2. Front chest mechanism part.

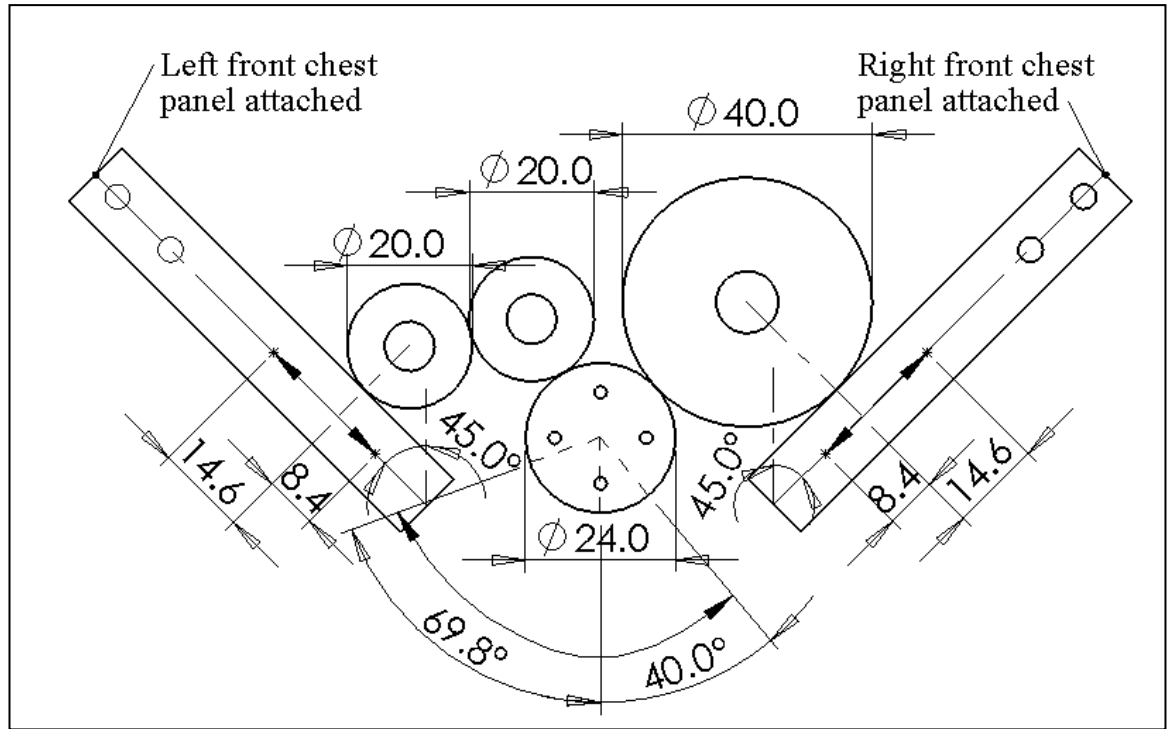


Figure 6-14. Front chest mechanism schematic diagram. The solid arrow shows the movement direction. All the linear dimensions are in mm.

The front chest mechanism realizes the shape variation at the front chest section.

Figure 6-14 describes kinematics of the mechanism. The gear of 24.0 mm is the driving gear, which drives the left and right front chest panel by rotation. The left and right front chest panel are able to go inward for 8.4 mm and outward for 14.6 mm simultaneously, resulting in a variation of the front under-bust girth from 38.5 mm to 44.5 mm. The slider force ($F_{\text{front_chest_slider}}$) is the force to move the front chest panel and overcome the friction and the external force applied on the chest panels which mainly are the tension of the cladding. It can be calculated as follows,

$$F_{\text{front_chest_slider}} = \frac{T\eta_g^3}{2R} \quad (6.2)$$

Where, $F_{\text{front_chest_slider}}$ is the driving force on a single front chest slider. The driving force on the left and right front chest will be different as the left one has one more gear. The value of $F_{\text{front_chest_slider}}$ is determined the smaller force, which is the driving force of the left front chest slider, as a low-ball estimate.

T is the torque of the motor which is 1.27 Nm. R is the radius of the driving gear which is 12 mm. η_g is the efficiency of cylinder gear transmission, which is 0.9.

Thus the quantity of $F_{\text{front_chest_slider}}$ is 38.5 N.

3. Back chest mechanism part.

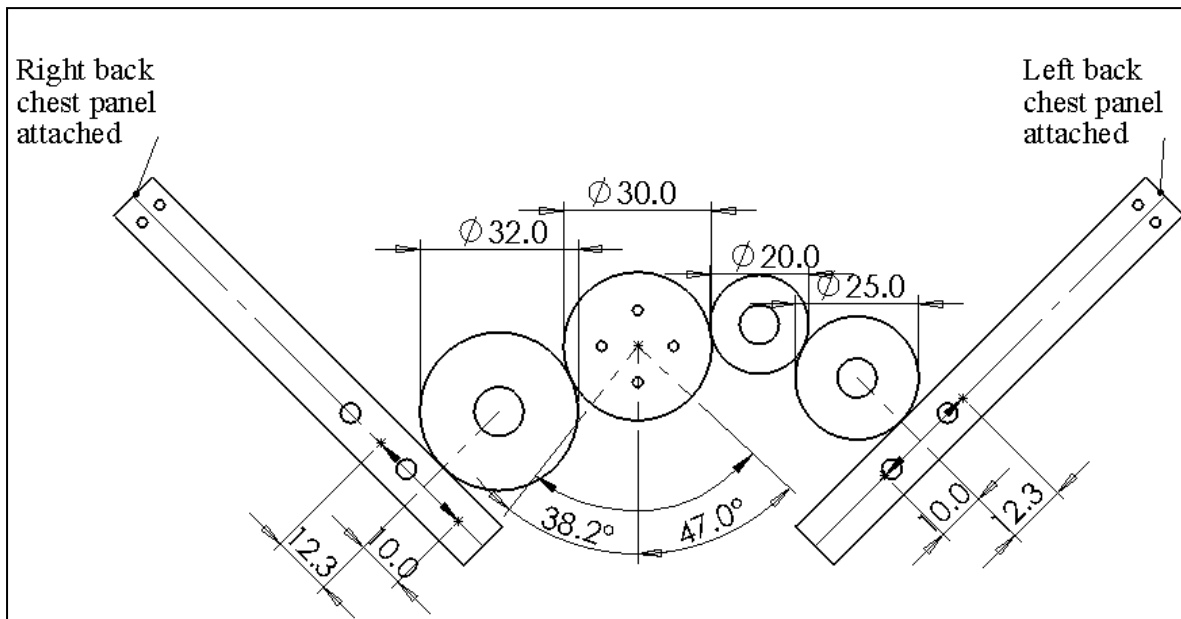


Figure 6-15. Back chest mechanism schematic diagram. The solid arrow shows the movement direction. All the linear dimensions are in mm.

The back chest mechanism realizes the shape variation at the back chest section.

Figure 6-15 describes kinematics of the mechanism. The gear of 30.0 mm is the driving gear, which drives the left and right back chest panel by rotation. The left and right front chest panel are able to go inward for 10.0 mm and outward for 12.3 mm simultaneously, resulting in a variation of the back under-bust girth from 29.5 mm to 39.5 mm. The slider force ($F_{\text{back_chest_slider}}$) is the force to move the back chest panel and overcome the friction and the external force applied on the back chest panels which mainly are the tension of the cladding. It can be calculated as follows,

$$F_{\text{back_chest_slider}} = \frac{T\eta_g^3}{2R} \quad (6.3)$$

Where, $F_{\text{back_chest_slider}}$ is the driving force on a single back chest slider. The driving force on the left and right back chest will be deferent as the left one has one more gear resulting a reducing in force transmission. The value of $F_{\text{back_chest_slider}}$ is determined by the smaller force, which is the driving force of the left back chest slider, as a low-ball estimate. T is the torque of the motor which is 1.27 Nm. R is the radius of the driving gear which is 15 mm. η_g is the efficiency of cylinder gear transmission, which is 0.9. Thus the quantity of $F_{\text{back_chest_slider}}$ is 30.8 N.

4. Bust mechanism part

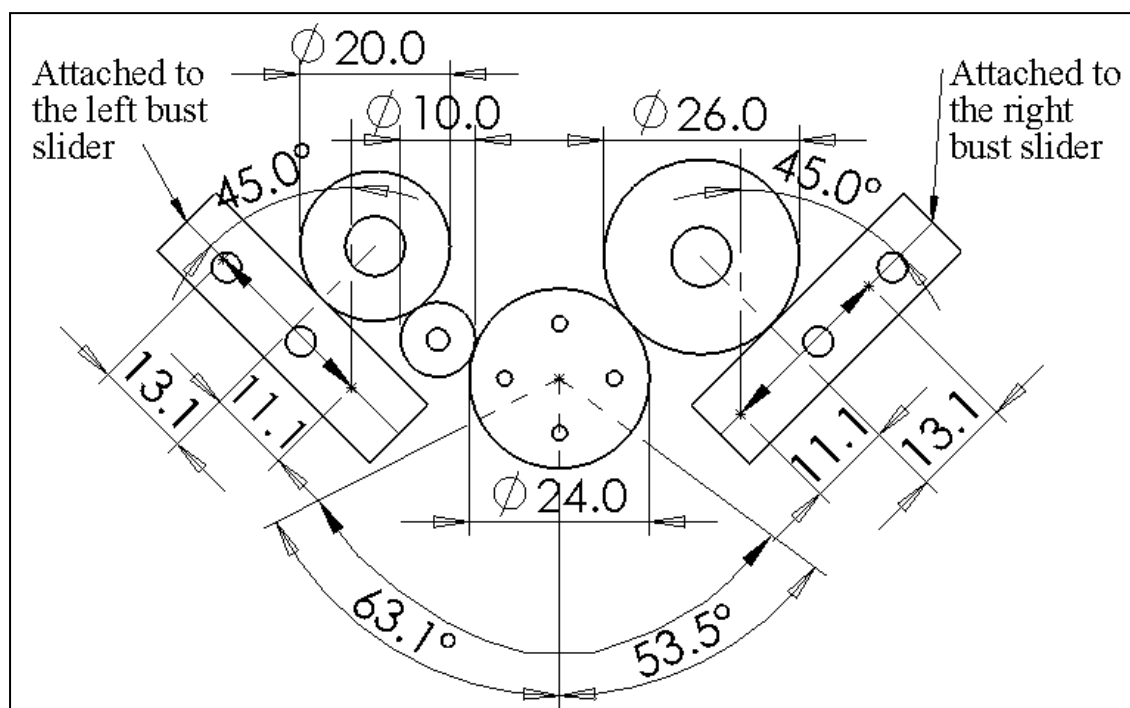


Figure 6-16. Bust mechanism schematic diagram. The solid arrow shows the movement direction. All the linear dimensions are in mm.

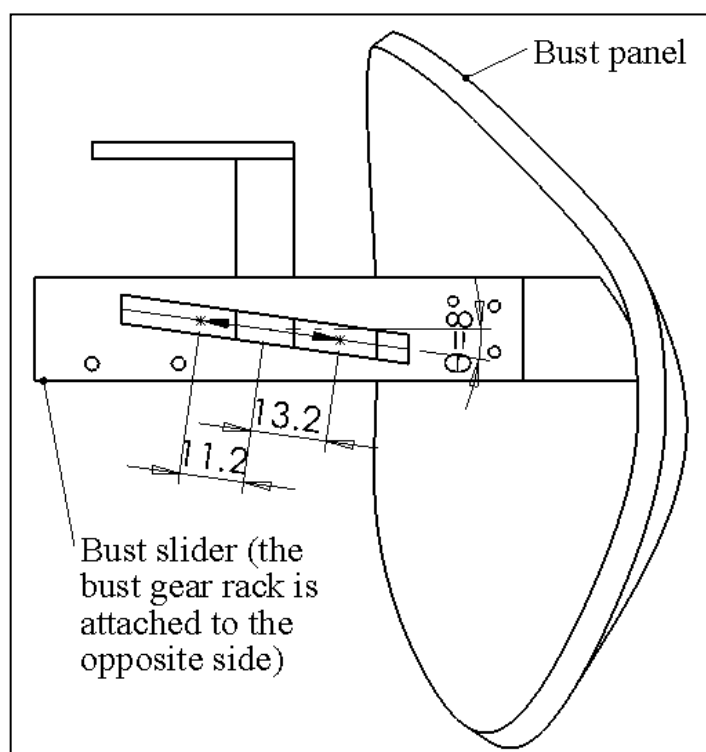


Figure 6-17. Side view of the right bust slider and panel, the movement of left bust panel is identical. All the linear dimensions are in mm.

The bust mechanism realizes the shape variation at the bust section. Figure 6-16 describes the kinematics of the mechanism. The gear of 24.0 mm is the driving gear, which drives the left and right bust panel by rotation. The left and right bust panel are able to go inward for 11.2 mm and outward for 13.2 mm simultaneously as shown in Figure 6-17. The slider force ($F_{\text{bust_slider}}$) is the force to move the front chest panel and overcome the friction and the external force applied on the bust panels which mainly are the tension of the cladding. It can be calculated as following:

$$F_{\text{bust_slider}} = \frac{T\eta_g^3 \cos \theta}{2R} \quad (6.4)$$

Where, $F_{\text{bust_slider}}$ is the driving force on a single bust slider force. The driving force on the left and right bust will be deferent as the left one has one more gear. The value of $F_{\text{bust_slider}}$ is determined by the smaller force, which is the driving force of the left bust slider, as a conservative estimate. T is the torque of the motor which is 1.27 Nm. R is the radius of the driving gear which is 12 mm. η_g is the efficiency of cylinder gear transmission, which is 0.9. θ is the angle between the movement and the horizontal plane, which is 8° . Thus the quantity of $F_{\text{bust_slider}}$ is 38.2 N.

6.2.2.4. Waist module design

The waist module is designed to realize the driving dimensions variations such as front waist girth, back waist girth, upper abdomen shape and chest to waist length.

Figure 6-18 shows the front overview of the waist module. The module is located between the chest module and the hip module, suspended on the chest module and providing support to the lower modules. Girth transmission is mainly using sliders and linkages which are designed to avoid interference with the linear motor during the movements. The chest to waist length variation is carried out by a linear motor.

The module consists of four parts as follows,

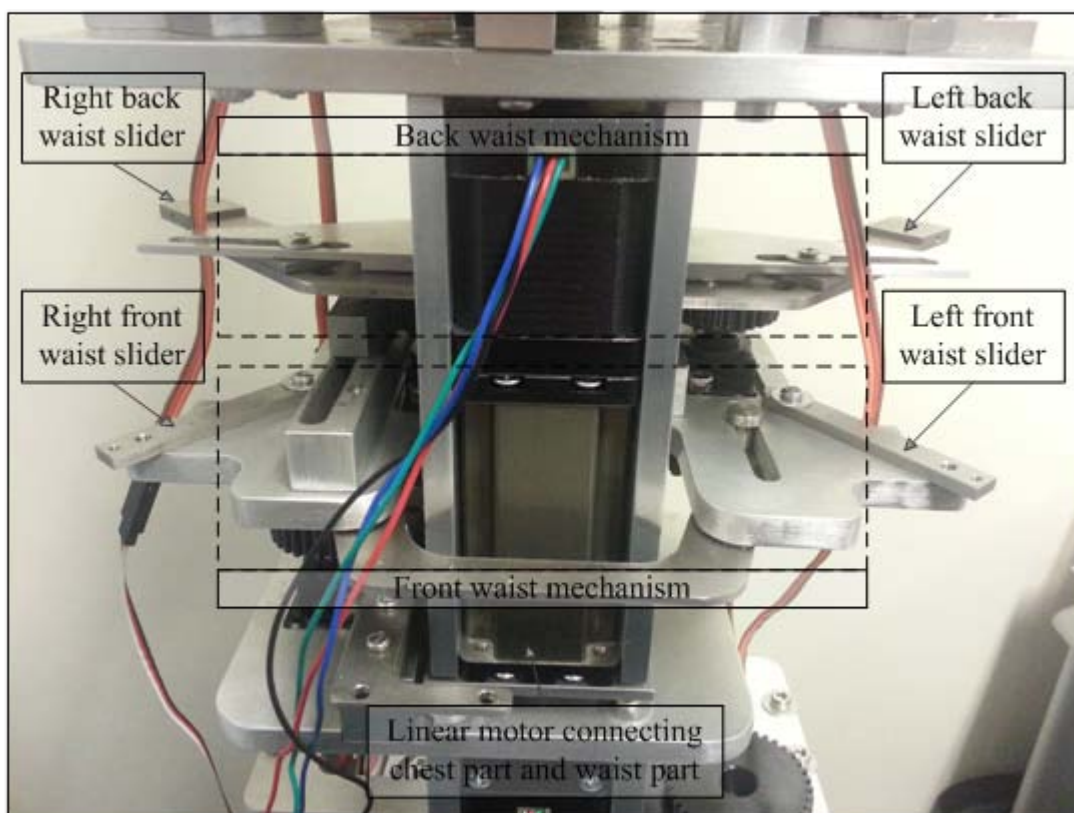


Figure 6-18. Front waist overview

1. Waist plate. The waist plate is designed to support the waist, and hip module by the self-locking of the linear motor. The entire waist module is able to lift and lower resulting in a variation of the bust to waist length from 155.0 mm to 175.0 mm at a constant low speed. The main external force is the weight of these modules which is 5.7 kg. Figure 6-19 shows the overview of the waist plate. The waist plate and suspension linkages are made of 6061 Aluminium alloy to reduce the weight. The flange is made of brass for smoothly sliding along the bar. The linear motor plate is used for the installation of the linear motor linking the waist and hip module. As the main force applied on the chest module is the weight, FEA is applied to ensure the safety. The result shows that the structure has a minimum FOS of 7.1, indicating the structure is safe. Figure 6-20 demonstrates the Von Mises stress distribution. It is observed that significant stress is located at the vicinity of the narrow part of the waist plate due to the bending force. The end of the linear motor is a 6 mm thread head made of stainless steel. It connects the waist plate with nut at the bottom. A washer of 16 mm is placed between the nut and waist plate to stress concentration. The stress on the thread head calculated with Solidworks FEA is listed in Table 6-3. Compared to the axial force, the resultant shear force and bending moment is negligible. So the main load on the thread is a axial force of 96.4 N which can be supported by a 6 mm thread head and self-locking of a common linear stepper

actuator.

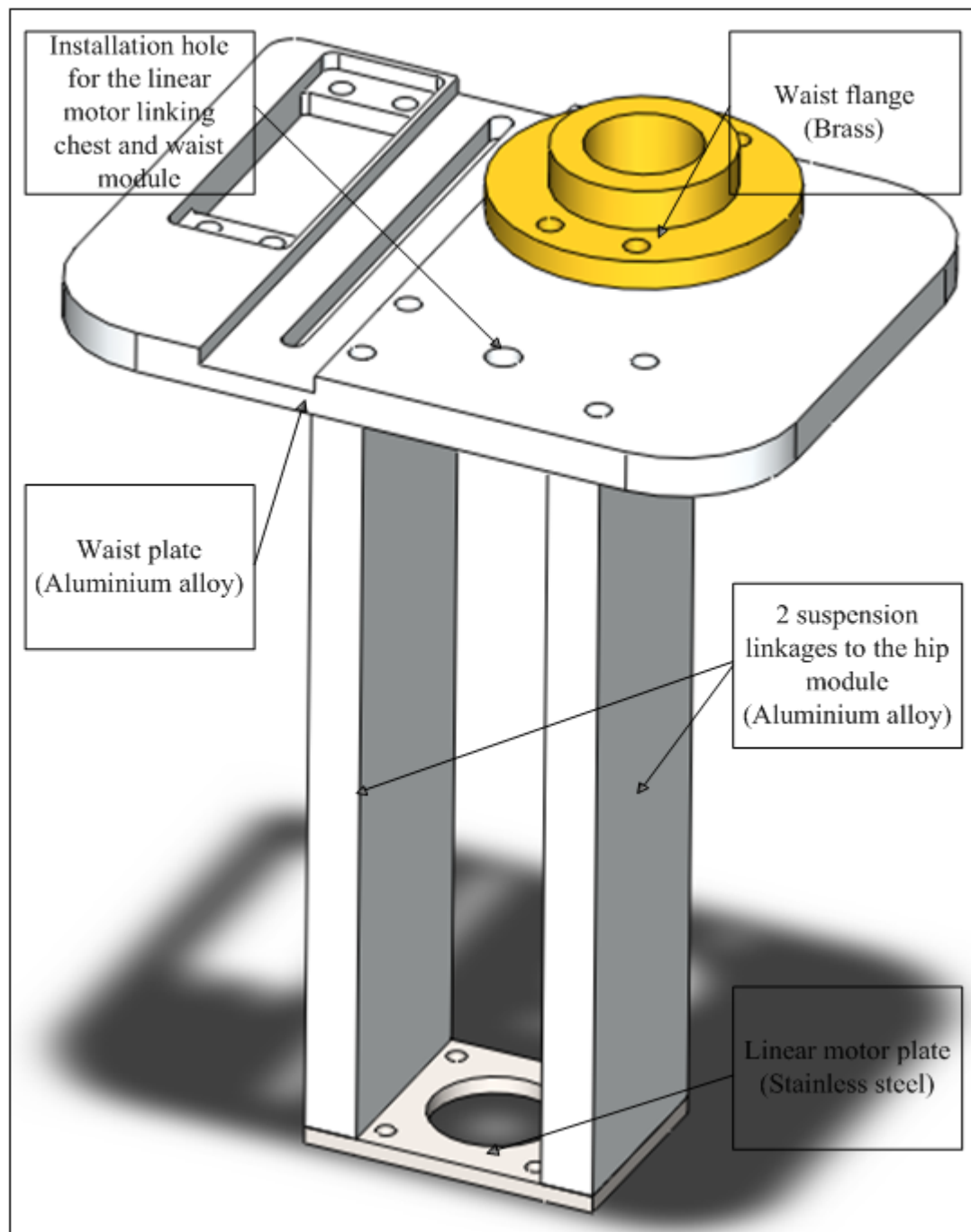


Figure 6-19. Chest plate part overview

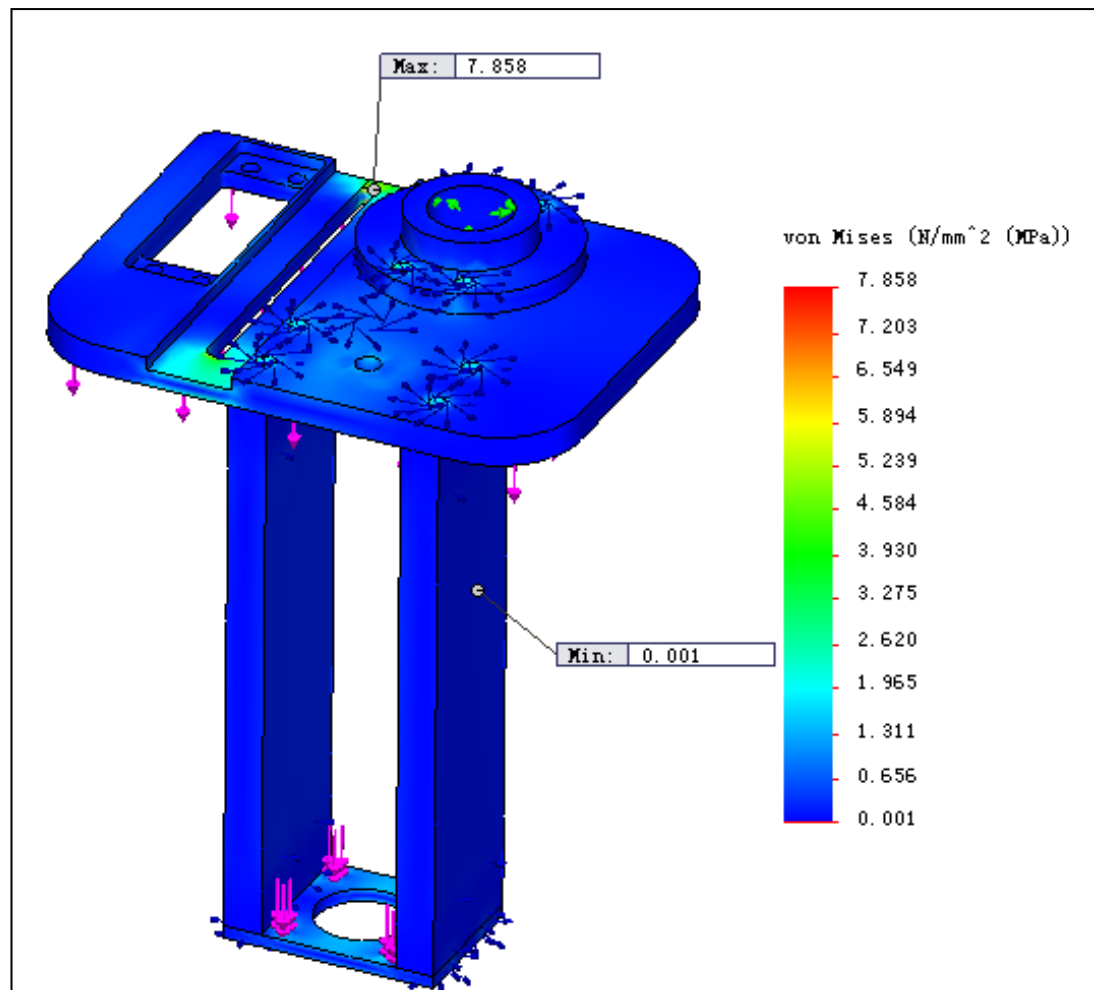


Figure 6-20. Von Mises stress distribution on waist plate part

Type	Resultant
Axial Force (N)	96.4
Shear Force (N)	0.3
Bending moment (Nm)	0.009

Table 6-3. Forces on the thread head of the linear motor of the waist module

2. Front waist part.

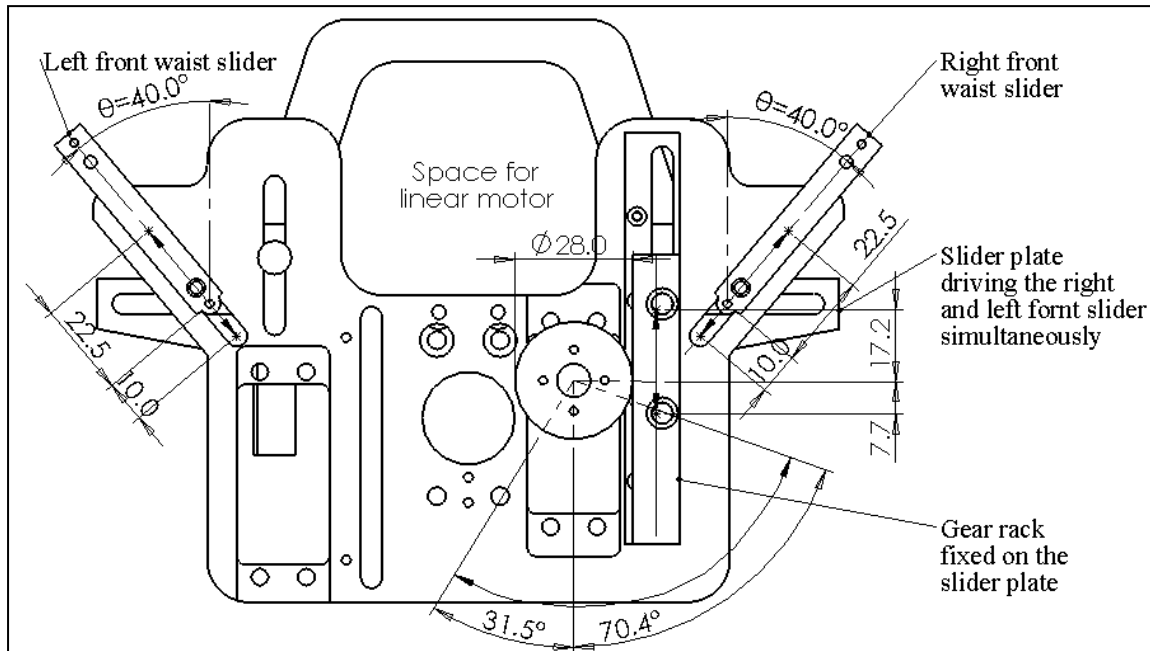


Figure 6-21. Front waist mechanism schematic diagram. The solid arrow shows the movement direction. All the linear dimensions are in mm.

The front waist mechanism realizes the shape variation at the front waist section.

Figure 6-21 describes the kinematics of the mechanism. The driving gear drives the left and right front waist slider attached to the waist panels. The left and right front waist panel are able to go inward for 10.0 mm and outward for 22.5 mm simultaneously, resulting in a variation of the front waist girth from 36.5 mm to 46.5 mm. The slider force ($F_{\text{front_waist_slider}}$) is the force to move the front waist panel and overcome the friction and the external force which mainly are the tension of the cladding. It can be calculated as follows,

$$F_{\text{front_waist_slider}} = \frac{T\eta_g \cos \theta}{2R} \quad (6.5)$$

Where, $F_{\text{front_waist_slider}}$ is the driving force on a single front waist slider. T is the torque of the motor which is 1.27 Nm. R is the radius of the driving gear which is 14 mm. η_g is the efficiency of cylinder gear transmission, which is 0.9. θ is the angle between the movement direction and front of body. Thus the quantity of $F_{\text{front_waist_slider}}$ is 31.3 N.

3. Back waist part.

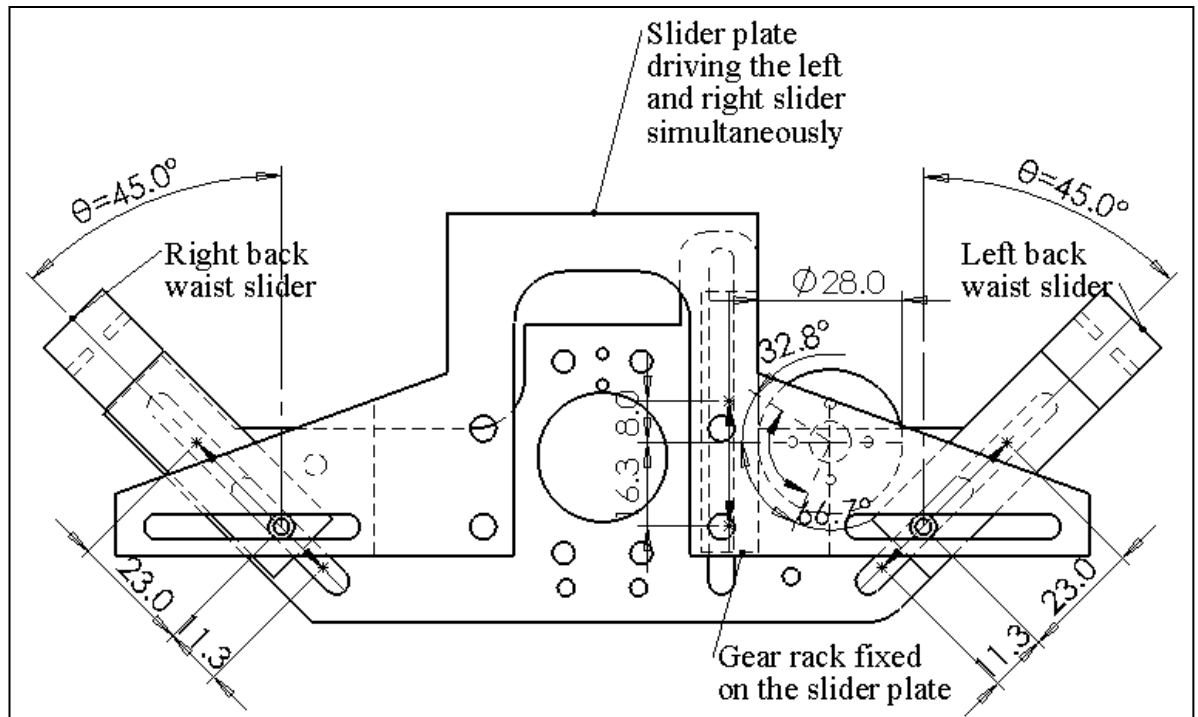


Figure 6-22. Back waist mechanism schematic diagram. The solid arrow shows the movement direction. All the linear dimensions are in mm.

The back waist mechanism realizes the shape variation at the back waist section.

Figure 6-22 describes kinematics of the mechanism. The gear is the driving gear,

which drives the left and right back waist slider attached to the back waist panels. The left and right back waist panels are able to go inward for 11.3 mm and outward for 23.0 mm simultaneously, resulting in a variation of the front chest girth from 25.5 mm to 35.5 mm. The slider force ($F_{\text{back_waist_slider}}$) is the force to move the back waist panel and overcome the friction and the external force which mainly are the tension of the cladding. It can be calculated as follows,

$$F_{\text{back_waist_slider}} = \frac{T\eta_g \cos \theta}{2R} \quad (6.6)$$

Where, $F_{\text{back_waist_slider}}$ is the driving force on a single back waist slider. T is the torque of the motor which is 1.27 Nm. R is the radius of the driving gear which is 14 mm. η_g is the efficiency of cylinder gear transmission, which is 0.9. θ is the angle between the movement direction and front of body. Thus the quantity of $F_{\text{back_waist_slider}}$ is 28.9 N which is sufficient to overcome the friction and external force.

4. Upper abdomen part. The abdomen mechanism realizes the shape variation at the upper abdomen section and provides the front waist shape with more freedom. Figure 6-23 describes the kinematics of the mechanism. The driving gear drives the upper abdomen slider attached to the upper abdomen. The upper abdomen panel is able to go inward for 9.0 mm and outward for 26.5 mm. The slider force

($F_{\text{upper_abs_slider}}$) is the force to move the upper abdomen panel and overcome the friction and the external force which mainly is the tension of the cladding. It can be calculated as follows,

$$F_{\text{upper_abs_slider}} = \frac{T\eta_g}{R} \quad (6.7)$$

Where, $F_{\text{upper_abs_slider}}$ is the driving force on a the upper abdomen slider. T is the torque of the motor which is 1.27 Nm. R is the radius of the driving gear which is 16 mm. η_g is the efficiency of cylinder gear transmission, which is 0.9. Thus the quantity of $F_{\text{upper_abs_slider}}$ is 71.4 N.

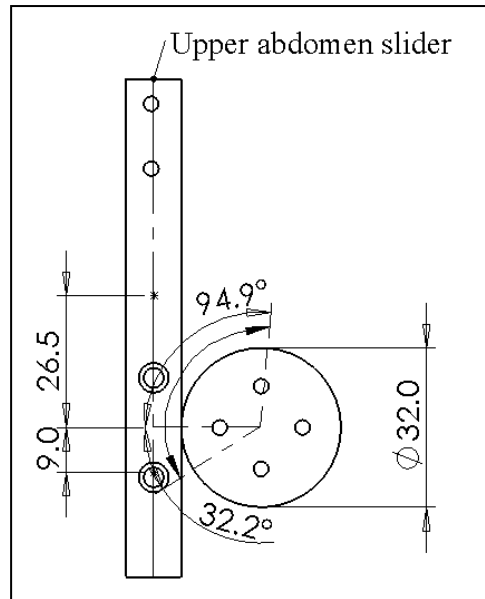


Figure 6-23. Upper abdomen mechanism schematic diagram. The solid arrow shows the movement direction. All the linear dimensions are in mm.

6.2.2.5. Hip module design

Figure 6-24 and Figure 6-25 show the overview from the front and rear for the

hip module.

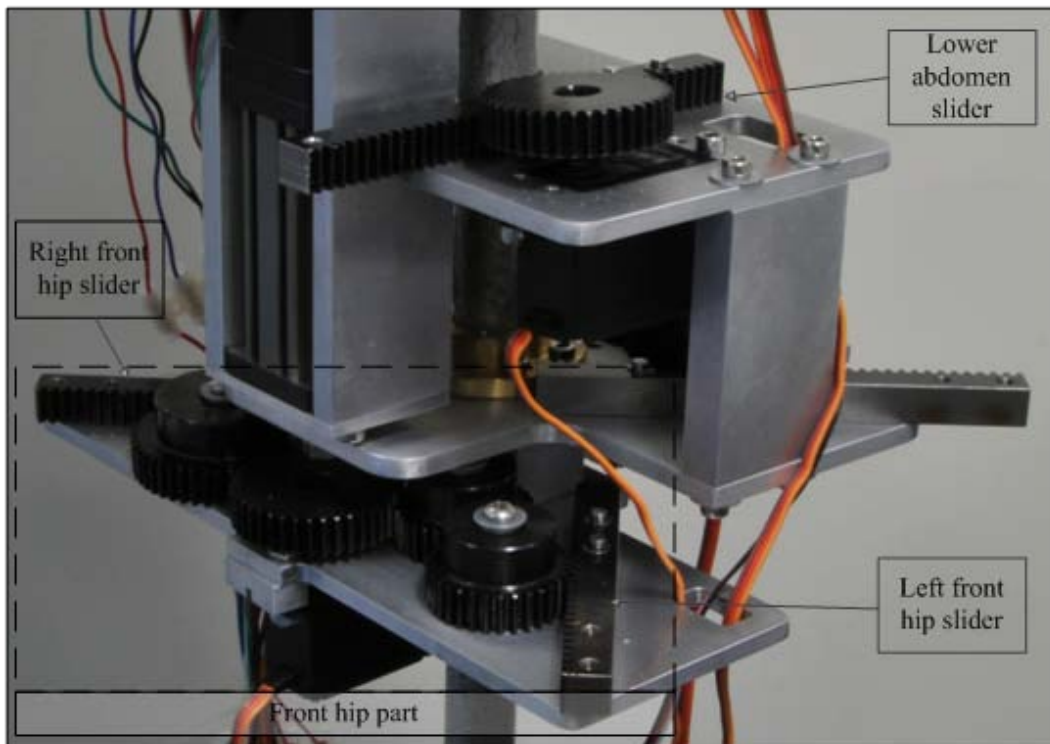


Figure 6-24. Front 45 degree angle overview of the hip module

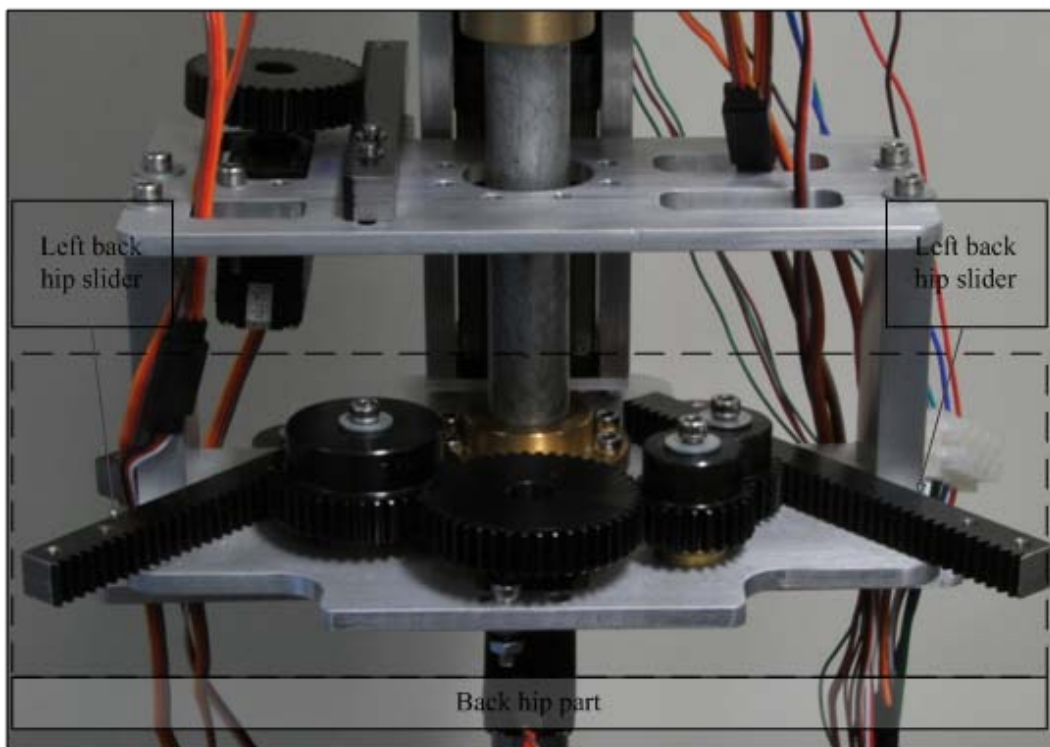


Figure 6-25. Rear overview of the hip module

The hip module is designed to realize the driving dimension variations such as front hip girth, back hip girth, lower abdomen dimensions and waist to hip length. The module is located at the bottom of the robotic mannequin, suspended on the waist module. Girth transmission is mainly using cylinder gearing, which is high in efficiency and compact in structure. The waist to hip length variation is carried out by a linear motor. The module is consists of four parts as follows,

1. Hip plate part. The hip plate part is designed to support the hip module by the self-locking of the linear motor. The entire hip module is able to lift and lower resulting in a variation of the waist to hip length from 184.0 mm to 216.0 mm at a constant low speed. The main external force is the weight of these modules which is 3.2 kg. Figure 6-26 shows the overview of the hip plate part. The hip plate is made of 6061 Aluminium alloy to reduce the weight. The flange is made of brass for smooth sliding along the bar. As the main force applied on the hip module is the weight, FEA is applied to ensure the safety. The result shows that the structure has a minimum FOS of 9.2, indicating the structure is safe. Figure 6-27 demonstrates the Von Mises stress distribution. It is observed that significant stress is located in the vicinity of the bolt thread hold of the hip plate. The end of the linear motor is a 6 mm thread head made of stainless steel. It connects the hip plate with nut at the bottom. A washer of

16 mm is placed between the nut and hip plate to stress concentration. The stress on the thread head calculated with Solidworks FEA is listed in Table 6-4. Compared to the axial force, the resultant shear force and bending moment is negligible. So the main load on the thread is a axial force of 99.1 N which can be supported by a 6 mm thread head and self-locking of a common linear stepper actuator.

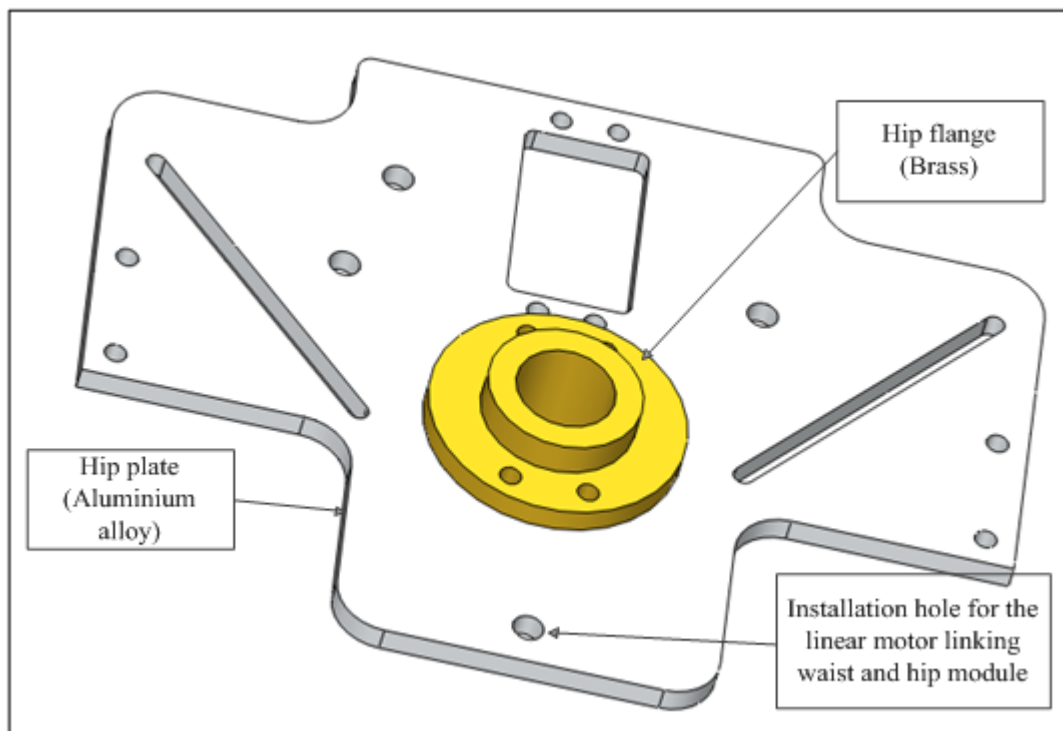


Figure 6-26. Hip plate part overview

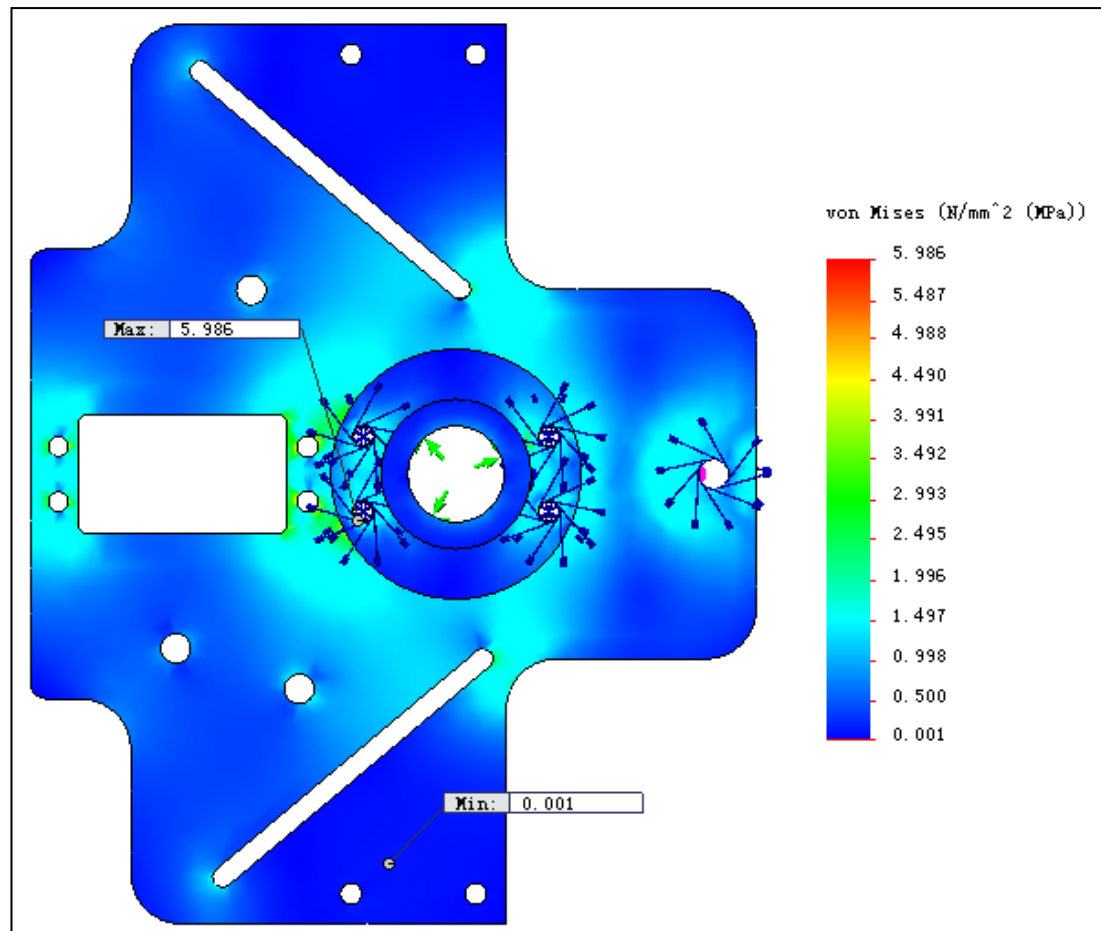


Figure 6-27. Von Mises stress distribution on hip plate part

Type	Resultant
Axial Force (N)	99.1
Shear Force (N)	7.0
Bending moment (Nm)	0.01

Table 6-4. Forces on the thread head of the linear motor of the hip module

2. Front hip part

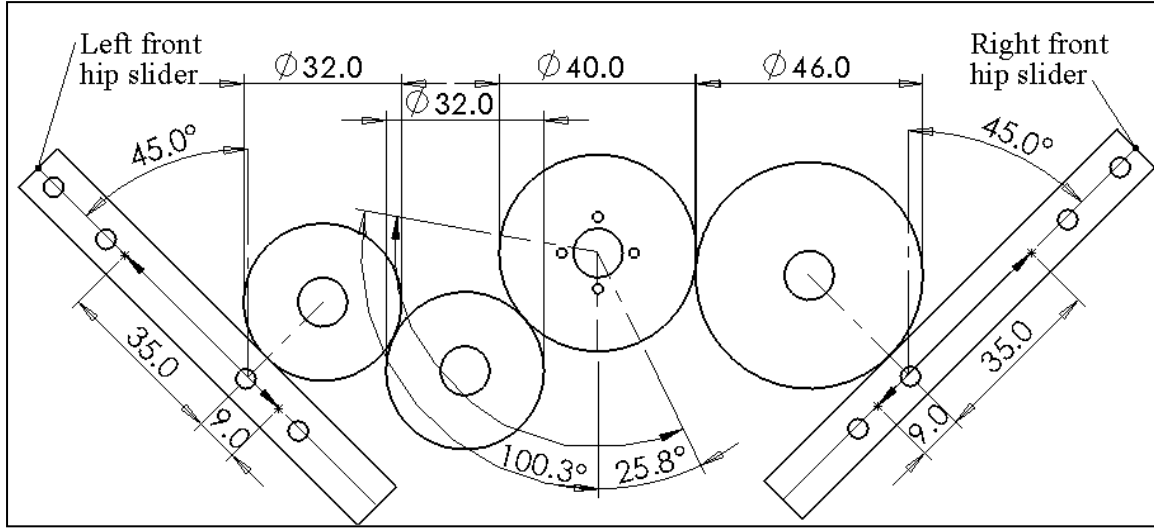


Figure 6-28. Front hip mechanism schematic diagram. The solid arrow shows the movement direction. All linear dimensions are in mm.

The front hip mechanism realizes the shape variation at the front hip section.

Figure 6-28 describes kinematics of the mechanism. The gear of 40.0 mm is the driving gear, which drives the left and right front hip slider attached to the waist panels. The left and right front hip panel are able to go inward for 9.0 mm and outward for 35.0 mm simultaneously, resulting in a variation of the front hip girth from 43.0 mm to 55.0 mm. The slider force ($F_{\text{front_hip_slider}}$) is the force to move the front hip panel and overcome the friction and the external force which mainly are the tension of the cladding. It can be calculated as follows:

$$F_{\text{front_hip_slider}} = \frac{T\eta_g^3}{2R} \quad (6.8)$$

Where, $F_{\text{front_hip_slider}}$ is the driving force on a single front hip slider force. T is the torque of the motor which is 1.27 Nm. The value of $F_{\text{front_hip_slider}}$ is determined the smaller force, which is the driving force of the left front hip slider, as a low-ball estimate. R is the radius of the driving gear which is 20 mm. η_g is the efficiency of cylinder gear transmission, which is 0.9. Thus the quantity of $F_{\text{front_hip_slider}}$ is 23.2N.

3.Back hip part.

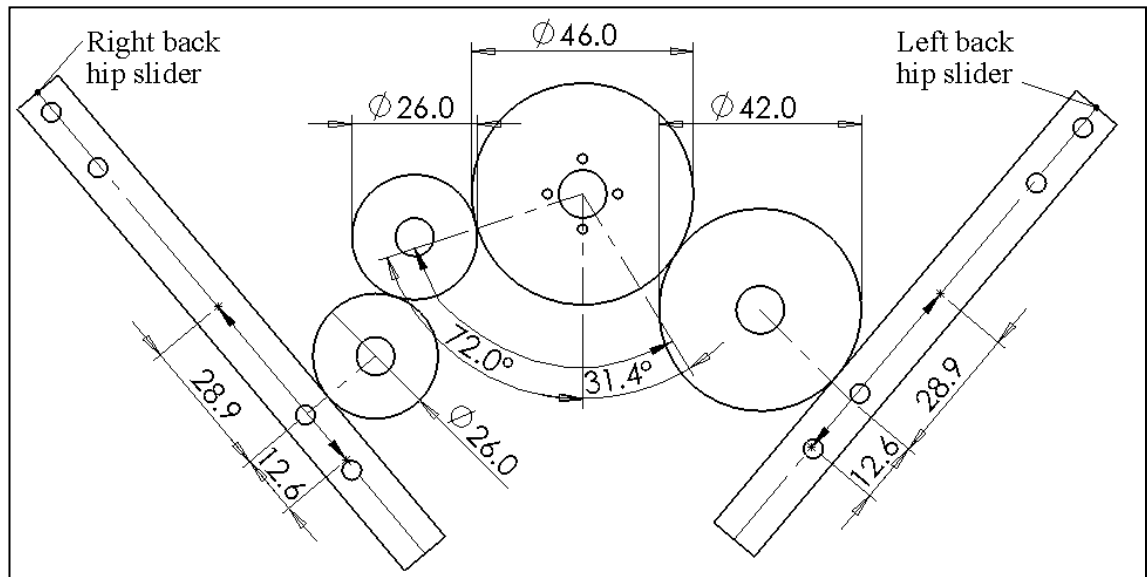


Figure 6-29. Back hip mechanism schematic diagram. The solid arrow shows the movement direction. All linear dimensions are in mm.

The back hip mechanism realizes the shape variation at the back hip section.

Figure 6-29 describes kinematics of the mechanism. The driving gear drives the left and right back hip slider attached to the hip panels. The left and right back hip panel

are able to go inward for 12.6 mm and outward for 28.9 mm simultaneously, resulting in a variation of the back hip girth from 44.0 mm to 57.0 mm. The slider force ($F_{\text{back_hip_slider}}$) is the force to move the back hip panel and overcome the friction and the external force which mainly are the tension of the cladding. It can be calculated as following:

$$F_{\text{back_hip_slider}} = \frac{T\eta_g^3}{2R} \quad (6.9)$$

Where, $F_{\text{back_hip_slider}}$ is the driving force on a single back hip slider. T is the torque of the motor which is 1.27 Nm. R is the radius of the driving gear which is 23 mm. η_g is the efficiency of cylinder gear transmission, which is 0.9. Thus the quantity of $F_{\text{back_hip_slider}}$ is 20.1 N which is sufficient to overcome the friction and external force.

4. Lower abdomen part. The lower abdomen mechanism realizes the shape variation at the lower abdomen section and provides the hip girth shape with more freedom. Figure 6-30 describes kinematics of the mechanism. The gear is the driving gear, which drives the lower abdomen slider attached to the lower abdomen. The lower abdomen panel is able to go inward for 7.4 mm and outward for 37.8 mm. The slider force ($F_{\text{lower_abs_slider}}$) is the force to move the lower abdomen panel and overcome the friction and the external force which mainly are the tension of the

cladding. It can be calculated as follows,

$$F_{\text{lower_abs_slider}} = \frac{T\eta_g}{R} \quad (6.10)$$

Where, $F_{\text{lower_abs_slider}}$ is the driving force on the lower abdomen slider. T is the torque of the motor which is 1.27 Nm. R is the radius of the driving gear which is 20 mm. η_g is the efficiency of cylinder gear transmission, which is 0.9. Thus the quantity of $F_{\text{lower_abs_slider}}$ is 57.2 N.

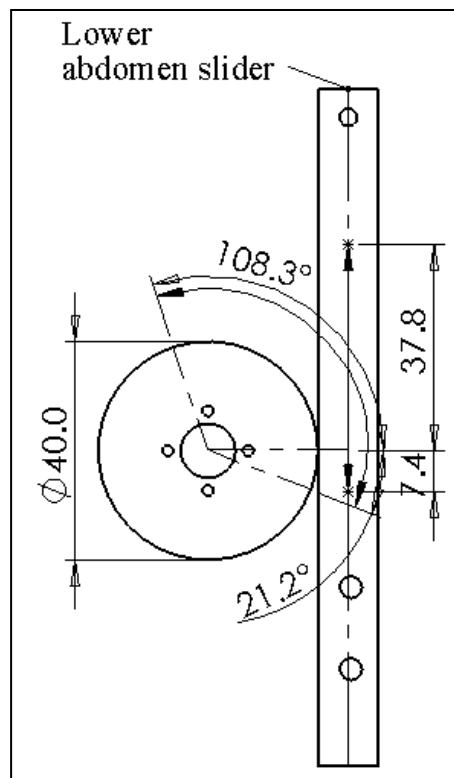


Figure 6-30. Lower abdomen mechanism schematic diagram. The solid arrow shows the movement direction. All linear dimensions are in mm.

6.3. Electrical & Electronic part

The driving unit design describes the actuators which provides the robotic

mannequin with required driving force and controllers which provide power and control the actuators. The robotic mannequin has 20 adjustable panels and 22 degree of freedoms. The mechanical design simplifies the required driving force to two types: rotation and linear motion.

6.3.1. Rotation actuator system

1. Radio control (RC) servo



Figure 6-31. RobotBase RB-150MG RC servo

A servo (Figure 6-31) is a system containing a motor and a controller to achieve self contained motion control for its speed or position. The wire from the servo is for control pulse, power and ground. An RC servo is a position control subsystem that is controlled remotely and widely used in hobby modeling and robot building as they

are relatively light, small, powerful and low cost. The device has a significant amount of torque for its size and weight. This is achieved by having a small motor and a large reduction gearing system providing an effective way of obtaining proportional rotary position control on the output shaft. As the servo has its own internal dynamic feedback, it may thus be treated as an independent sub-system.

RC model servo is a relatively sophisticated device incorporating both position and speed feedback to provide a precision position control system. It is driven by an input pulse of 1-2 millisecond (ms) duration at a repetition rate of 50-100 Hz. Figure 6-32 shows the schematic block diagram. The input pulse is compared with a pulse generated internally. This pulse is controlled by the position feedback potentiometer and the back electromotive force (EMF) generated by the motor, which provides speed feedback. The difference between the pulses forms an error signal, which is amplified by a pulse stretcher, which dictates controller gain. The output of this stage drives the servomotor through an H Bridge power amplifier. The velocity feedback is only used to provide stability in the system as the servo drives to its desired command position with minimal overshoot.

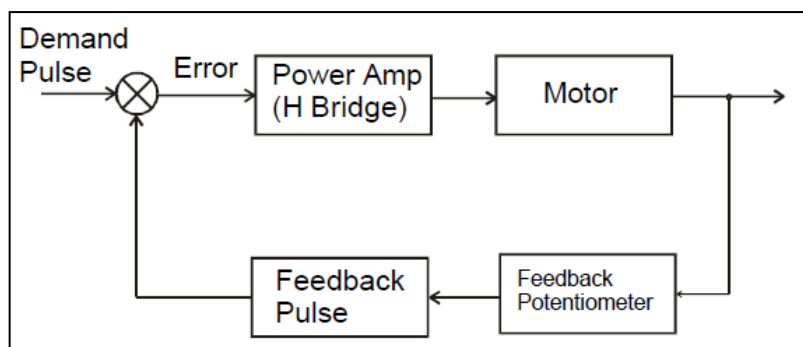


Figure 6-32. Schematic block diagram for RC servo system

RC servo system is easy to operate. It works with a 5V supply and TTL level input pulses so it can be supplied directly by a micro-controller or computer I/O port. As shown in Figure 6-33, a pulse width of 1.5 ms provides a neutral or straight ahead shaft output. Longer pulses move the output anti-clockwise and shorter ones move it clockwise. The RC servo has a limitation of rotate angle which is normally around 200°, but it may be modified to a continues rotation motor. The servo can be driven from extreme position to another by the pulses between 0.5 ms and 2.5 ms wide depending on the specific RC servo used.

Table 6-5 lists the specification of the RC servo used. The dead band width indicates the minimum width of control pulse which is 10 microsecond (us). In another word, the precision of this RC servo is 0.9°. The RC servo drives the mechanism by gear, so the precision of the linear position relates to the radius of the driving gear. The biggest driving gear has a radius of 23 mm which drives the back

hip part. So the lowest linear precision for mechanism is 0.4 mm. The girth variation is controlled by the linear position variation of the sliders which is along the radial direction. The girth is an approximation of circle and the circumference is $2\pi R$. The precision of R is equal to the linear precision, so the estimation of the lowest girth tolerance is 2.5 mm which is sufficient for the garment fitting and design whose requirement of tolerance is 1 cm. The torque of the RC servo meets the design requirement as well.

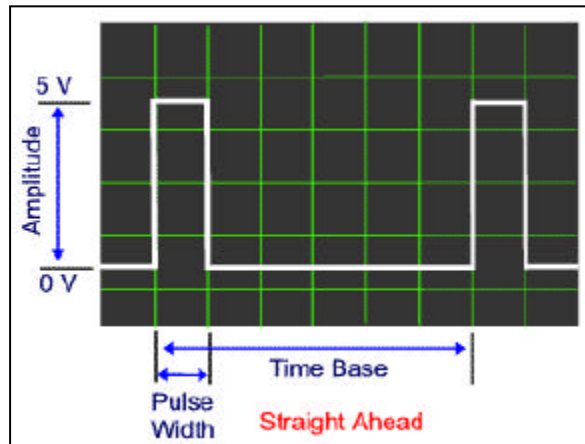


Figure 6-33. Input pulse for RC servo

Control pulse width	0.5-2.5 ms, 1.5 ms for neutral position
Operation voltage	5 -7.2 V
Current Drain	7.9 mA (idle) and 180 mA (no-load operation) at 5 V
	15.8 mA (idle) and 220 mA (no-load operation) at 7.2 V
Operating temperature	0 - 60 °C
Operating speed	0.16 second/60° without load at 6.0 V
	0.14 second/60° without load at 6.0 V
Torque	1.27 Nm at 5.0 V
	1.47 Nm at 6.0 V
	1.57 Nm at 7.2 V
Dead band width	10 us

Table 6-5. Specification for RobotBase RB-150MG RC servo (RB-150MG product homepage)

2. Control board.

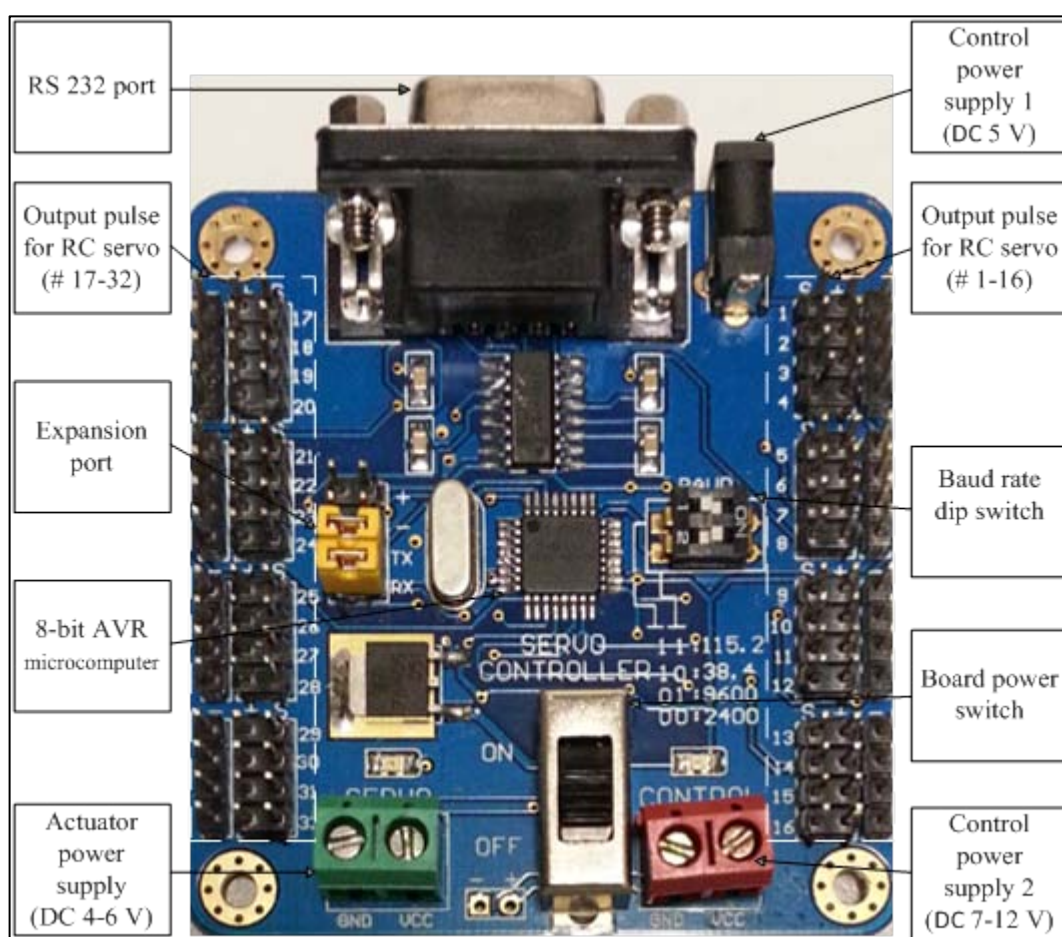


Figure 6-34. RobotBase Co. Ltd RC servo control board

The RC servo can be controlled directly using microcomputer such as AVR, AT51 and STC51. A control board using 8-bit AVR microcomputer is selected for the robotic mannequin as shown in Figure 6-34. It has the following advantages:

- 32 pulse output for RC servo.
- It is able to communicate using Standard RS232 communication protocol via cable or Bluetooth. So the robotic mannequin can be controlled by computer, mobile phone, or via network. The Bluetooth technology makes the robotic mannequin can be placed as request.
- The power of the control part can be supplied through either control power supply 1 or 2 port, so it can be powered via USB, battery or power supply.
- The expansion port is able to connected to Bluetooth I/O module or motion memory card if needed.
- Small size and low price.

6.3.2. Linear actuator system

1. Hybrid linear stepper actuator

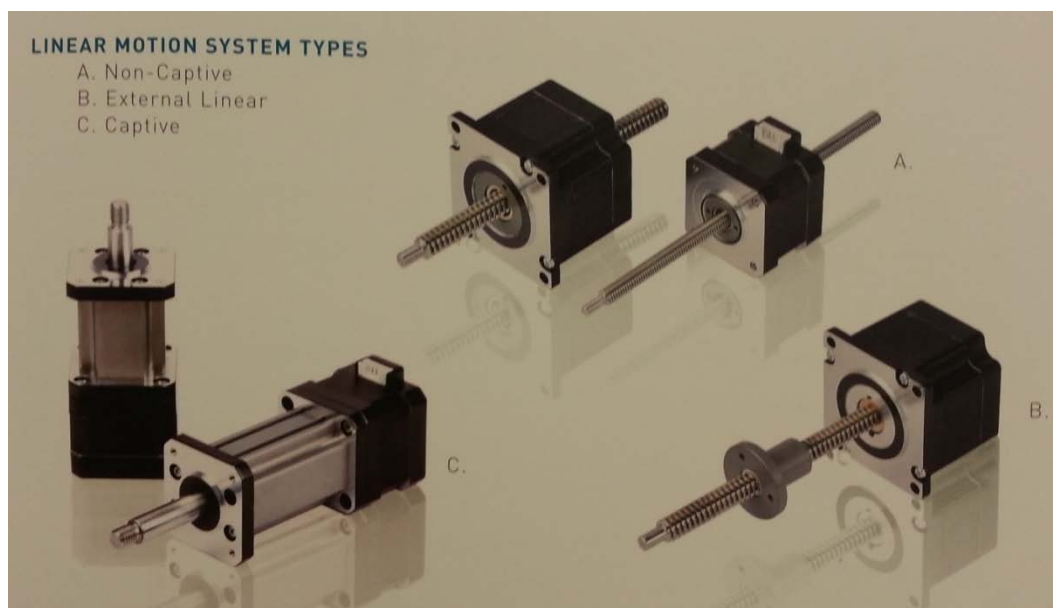


Figure 6-35. Hybrid linear stepper actuators (DINGS' electrical & mechanical Co., Ltd product brochure, 2012)

Hybrid linear stepper actuators belong to a branch of stepper motor, which is modified to convert the rotary motion into linear motion with the use of worm gear mechanism. A stepper motor is a brushless DC electric motor which divides a full rotation into a number of equal steps. There are several advantages to use a hybrid linear stepper motor for the robotic mannequin. First, although it is an open-loop device, but it is able to hold the motor's position at any steps without feedback. Second, it has an excellent repeatability, able to return to the same position accurately. Third, it offers excellent low speed torque, which means it can drive many loads without gearing. Hybrid stepper actuators use a combination of permanent magnet and variable reluctance techniques to achieve maximum power in a relatively small

package size. Fourth, it is able to maintain position by self-locking without power. Fifth, it is safe to use. when overload happens, it only stops instead of being damaged. Sixth, the price is relatively low among linear actuators. According to the form of output shaft, the linear stepper actuators can be divided into non-captive (A), external linear (B) and captive (C) types as shown in Figure 6-35.

A stepper actuator can be driven by sinusoidal wave current. By modifying the input wave to the actuator's phases, various drive wave modes have been developed for better performance. The common types are full stepping, half stepping and microstepping. The full stepping method drive the motor to rotate by a full step with full rated torque. Half stepping increases the angular resolution by rotating for half of step, but the torque is less. The microstepping usually uses an approximation of sinusoidal waveform. It can greatly increase the angular resolution of the motor by divide a full step into 1,2, 4 and even 128 micro steps, therefore the motor operation becomes more smooth.

14C2047D4-200-915 hybrid linear captive stepper actuator is selected for the robotic mannequin. Table 6-6 lists the specification. The travel per step is 0.0635 mm which is sufficient for garment fitting and design, whose precision is normally 1 cm.

Figure 6-36 shows the thrust diagram. The linear actuator operates at a speed of 800 pulse per second, thus the thrust is about 340 N which meets the requirement.

Step angle	2-Phase with 1.8° step angle
Phase current	2.0 A
Phase resistance	1.2 $\Omega \pm 10\%$
Lead wire number	4
Travel per step (1.8°)	0.0635 mm
Travel range	38.1 mm

Table 6-6. Specification for 14C2047D4-200-915 hybrid linear captive stepper actuator (DINGS' electrical & mechanical Co., Ltd product brochure, 2012)

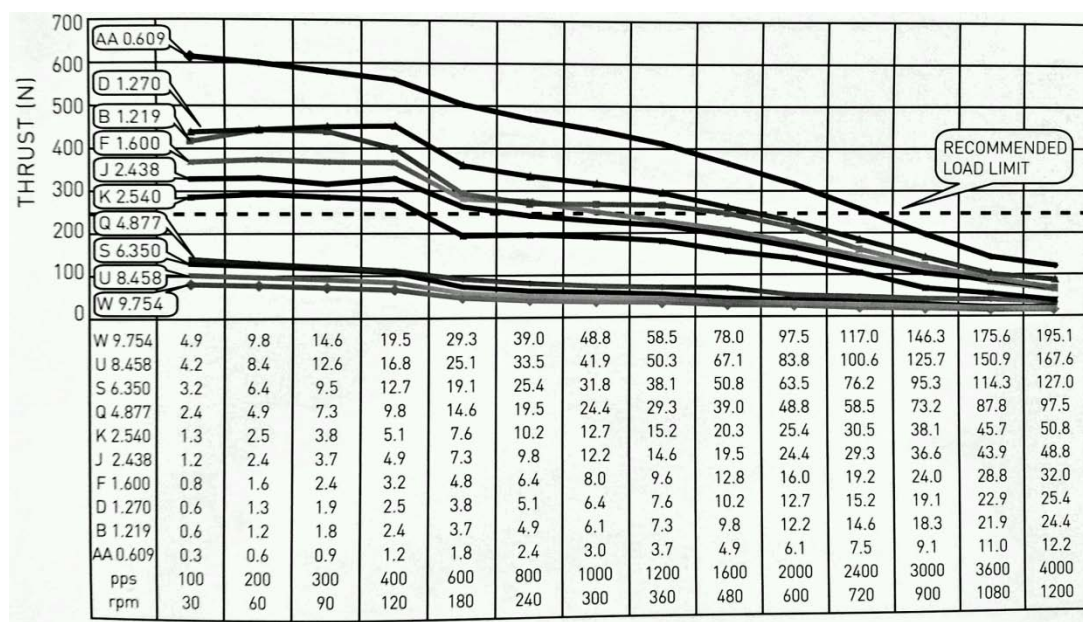


Figure 6-36. Thrust diagram for hybrid linear captive stepper actuator. Lines with different label are corresponding to different model of linear actuator. The values in lower table stand for the linear speed (mm/s), pulse speed (pps) and rotary speed (rpm) (DINGS' electrical & mechanical Co., Ltd product brochure, 2012).

2. Controller and driver board.

The integral stepper actuator system consists of controller, driver and stepper actuator. The controller (or indexer) is a microprocessor capable of the generating step pulses and perform the communication to upper system and other command functions. The Driver amplifies the controller step pulses into the power necessary to energize the motor windings. A controller using STC11F32XE microcomputer is selected for the robotic mannequin as shown in Figure 6-37. It provide with the following advantages:

- It integrates the controller and driver board.
- DC and AC power supply are both acceptable.
- Communicate using Standard RS232 protocol.
- Microstepping control at the rate of 1/1, 1/2, 1/4, 1/8, 1/16, 1/32, 1/64 and 1/128.
- 30 kilobyte read only memory (ROM). The settings of actuator will not be lost after power off.
- Small size and low price.

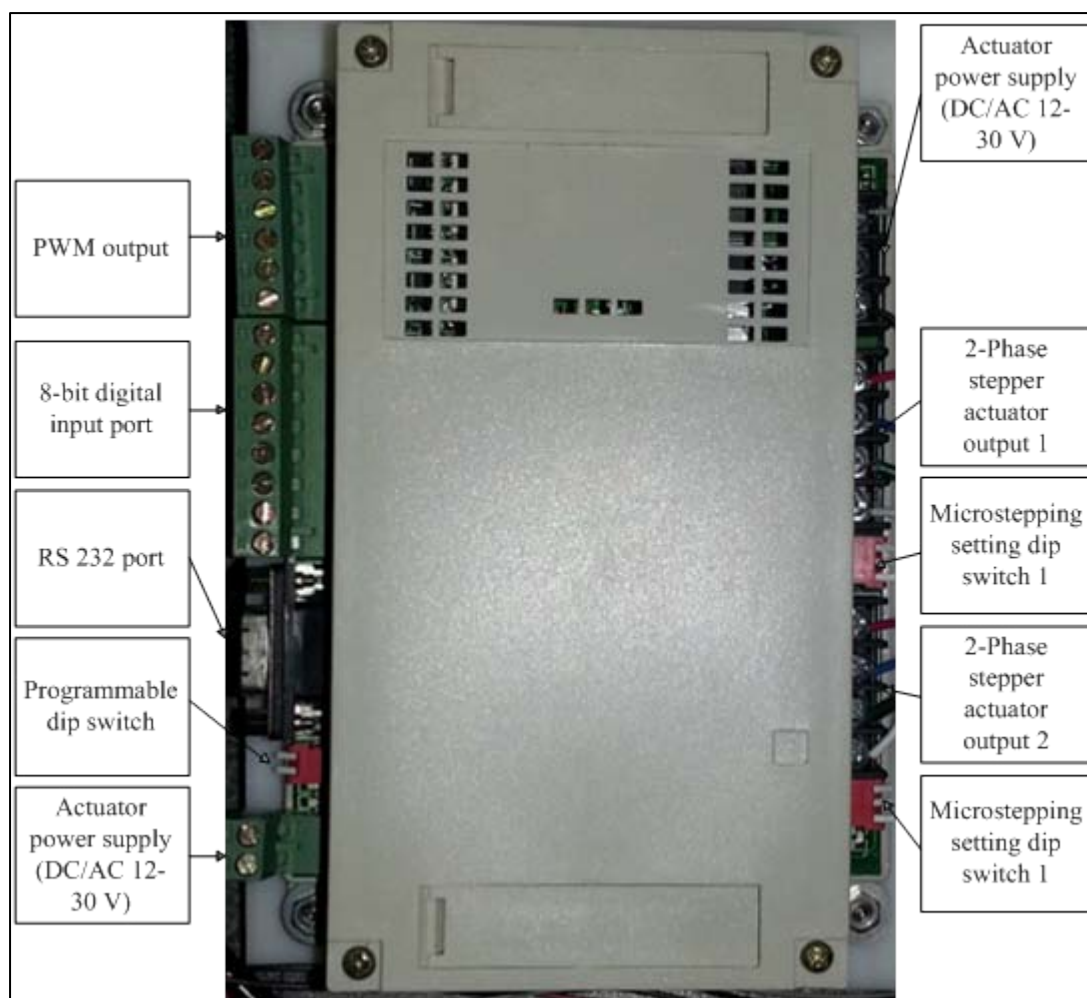


Figure 6-37 JMDM-COMTSM double stepper controller from JMDM Co., Ltd

6.4. Cladding part

A cladding is designed to be the "skin" of the robotic mannequin. It is tight and made of elastic fabric (80% Nylon, 20% Spandex, 190 g/m²) according to the patterns in Appendix III. The cladding is able to cover the gaps between the panels and reduce the backlash problem of the mechanism as it can reduce the clearance between the mating components by its elasticity on the panels. Soft films are attached to the edge of the panel to provide the cladding with support as shown in

Figure 6-38.

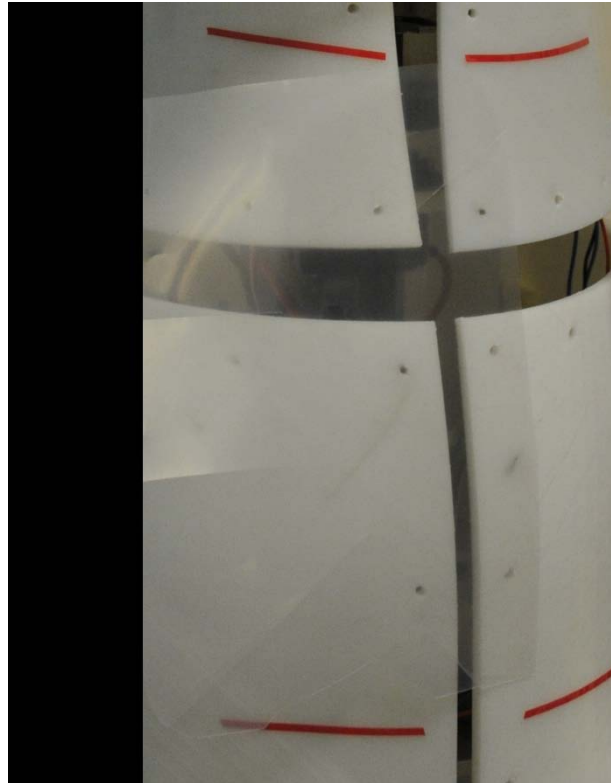


Figure 6-38. Soft films are attached to the edge of panels so it can support the cladding over the gap when the cladding is covered on them.

6.5. Controlling software part

The software design focus on building a PC software which is able to control the robotic mannequin and inform user the status with a user-friendly graphical user interface (GUI). The entire software part is developed using Matlab R2010b version. The control instruction is in the form of character string using RS232 communication protocol. Figure 6-39 shows the flowchart of the robotic mannequin

control software. Following is explanation for the stages inside it:

1. The actuators' position file record the position for the linear stepper actuators and RC servo as a the reference for the control system at the beginning. It also provides valuable information for system debugging.

2.The robotic mannequin shape library contains the preset body shapes. User can add new preset body shapes into it.

3. The modified parameters will be checked if they are legal before the transformation to ensure the robotic mannequin will be not be damaged and the surface maintains smooth.

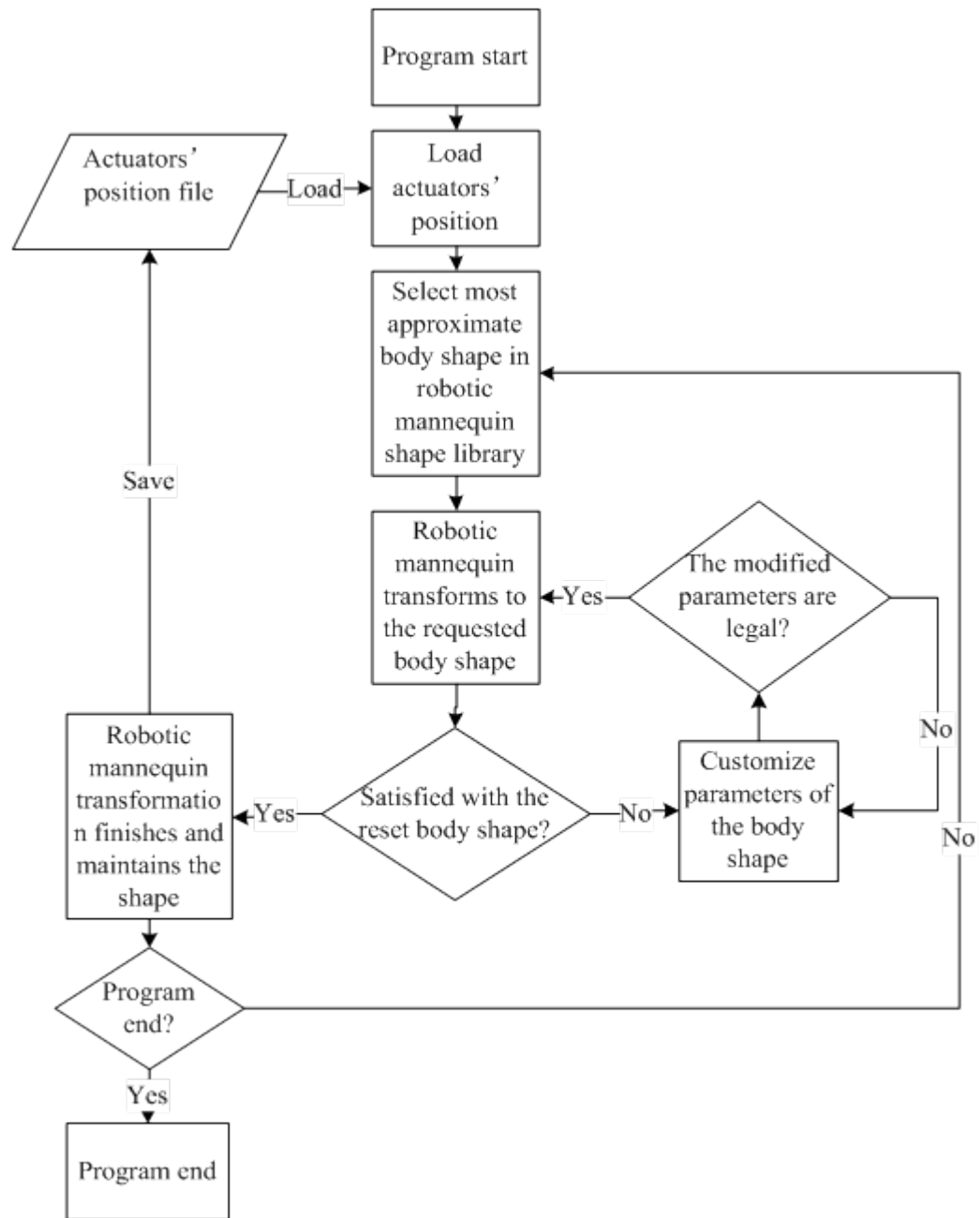


Figure 6-39. Robotic mannequin control software flowchart

The GUI is shown as Figure 6-40.

1. The "Mannequin size" drop-down list contains the present mannequin sizes as shown in Figure 6-41. This drop-down list can be edited by the user to add new

customized mannequin sizes.

2. The "Notification display area" shows the notification which describes the current mannequin size, system status, and warnings.

3. The "Connection control area" control the connection to the robotic mannequin. The connection should be established in the beginning of the control and disconnected before closing the software.

4. The "Dimension display area" display the current dimensions of the robotic mannequin.

5. The "Dimension customization area" contains buttons for dimension customization buttons. The "-" and "+" buttons are corresponding the dimensions on their left side in the same line. The words between them describe the sort of variation. "Girth" means the entire girth is modified by the clicking the button. "Front" and "Back" mean only the front part or the back part of the girth is modified by clicking the button. "Length" means the length is modified by clicking the button. Every click of the button "+" or "-" resulting in a step of position variation of the corresponding actuator. The step of RC servo is set to 4.5° and the step for linear actuator is set to 1 mm. The modified dimension will be checked before variation happening, as the modified dimension must be legal to protect the mechanism and maintain a realistic body shape. Firstly, it must within the range of dimensional variation of the robotic

mannequin. Secondly, and the difference between modified and original dimension is less than 20% of the original dimension. The customized control instruction will only be sent to the driving unit, when these two requirement is met.

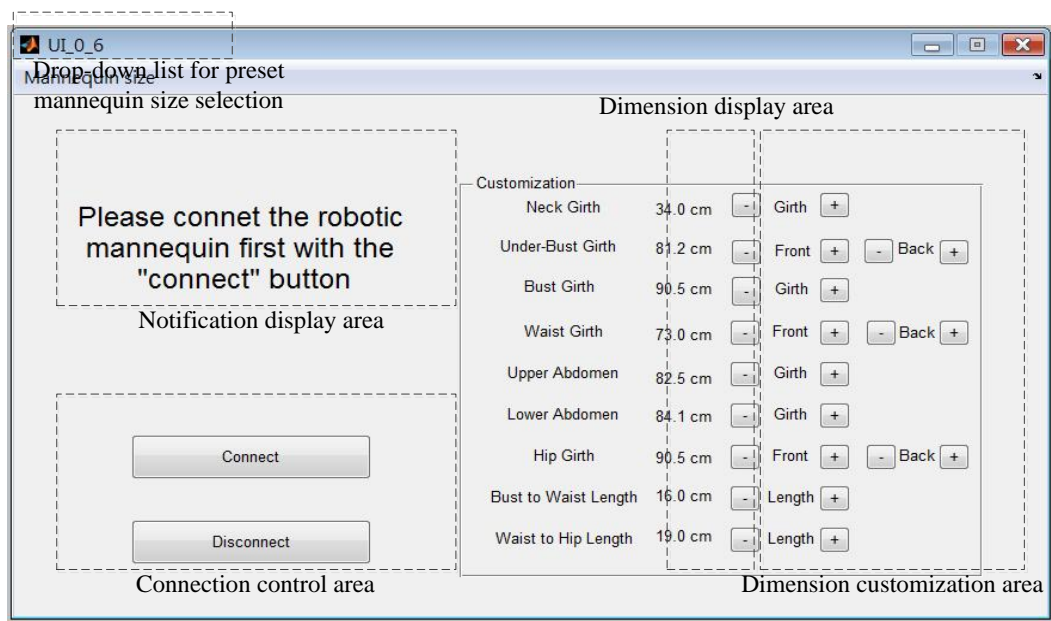


Figure 6-40. GUI for robotic mannequin



Figure 6-41. Preset mannequin sizes in the "Mannequin size" drop-down list

6.6. Production and integration

6.6.1. Production

The panels are made of engineering plastics using the rapid prototype machine.

The other parts were made by the Industrial Centre in The Hong Kong Polytechnic university according to the CAD drawings, which indicate the dimensions, material, tolerance and assembling of the parts.

6.6.2. Integration

The robotic mannequin is integrated in the following steps,

1. Assemble the neck module, chest module, waist module and hip module
orderly as indicated by the assembly drawings.
2. Connect the actuators to the driving unit.
3. Install the panels as shown in Figure 6-42.
4. Cladding the robotic mannequin as shown in Figure 6-43.
5. Connect the driving unit to PC via RS232 port, USB or bluetooth.



Figure 6-42. From left to right, the front, side and back view of the robotic mannequin with panels installed



Figure 6-43. From left to right, the front, side and back view of the robotic mannequin with panels and cladding

6.7. Summary of chapter

This chapter describes the detailed design of the robotic mannequin, covering the mechanical design, driving unit design, cladding design and software design. The mechanical design covers the mechanism of the robotic mannequin. The driving unit provides the robotic mannequin a precise and controllable movement. The cladding is designed to the "skin" of the robotic mannequin. The software design cover the code programming and GUI development. The parts of robotic mannequin was produced manufactured and integrated as described section 6.6. Next chapter will validate the robotic mannequin system performance.

Chapter 7 System validation

7.1. Introduction

This chapter reports the validation result of the robotic system. The robotic mannequin is designed for the usage of garment fitting, thus the range of dimensional variation, dynamic performance (accuracy, repeatability, and speed), and the elastic properties of the cladding are tested.

7.2. Range of dimensional variation and transformation time

The range of dimensional variation of the robotic mannequin is the range defined by the minimum size and maximum size it can transform. Dimensions for describing the shape of mannequin are selected for testing as shown in Table 7-1. The tools for measurement and the methods of measuring are adopted according to the standard “ISO 8559: Garment construction and anthropometric surveys – Body dimensions”. The mark point of body is marked with red tapes on the surface of the robotic mannequin as shown in Figure 6-42.



Figure 7-1. Front view of the robotic mannequin of the minimum and maximum size.



Figure 7-2. Side view of the robotic mannequin of the minimum and maximum size



Figure 7-3. Back view of the robotic mannequin of the minimum and maximum size

	Minimum size(cm)	Maximum size(cm)
Neck girth	30.6	38.0
Neck-base girth	33.7	42.5
Shoulder width	34.2	38.2
Bust girth	78.6	98.9
Under-bust girth	68.0	84.2
Waist girth	63.5	83.3
Hip girth	87.3	111.5
Bust to waist vertical length	15.5	17.5
Waist to hip vertical length	18.4	21.6
Shoulder length	12.5	13.9
Back width	29.2	33.6
Bust width	17.0	21.1
Neck to bust point	22.3	27.6

Table 7-1. Range of dimensional variation of the robotic mannequin. All units are in cm.

	Designed range of variation of the robotic mannequin	Actual range of variation of the robotic mannequin	Percentage of range covered
Neck girth	30.3 to 38.1	30.6 to 38.0	94.9%
Bust girth	75.7 to 100.0	78.6 to 98.9	83.5%
Waist girth	60.0 to 82.8	63.5 to 83.3	84.6%
Hip girth	85.1 to 111.1	87.3 to 111.5	91.5%
Bust to waist vertical length	15.5 to 17.5	15.5 to 17.5	100%
Waist to hip vertical length	18.4 to 21.6	18.4 to 21.6	100%

Table 7-2. Comparison between the designed and actual range of dimensional range of the robotic mannequin. All units are in cm.

The result shows that the actual range of dimensional variation of the robotic mannequin covers 92.4% of the designed range averagely, as shown in Table 7-2.

The time used for the transformation from the minimum size to maximum size transformation and vice versa are tested 5 times for each and listed as shown in Table 7-3. As the actuators are running at a constant speed, the time for transformation between the extreme sizes is the maximum transformation time for the robotic mannequin. The result shows that the average transformation time is 8.1 second. As this robotic mannequin is the first robotic mannequin used for garment fitting and display, there is no relevant product to be used as a benchmark.

Test	1	2	3	4	5	Average
From maximum size to minimum	8.1s	8.1s	8.1s	8.1s	8.1s	8.1s
From minimum size to maximum	8.1s	8.1s	8.1s	8.1s	8.1s	8.1s

Table 7-3. Transformation time testing result

7.3. Accuracy and repeatability

The ISO 9283:1998 "Manipulating industrial robots - performance criteria and related test methods." depicts the performance criteria and related testing methods to determine performance characteristics of manipulating industrial robots. According to this standard, accuracy refers to a robot's ability to position its mechanism end at a desired target point within the work volume. It depends on the mechanical inaccuracies, the computer control algorithms, and the system resolution. It will also be affected by the work volume, so in the case of the robotic mannequin, it will be affected by the elasticity of the cover, friction of the mechanism and other external forces. The repeatability describes how a point is repeated by moving the robot mechanism from a certain point a number of times, with equal environmental conditions. Figure 7-4 shows the relation between the measurements of accuracy and repeatability. The accuracy is the average displacement between the required position and repeated actual positions. And the repeatability is the positional deviation from

the average position of the repeated actual positions.

$$P_{\text{accuracy}} = \frac{\sum_{i=1}^n |P_i - P_r|}{n} \quad (8.1)$$

$$P_{\text{repeatability}} = |P_{e1} - P_{e2}| \quad (8.2)$$

Where,

P_{accuracy} is the accuracy of position.

$P_{\text{repeatability}}$ is the repeatability of position.

P_i is the actual repeated position for the i times.

P_r is the required position.

P_{e1} and P_{e2} are the two ends of the range of the repeated positions.

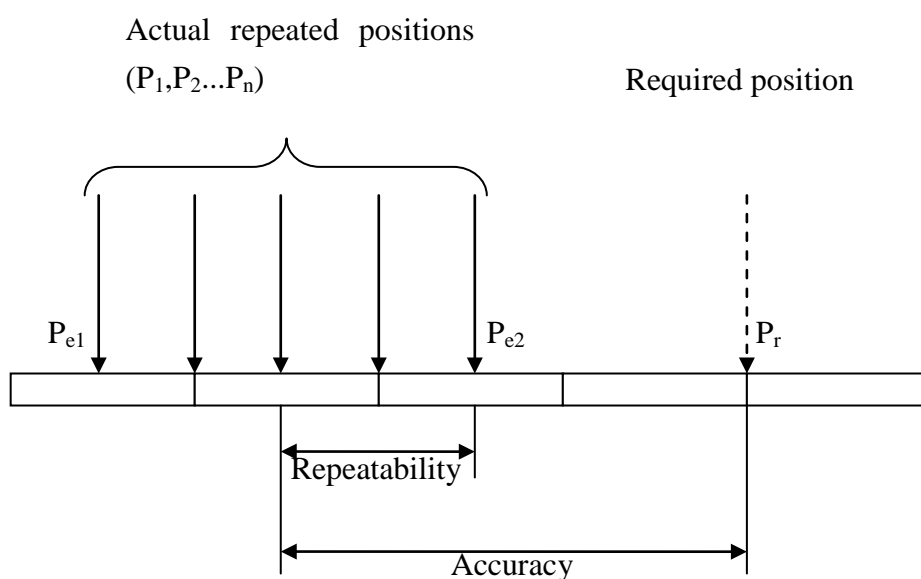


Figure 7-4. The Accuracy and repeatability measurements

For garment design, the commercial accuracy in girth and length measurements

is ± 0.5 cm, thus the robot system is tested to validate that it can fulfill this requirement. All the driving dimensions are tested separately by changing to the required position from the minimum size to the maximum size with an increment of 20% of the total travel range. As the size change motions can be divided into decreasing and increasing, these two different situations are tested correspondingly by setting the starting point at the minimum size and maximum size. The accuracy and repeatability are calculated using equation 8.1 and 8.2.

Neck girth (30.6 – 38.0)		0% (30.6)	20% (32.1)	40% (33.6)	60% (35.0)	80% (36.5)	100% (38.0)	Mean differe nce
Start from minimum position	Test 1	30.5	31.9	33.4	35.0	36.1	37.9	0.17
	Test 2	30.6	32.1	33.8	34.8	36.6	38.0	0.17
	Test 3	30.7	31.9	33.4	35.0	36.6	38.1	0.12
Start from maximum position	Test 4	30.6	32.1	33.8	35.4	36.9	38.2	0.20
	Test 5	30.7	32.5	33.6	35.3	36.7	37.8	0.20
	Test 6	30.6	32.2	33.8	35.0	36.6	38.0	0.07
		Average Accuracy: 0.2			Average Repeatability:0.5			

Table 7-4. Accuracy and repeatability for neck girth (all units in cm)

Bust girth (78.6 – 96.6)		0% (78.6)	20% (82.2)	40% (85.8)	60% (89.4)	80% (93.0)	100% (96.6)	Mean difference
Start from minimum position	Test 1	78.6	82.0	85.5	89.3	93.0	96.5	0.12
	Test 2	78.3	82.0	85.7	89.4	92.8	96.4	0.17
	Test 3	78.5	82.2	85.8	89.2	93.0	96.6	0.05
Start from maximum position	Test 4	78.5	82.3	85.8	89.5	92.9	96.6	0.07
	Test 5	78.6	82.3	85.5	89.4	93.1	96.9	0.13
	Test 6	78.7	82.4	85.7	89.3	93.0	96.7	0.10
		Accuracy:0.1			Repeatability:0.4			

Table 7-5. Accuracy and repeatability for bust girth (all units in cm)

Waist girth (63.5 – 83.3)		0% (63.5)	20% (67.5)	40% (71.4)	60% (75.4)	80% (79.3)	100% (83.3)	Mean difference
Start from minimum position	Test 1	63.5	67.3	71.4	75.5	79.0	83.0	0.15
	Test 2	63.5	67.3	71.5	75.4	79.2	83.3	0.07
	Test 3	63.6	67.4	71.3	75.2	79.2	83.1	0.13
Start from maximum position	Test 4	63.6	67.6	71.5	75.4	79.3	83.5	0.08
	Test 5	63.6	67.5	71.5	75.6	79.3	83.4	0.08
	Test 6	63.5	67.7	71.6	75.5	79.5	83.3	0.12
		Accuracy:0.1			Repeatability:0.4			

Table 7-6. Accuracy and repeatability for waist girth (all units in cm)

Hip girth (87.3 – 111.5)		0% (87.3)	20% (92.1)	40% (97.0)	60% (101.8)	80% (106.7)	100% (111.5)	Mean difference
Start from minimum position	Test 1	87.3	92.0	96.8	101.8	106.5	111.4	0.10
	Test 2	87.2	92.0	97.0	101.7	106.5	111.4	0.10
	Test 3	87.3	92.1	97.1	101.8	106.7	111.3	0.05
Start from maximum position	Test 4	87.4	92.2	97.1	101.9	106.7	111.3	0.10
	Test 5	87.2	92.1	97.0	101.9	106.6	111.5	0.05
	Test 6	87.4	92.1	97.0	101.8	106.6	111.3	0.07
		Accuracy:0.1			Repeatability:0.2			

Table 7-7. Accuracy and repeatability for hip girth (all units in cm)

Bust to waist length (15.5 – 17.5)		0% (15.5)	20% (15.9)	40% (16.3)	60% (16.7)	80% (17.1)	100% (17.5)	Mean difference
Start from minimum position	Test 1	15.5	16.0	16.4	16.7	17.0	17.6	0.07
	Test 2	15.5	15.9	16.3	16.8	17.1	17.5	0.02
	Test 3	15.6	15.9	16.3	16.8	17.2	17.6	0.07
Start from maximum position	Test 4	15.5	16.0	16.4	16.7	17.1	17.7	0.07
	Test 5	15.6	16.1	16.3	16.8	17.2	17.6	0.10
	Test 6	15.6	16.1	16.4	16.7	17.1	17.5	0.07
		Accuracy:0.1			Repeatability:0.2			

Table 7-8. Accuracy and repeatability for bust to waist vertical length (all units in cm)

Waist to hip length (18.5 – 20.5)		0% (18.5)	20% (18.9)	40% (19.3)	60% (19.7)	80% (20.1)	100% (20.5)	Mean differe nce
Start from minimum position	Test 1	18.5	18.9	19.2	19.7	20.0	20.7	0.07
	Test 2	18.6	18.9	19.0	19.8	20.1	20.6	0.10
	Test 3	18.6	20.0	19.1	19.7	20.1	20.6	0.08
Start from maximum position	Test 4	18.6	20.0	19.3	19.8	20.0	20.7	0.10
	Test 5	18.5	18.9	19.3	19.8	20.1	20.6	0.03
	Test 6	18.5	18.9	19.2	19.7	20.0	20.6	0.05
		Accuracy:0.1			Repeatability:0.1			

Table 7-9. Accuracy and repeatability for waist to hip vertical length (all units in cm)

The results show that the lowest accuracy of the driving dimensions is ± 0.1 cm while the lowest repeatability is 0.5 cm and they are both observed at the neck girth. It is mainly because the mechanism which uses 1 actuator to drive 4 neck panels simultaneously due to the limited space. The friction is higher compared to other parts so the accuracy and repeatability is lower. The commercial accuracy of garment design is ± 0.5 cm so the robotic mannequin is suitable to be used in fashion industry.

7.4. Cladding elasticity test

The range of dimensional variation result (Table 7-1) shows that the waist girth has the maximum growth percentage, which is 31.2%, from the minimum size to the maximum size. The cladding is the surface of the robotic mannequin, therefore it's

stretch percentage should be higher than 31.2% to be stretchable during the variation. The elasticity of the cladding is tested according to ASTM D6614 – 07 (2011): standard test method for stretch properties of textile fabrics. According to the standard, A specified load (1814 ± 1.0 g) is applied to a fabric specimen, using a constant rate of extension tensile tester at a prescribed rate of extension. After holding at the specified load is removed from the specimen and allowed to relax for a specified time. A small amount of force, enough to remove any wrinkles or folds, is applied and the specimen length measured. The amount of fabric stretch is calculated from the difference in length prior to load and under load. Fabric growth is calculated from the difference in length prior to loading and after relaxation. The cladding is made of elastic fabric shown in Figure 7-5. Four specimens are prepared as follows,

1. To test stretch properties in wale direction, two specimens whose dimension is 50 ± 0.5 mm wide by 350 mm with the long dimension parallel to the wale direction are cut from different part of the cloth for wale direction test 1 and 2.

2. To test stretch properties in course direction, two specimens whose dimension is 50 ± 0.5 mm wide by 350 mm with the long dimension parallel to the course direction are cut from different part of the cloth for the course direction test 1 and 2.

The machine gradually increases the pull strength to 1814 ± 1.0 g and record

the length of specimen as shown in Figure 7-6. The fabric stretch and the fabric growth percentage can be calculated using equation 7.3 and 7.4.

$$\text{Fabric stretch percentage} = \frac{B - A}{A} \times 100 \quad (7.3)$$

$$\text{Fabric growth percentage} = \frac{C - A}{A} \times 100 \quad (7.4)$$

Where,

A = original distance between jaw faces, which is set to 250 mm.

B = distance between jaw faces measured while the specimens under 1814 ± 1.0

g.

C = distance between jaw faces measured after removal of slack.

Test results are shown in Table 7-10.

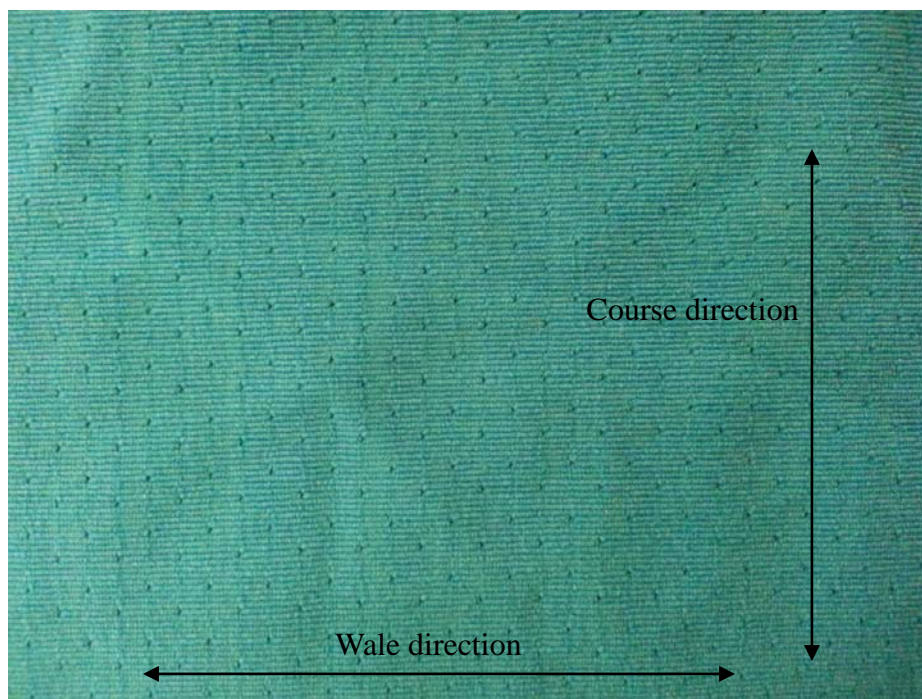


Figure 7-5. Elastic fabric used for cladding

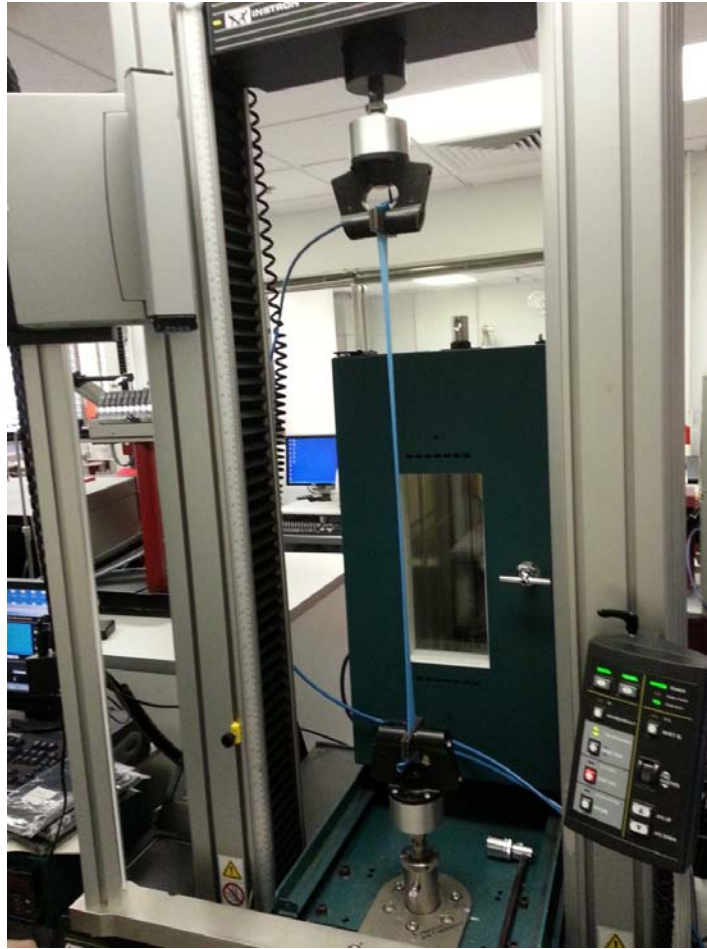


Figure 7-6. Elasticity test using Instron 5566 device

	A	B	C
Wale direction test 1	250.0 mm	430.2 mm	270.2 mm
Wale direction test 2	250.0 mm	443.6 mm	274.2 mm
Course direction test 1	250.0 mm	496.0 mm	279.0 mm
Course direction test 2	250.0 mm	490.3 mm	278.3 mm

Table 7-10. Stretch properties test result. A is the original distance between jaw faces (250 mm). B is the distance between jaw faces measured while the specimens under 1814 ± 1.0 g. C is the distance between jaw faces measured after removal of slack.

So the average stretch percentage of wale direction is 74.76% and the average

growth percentage of it is 8.88%; the average stretch percentage of course direction is 97.26 and average growth percentage of it is 11.46%. The tension force of the cover is relevant to stretch percentage of the cloth, the smaller the percentage, the larger the force. The growth percentage indicate the capability of recover, the smaller the percentage, the better the cover can fit to the surface of the robotic mannequin during transformation. So it is suggested that the cloth of the cover should be with stretch percentage lager than 74.76% and growth percentage less than 11.46%.

7.5. Summary of chapter

This chapter describes the range of dimensional variation, transformation time, accuracy, repeatability, and elasticity of the cladding. The actual range of dimensional variation, and covers 92.4% of the design range, which is adequate to cover the entire size range of the popular mannequins in the market as described in section 4.3.1. The transformation time is less than 8.1 second. The accuracy achieves ± 0.1 cm and the repeatability is 0.5 cm better than what the industry is accepting, i.e. ± 0.5 cm. The elasticity of the cladding was tested for setting the standard of the fabric used for the cladding.

Chapter 8 Conclusion and future work

This chapter presents a summary of the research project, discuss contribution and limitation of this research and identifies the major implications of the research for both academic and industrial application. The first part summarizes the design and development of the robotic mannequin system. The second part concludes the feedbacks from professionals from the fashion industry and academic field. The third part discusses the performance of the robotic mannequin system, outlines its advantages and limitations. The fourth part suggests future work for improving the robotic mannequin system for commercial application.

8.1. Summary of research project

This research project completed a robotic mannequin system for fashion industry. First the variation ranges and manners are analysed based on 130 Chinese females, existing mannequin on the market and anthropometric surveys, in order to reconstruct the realistic body shape to meet the market demand. Next the kinematic of the mechanism was designed to determine the movements for transformation of the robotic mannequin. A virtual adjustable mannequin was built to visualise the transformation of the body shape, which was validated by the pilot survey. In the

following mechanical design stage, the mechanisms were designed to realize the designed functions. Then the driving and control modules were completed to ensure the movement is controllable and precise. The standardization and module design are adopted in the mechanical and electronic parts to reduce the difficulties and cost in manufacturing and maintenance. A elastic fabric cladding was made to give the robotic mannequin a smooth contour, protects the mechanism from dust and improves the accuracy of the transformation by limiting the backlash problem. Lastly, a GUI was finished to provide a friendly user experience. To protect the design, the system was patented in China (201210279971.5) and Hong Kong (12111456.0). Visitors from academic and industry were invited to provide valuable feedbacks with their professional knowledge on the performance of the robotic mannequin.

8.2. Feedback from professionals

Professionals from the fashion industry and academic were invited to review the robotic mannequin. To obtain comprehensive feedbacks from both the view of academics and industry, visitors with various positions were invited to provide the comments upon viewing the working of the mannequin. The collected comments are from the visitors as teachers, researchers, engineers, designers, managers, and CEO. Table 8-1 lists the significant comments of the feedbacks,

Name	Date	Comments
Ms Sally from textile institute	2012. 11.16	1. The robotic mannequin will be useful for fashion industry. 2. The shape of robotic mannequin is realistic.
Mr Zhang from "A" company	2012. 11.24	1. The shape of the robotic mannequin is realistic. 2. The surface of the robotic mannequin is smooth. 3. The robotic mannequin can be used in retail stores to attracting customers. It can be added an image recognition system to acquire the general body size of the customers and automatically change its shape to actually show the performance of the garment dressed on the customer. 4. The robotic mannequin will be useful for garment manufacturers and retailers.
Mr. Zhou from "N" company	2012. 12.4	1. The shape of robotic mannequin is realistic. 2.The range of dimensional range is sufficient for garment design. 3. The transform procedure is quick and interesting. 4. The precision is sufficient for using in fashion industry.
Prof. Tao, Prof. Au from university	2012. 12.13	1. The robotic mannequin has a realistic body shape and realistic variation process. It can be used for teaching of pattern design and grading.
Ms Sin from "AU" company	2012. 12.18	1. The robotic mannequin will be useful for fashion industry. 2.It can be designed for tight fitting clothes.
Mr Lai and Lee from "W" company	2012. 1.8	1. The shape of robotic mannequin is realistic. 2. The range of dimensional range is sufficient for garment design. 3. The robotic mannequin will be useful for fashion industry.
Mr. Edmond from university	2012. 1. 18	1. The robotic mannequin is a innovative product which can mimic the female body shape precisely. 2. It shows great potential for uses in fashion industry. 3. It is easy to set up and use

Mr Lui and Lai from "L" company	2012. 1.31	<p>1. The range of dimensional range is sufficient for garment design.</p> <p>2. The variation of shape is realistic and the adjustable parts are sufficient for fashion industry.</p> <p>3. The design of replaceable panel is good for covering the uncommon types of body shape.</p> <p>4. It will be useful for customized clothes design.</p> <p>5. It is easy to set up and use</p> <p>6. It is useful for online shopping by visualise the looking of the garment on the body shape of the customer through online video. It can help the customer to choose the nice fit cloth even they cannot try it on. It will also help to reduce the return of the goods to reduce the cost of sellers.</p> <p>7. The system is safe, as the torque force of the actuators is within safe range and will not damage the clothes. The cover prevents the user from getting hurt by the mechanism inside.</p>
---------------------------------	------------	---

Table 8-1. Feedbacks for professionals about the robotic mannequin system

According to the comments, the feedback is positive on the robotic mannequin system generally. The range of the dimensional variation is sufficient for the fashion industry. The shape variation is realistic and precise. In the fashion industry, it is a useful, user-friendly, cost-effective, easy to maintenance, and practical system for the garment design and garment e-retailing. It can also be used in the teaching and training for the demonstration of body size variation.

8.3. Discussion

The apparel industry relies very much on the availability of the “mannequin” for many of the tasks involved in apparel design, fitting and alteration, and size gradation, however the tradition mannequins (only one size per mannequin) are costly and occupy a lot of storage space. The robotic mannequin is developed to solve the problem of having multiple sized mannequins. It is a revolutionary novel robotic system for the fashion industry with the ability to increase/decrease automatically over a size range or customized size dimensions suitable for garment fitting, tailoring, training and display. It has following significant,

1. The robotic mannequin can change its shape, size and dimension precisely and quickly. The accuracy achieved ± 0.1 cm and the repeatability is 0.5 cm better than what the industry is accepting, i.e. ± 0.5 cm. The maximum time for transformation is 8.1 s, which is quick enough for all profile change.

2. The range of dimensional variation of the robotic mannequin is sufficient for fashion industry. It can cover the major sizes of mannequin used in the fashion industry.

3. The shape of the robotic mannequin is realistic and the adjustable parts are sufficient for fashion industry. The shape of the robotic mannequin is confirmed by professionals to be realistic. Its surface is smooth as the cladding covers the gaps. The robotic mannequin has 20 adjustable panels and 20 degree of freedom, which can realize the body shape variation for garment design and fitting.

4. The robotic mannequin system is easy to set up, use and maintain. It can be control using Windows platform directly via wire or wireless connection. The system is controlled with a user-friendly graphical user-interface. The software can be edited by the user to add their customized types of the body shape, connect with 3-D body scanner, or communicate with other software.

5. The panels of the robotic mannequin are replaceable, so the robotic mannequin can mimic more types of body shape by changing the panels.

6. The system is safe to use. The maximum torque of the actuators is not big enough to damage normal clothes. The surface of the robotic mannequin is covered by a cladding to provide a continuous human-like surface for clothes fitting.

With the above features, the system can be used in the following applications,

1. Garment design, development and styling.
2. Quality control relating to garment fitting. The garment can be tested on the desired body shape by using the mannequin.
3. Garment factories producing for multiple international buyers, as it can change to the dimensions over a wide range for the people in different countries.
4. Customized garment design. It can be used for tailoring of clients with various body profiles.
5. E-retailing and on-line purchase.
6. Education and training. It can demonstrate the process of body shape variation and garment grading.

8.4. Future work

The robotic mannequin generally fulfil the project objectives, however, it is limited by the funding, time, and manpower. It is only a prototype but with potentials.

Improvements can be made in the following aspects:

1. The mechanism can be refined further to achieve commercial stability.

Stronger material and better gearing can be adopted in the mechanism. Currently, sliding is applied for the panel motion, it may cause problem due to normal wear. It can be solved by using rolling motion to replace the contact parts. In this way, the problem of wear will be limited and the accuracy will be improved. The prototype is mainly for fulfilling the function so the parts can be refined to save more material and lower the weight and reduce the cost. Non-critical parts can be made of engineering plastics.

2. More body shapes should be studied for the panel design, and panels for more body types should be designed. For example, panels can be designed for elderly, extreme leanness, outsizes, pregnant women and etc.

3. Hand, foot and other body part can be added on for other design purposes. A

suspension type of support module could be developed for trousers design. A rotation system can be added to the bar, so the robotic mannequin can rotate automatically for better demonstration.

4. The GUI can be improved to include more preset body shapes and to be more convenient. The software can featured more functions and the bugs fix work should be continued

.

5. The programme linking the robotic system to the 3-D body scanner can be developed.

6. The control software on other platform, such as IOS or Android can be developed so the user can use smart phone to control the system.

Appendices

Appendix I. Anthropometric measurements of Chinese female

Subject	Neck Full	Bust Full	Waist Full	Waist Front	Waist Back	Abdo men Full	Hips Full	Hips Front	Hips Back	Should er Length	Bust width	Neck to bust	Sceye circum ferenc e
G1	34.4	85.4	78.9	38.1	40.7	97.4	98.1	47.7	50.4	11.4	18.6	26.5	37.3
G2	34.0	84.1	77.5	37.6	40.0	82.5	93.3	46.3	46.9	13.8	17.6	22.3	33.8
G3	34.0	81.8	69.2	33.4	35.8	85.6	89.5	44.7	44.8	10.1	18.4	24.3	34.0
G4	31.2	79.9	62.9	30.2	32.7	73.8	85.0	44.7	40.3	10.4	18.9	24.3	31.4
G5	34.3	81.8	69.1	33.3	35.8	79.6	93.3	49.1	44.3	9.6	18.8	25.7	35.9
G6	32.9	85.4	74.4	36.0	38.4	84.3	94.4	46.8	47.5	10.1	17.3	23.9	37.3
G7	28.6	75.4	69.6	33.6	36.0	74.9	91.4	45.9	45.5	13.0	16.9	26.6	34.0
G8	36.1	87.6	78.4	38.0	40.4	90.4	106.2	53.9	52.3	15.7	20.0	29.9	36.0
G9	30.6	79.0	61.4	29.5	31.9	71.4	88.0	44.0	43.9	11.3	14.6	20.7	30.6
G10	34.1	75.7	66.2	31.9	34.3	67.2	89.2	45.7	43.5	11.5	18.4	25.8	33.3
G11	34.4	76.7	74.1	35.8	38.3	87.2	91.4	46.9	44.4	11.8	14.8	22.4	33.2
G12	35.0	85.9	78.9	38.3	40.7	82.4	95.5	48.1	47.5	11.4	17.1	27.2	38.3
G13	36.0	101.6	77.7	37.8	40.0	90.6	104.3	51.3	52.9	12.2	22.8	30.0	41.6
G14	37.7	92.2	82.4	40.0	42.4	86.3	100.3	47.0	53.3	13.1	19.9	29.7	37.3
G15	36.3	84.7	77.5	37.5	40.0	82.1	96.6	50.1	46.5	13.1	17.3	23.2	32.6
G16	30.3	74.9	63.7	30.6	33.1	72.2	87.7	44.7	43.0	11.8	16.4	26.7	31.0
G17	32.5	84.3	73.8	35.7	38.2	84.0	98.2	49.6	48.6	11.8	18.1	24.9	35.1
G18	35.1	81.4	78.6	38.1	40.5	84.7	98.2	48.6	49.6	11.1	18.9	25.6	38.0
G19	33.3	81.4	73.3	35.4	37.9	85.1	92.1	47.2	44.9	11.6	18.0	23.3	33.0
G20	35.4	83.9	78.9	38.2	40.7	96.9	100.6	50.9	49.7	12.6	17.0	26.4	36.6
G21	31.8	78.4	64.5	30.8	33.6	77.7	89.7	47.0	42.7	12.6	19.7	24.6	31.0
G22	31.9	76.8	59.9	28.6	31.3	59.6	86.4	44.5	42.0	12.0	17.4	27.3	31.0
G23	33.1	82.8	70.1	33.8	36.3	78.3	92.4	47.6	44.8	11.7	15.8	24.1	32.2

G24	35.5	74.5	68.1	32.8	35.3	76.0	89.5	44.6	44.9	7.7	16.3	25.6	33.5
G25	34.2	80.5	64.4	31.0	33.4	80.1	90.7	47.0	43.7	10.0	17.0	22.8	33.4
G26	31.3	86.3	62.8	30.0	32.8	64.3	86.0	43.3	42.7	12.1	14.2	24.2	33.8
G27	32.0	83.4	73.8	35.7	38.1	82.2	92.5	48.1	44.4	9.6	18.4	21.7	35.6
G28	34.5	77.1	65.7	31.5	34.2	79.8	93.9	48.5	45.4	11.5	17.1	25.1	28.6
G29	34.3	85.1	74.3	35.8	38.5	83.3	94.7	49.7	45.1	10.4	18.9	25.1	34.4
G30	33.9	73.2	64.2	30.9	33.3	80.8	89.3	46.6	42.7	8.6	14.2	22.5	30.5
G31	33.3	90.9	79.2	38.4	40.8	97.4	99.7	50.4	49.3	9.5	19.0	26.7	37.4
G32	36.2	80.2	69.5	33.4	36.1	77.6	95.7	48.7	47.0	11.7	16.1	23.6	34.7
G33	36.2	75.3	68.1	32.8	35.3	78.5	89.1	45.0	44.1	9.5	17.3	23.3	30.8
G34	33.1	84.2	65.3	31.4	33.9	69.2	88.8	46.3	42.5	13.1	14.8	26.1	32.7
G35	35.5	86.1	74.6	36.1	38.5	83.3	93.8	46.4	47.5	11.0	15.5	23.2	36.0
G36	35.5	87.8	74.0	35.6	38.4	82.6	99.4	50.3	49.1	10.6	18.6	24.1	37.6
G37	35.0	85.4	75.7	36.6	39.1	84.2	92.4	47.7	44.7	12.0	17.7	22.6	36.8
G38	33.4	83.3	68.4	32.8	35.6	88.1	94.2	47.5	46.7	11.3	17.7	25.0	35.3
G39	32.3	78.2	63.9	30.8	33.1	81.4	82.1	41.9	40.2	10.9	16.7	24.7	30.5
G40	31.6	85.0	64.6	31.0	33.7	76.9	89.3	46.1	43.2	11.1	18.8	24.1	32.8
G41	34.1	88.2	78.1	37.8	40.3	84.6	97.1	49.6	47.5	11.7	17.0	24.2	36.4
G42	32.4	86.4	73.8	35.7	38.2	80.5	94.9	48.7	46.2	11.8	17.9	25.4	32.6
G43	34.0	81.5	72.8	35.2	37.6	80.8	93.5	57.1	36.4	11.2	18.5	24.6	34.4
G44	33.8	83.1	72.4	34.7	37.6	85.2	98.2	49.7	48.6	11.5	12.7	27.1	38.4
G45	36.2	87.9	72.1	34.7	37.4	85.7	94.5	46.3	48.3	12.5	21.9	24.4	34.8
G46	29.9	78.5	66.0	31.8	34.2	74.6	88.9	46.3	42.6	11.6	16.9	21.3	30.9
G47	31.3	88.2	65.5	31.5	34.1	77.4	82.1	41.0	41.0	8.6	18.7	26.0	34.1
G48	34.4	82.8	63.2	30.2	32.9	71.0	84.6	43.1	41.5	10.1	15.5	22.7	30.9
G49	33.8	77.6	66.9	32.2	34.7	75.0	95.2	48.2	47.0	11.6	15.9	24.3	31.9
G50	34.5	75.4	66.9	32.3	34.6	82.8	86.6	44.4	42.2	9.4	16.5	22.6	32.0
G51	32.4	74.7	71.1	34.3	36.8	73.9	81.0	42.4	38.7	10.1	13.9	23.7	30.7
G52	34.8	93.2	78.6	38.0	40.6	84.5	96.0	48.2	47.7	13.0	16.6	26.4	37.4
G53	33.5	75.4	71.6	34.6	37.1	78.0	91.1	47.2	43.9	10.0	15.7	24.3	32.1
G54	34.2	85.9	70.9	34.2	36.6	82.8	95.8	47.6	48.2	12.5	16.8	25.6	35.5
G55	35.5	88.7	76.6	37.1	39.5	87.2	104.6	53.3	51.3	10.9	17.4	26.6	36.7
G56	32.9	82.5	65.4	31.6	33.8	74.0	89.7	46.3	43.4	11.2	15.3	24.6	31.8
G57	32.8	85.3	71.4	34.3	37.0	83.3	95.8	47.9	47.9	11.4	14.3	24.8	35.9
G58	32.2	79.6	69.9	33.7	36.2	75.1	96.1	49.9	46.2	10.2	16.3	22.3	33.1
G59	32.9	89.8	76.2	36.9	39.3	86.3	100.2	48.8	51.4	12.3	21.0	23.1	37.5

Appendices

G60	31.7	83.0	68.5	33.1	35.4	81.9	96.5	48.7	47.7	12.9	20.1	27.0	34.6
G61	33.7	85.9	69.9	33.6	36.3	85.6	90.1	46.6	43.5	12.9	17.6	25.3	34.8
G62	34.8	86.8	67.9	32.7	35.2	82.1	90.8	45.4	45.4	11.7	16.2	23.9	37.0
G63	33.6	76.5	65.0	31.2	33.7	70.2	85.7	45.1	40.6	12.0	14.6	24.6	30.5
G64	31.6	74.1	62.5	30.0	32.4	72.7	92.5	53.0	39.5	11.0	15.7	22.4	32.1
G65	33.8	74.6	62.4	30.0	32.5	81.0	87.4	43.9	43.5	10.3	16.1	21.9	31.1
G66	38.1	107.4	82.8	40.1	42.8	84.7	111.1	55.9	55.2	14.6	21.4	30.6	41.1
G67	30.8	75.7	60.3	29.0	31.3	73.9	85.1	45.7	39.5	9.1	16.7	22.2	27.0
G68	29.8	78.3	63.4	30.4	33.0	65.2	84.5	49.8	34.7	10.2	16.5	22.9	31.5
G69	34.0	81.0	61.3	29.4	31.9	77.4	90.2	45.2	45.0	10.0	17.9	22.8	31.0
G70	32.7	82.8	67.0	32.0	35.0	76.8	91.6	47.8	43.8	10.8	14.8	26.7	35.4
G71	32.6	81.3	69.2	33.4	35.8	85.7	99.2	50.0	49.2	8.7	15.6	22.8	38.8
G72	33.0	78.8	68.4	33.0	35.4	81.5	93.1	47.8	45.3	14.6	17.3	27.0	38.7
G73	33.9	89.2	78.5	38.0	40.5	81.3	92.2	46.9	45.3	11.6	17.4	23.0	34.8
G74	32.7	84.0	70.0	33.8	36.2	72.9	87.9	45.8	42.0	11.3	16.8	24.0	36.7
G75	32.6	78.3	65.6	31.6	34.1	75.6	86.3	43.8	42.5	12.8	14.3	23.3	30.3
G76	34.2	94.3	76.8	37.2	39.5	88.5	99.0	51.5	47.4	15.1	20.9	28.5	36.6
G77	33.0	78.4	62.9	30.2	32.7	74.1	92.0	48.2	43.8	12.2	15.3	21.8	30.9
G78	33.4	77.8	63.4	30.5	32.9	68.9	86.2	44.6	41.6	10.5	13.9	21.2	29.5
G79	33.9	85.1	75.4	36.5	38.8	81.6	88.9	45.1	43.8	10.8	16.5	23.0	36.7
G80	37.1	102.8	80.4	38.8	41.5	97.8	103.8	51.5	52.4	11.8	16.8	27.6	45.2
G81	32.8	82.3	70.1	33.8	36.3	83.2	92.9	47.1	45.7	10.1	18.2	27.2	36.7
G82	35.3	87.6	67.1	32.3	34.8	81.4	101.1	51.2	49.9	12.0	17.6	28.1	37.2
G83	33.5	84.5	72.5	35.0	37.5	84.4	96.5	49.1	47.3	11.4	16.6	27.4	38.9
G84	32.4	91.6	74.1	35.9	38.2	87.6	96.4	44.4	52.0	12.4	20.2	26.9	39.7
G85	28.6	81.9	64.2	30.8	33.4	77.5	87.9	43.9	44.0	11.4	18.5	23.5	32.4
G86	35.9	89.3	74.7	36.1	38.5	84.3	93.8	46.7	47.1	11.8	17.0	26.2	39.1
G87	38.2	83.8	68.6	33.1	35.6	82.3	90.3	46.9	43.5	8.7	19.8	24.6	39.4
G88	30.5	85.4	62.1	29.7	32.4	73.0	81.0	42.0	38.9	11.8	16.0	24.5	35.5
G89	32.5	80.3	66.4	32.0	34.4	76.3	89.8	45.1	44.7	11.7	17.8	25.2	31.5
G90	28.8	74.4	69.9	33.7	36.2	85.2	89.5	45.8	43.7	12.5	16.8	23.2	31.0
G91	34.0	84.6	66.6	32.1	34.5	81.3	89.7	53.5	36.3	11.0	15.1	22.8	36.6
G92	35.4	82.4	66.2	31.8	34.5	86.1	95.0	48.0	47.0	7.0	17.4	26.7	94.7
G93	35.0	82.9	71.2	34.4	36.8	82.1	97.7	49.4	48.3	12.6	15.4	24.6	34.6
G94	31.9	78.3	64.9	31.0	33.8	77.3	91.8	48.4	43.4	10.7	14.9	25.6	30.2
G95	35.7	94.3	72.8	35.1	37.6	83.9	97.7	51.4	46.4	4.6	16.4	29.1	91.1

G96	34.3	79.8	70.8	34.0	36.8	77.6	93.1	47.9	45.2	11.4	16.6	24.2	33.1
G97	34.9	88.5	79.9	38.8	41.2	85.4	108.3	52.4	55.9	10.5	15.9	24.1	39.7
G98	34.8	84.2	75.3	36.4	38.9	77.4	95.0	49.2	45.8	10.3	16.7	24.3	33.5
G99	31.5	93.1	78.5	38.0	40.5	96.3	98.2	48.9	49.3	11.4	15.2	26.4	37.5
G100	31.7	87.7	67.2	32.3	34.9	81.0	95.3	48.6	46.7	10.8	17.4	24.1	40.7
G101	32.2	83.0	72.2	34.9	37.3	84.2	97.5	49.1	48.4	11.9	16.8	24.8	35.3
G102	35.1	82.6	64.6	31.1	33.5	73.8	91.7	45.9	45.8	8.9	18.6	23.4	35.6
G103	37.4	105.1	84.7	41.2	43.4	107.9	113.0	53.9	59.1	14.2	19.0	30.5	43.3
G104	31.9	74.0	63.2	30.4	32.9	71.6	88.1	45.2	42.9	7.6	15.0	26.1	34.8
G105	37.1	107.8	82.6	40.0	42.6	97.2	102.7	51.4	51.3	13.1	20.2	27.0	43.1
G106	31.7	77.7	58.3	27.8	30.5	57.8	80.7	41.2	39.6	9.5	14.6	23.2	30.8
G107	33.6	81.9	69.6	33.6	36.0	77.2	93.0	47.8	45.2	10.1	17.3	23.7	35.6
G108	31.9	86.9	66.2	31.9	34.3	72.1	90.0	46.5	43.4	10.7	15.7	25.7	35.4
G109	35.2	81.8	70.6	34.0	36.6	86.8	89.8	45.1	44.6	12.6	16.8	23.5	32.9
G110	28.2	77.0	65.5	31.4	34.1	66.1	86.6	43.0	43.7	9.5	15.2	26.0	32.9
G111	33.0	86.3	73.3	35.4	37.9	78.1	91.5	46.6	44.9	9.2	15.8	20.7	32.7
G112	33.4	86.0	72.1	34.8	37.3	80.1	95.9	48.4	47.5	12.2	17.8	24.4	31.3
G113	32.0	72.6	61.8	29.6	32.1	84.1	88.7	44.7	44.0	12.0	16.0	23.8	28.5
G114	36.5	86.9	73.3	35.4	37.9	80.2	99.3	50.6	48.7	12.1	20.5	27.3	39.8
G115	31.2	76.6	68.7	33.1	35.6	76.0	91.3	62.6	28.7	9.9	16.4	23.1	34.7
G116	34.2	88.2	69.0	33.3	35.8	79.1	85.5	43.5	41.9	11.0	16.3	26.5	36.9
G117	39.0	84.5	71.8	34.7	37.1	72.4	98.0	49.6	48.4	12.1	18.4	26.0	39.5
G118	31.7	79.1	62.7	30.1	32.6	66.6	87.7	57.3	30.4	12.5	15.4	23.9	30.2
G119	32.7	77.1	63.7	30.5	33.2	64.2	83.7	43.5	40.2	10.9	16.0	23.5	29.9
G120	32.8	80.6	61.8	29.6	32.2	85.2	89.5	46.7	42.8	10.9	18.1	26.2	31.5
G121	34.5	75.5	65.1	31.3	33.8	76.0	89.4	46.2	43.2	10.3	18.0	23.7	32.5
G122	33.6	89.2	71.2	34.2	37.0	72.1	93.6	46.6	47.0	11.5	19.1	25.6	37.1
G123	33.6	84.9	68.6	33.1	35.6	79.1	96.6	48.0	48.6	12.3	16.1	25.8	37.8
G124	35.1	78.6	66.8	32.1	34.7	81.1	97.2	50.2	46.9	11.0	14.4	25.5	32.1
G125	37.5	79.7	65.2	31.3	33.9	78.4	87.7	44.9	42.8	11.2	15.6	23.0	32.4
G126	31.2	84.5	64.6	31.2	33.4	79.9	91.4	47.0	44.4	11.1	17.6	24.2	35.8
G127	33.4	92.2	73.7	35.6	38.1	81.6	101.3	52.2	49.1	12.0	16.5	24.7	39.4
G128	34.7	88.7	76.0	36.8	39.2	84.7	100.7	49.2	51.5	11.2	18.2	25.1	41.3
G129	33.3	85.4	67.4	32.3	35.1	75.3	94.0	48.4	45.7	11.7	18.0	23.6	33.5
G130	33.5	83.8	72.2	34.8	37.3	86.2	93.4	47.2	46.2	14.0	16.1	25.5	38.2

Appendix II. Pilot survey result of concept design

Robotic Mannequin Shape Design Validation

機器人模特兒外形設計驗證

- By Dr. Chan (ITC), Dr. Luximon (ITC), Dr. Ip (ISE), Peng Sixiang (ITC)

Targets: Textile researchers, teachers and engineers and specialists.

訪問對象: 紡織專業研究人員, 教師, 工程師以及專家

Questionnaire:

The data collected from the questionnaire will be used for a research about the robotic mannequin development. In order to accomplish these goals, we need your complete and honest participation. We ensure the personal information and questionnaire result will be completely confidential for everyone who completes this survey.

以下收集的是為研究項目 - <機器人模特兒項目>提供資料.我們期待可以獲得您的真誠配合。 個人資料與調查結果會嚴格保密。

Confidential statement:

Please recognise that all the information provided about the robotic mannequin

project during this validation questionnaire procedure is highly confidential and should not be disclosed to any third party or person, or used for any purpose without our permission.

請閣下明白，在這次問卷調查中所有與機器人模特兒項目相關的信息與設計是機密而不可泄露給第三方的，并且在沒有我們允許的情況下不可被用作任何用途。

The questionnaire is divided in two parts to collect 問卷分為三部分:

A. Comments on the shape design of the robotic mannequin and whether it meets the requirement of research and industry use.

對機器人模特兒的外形設計也功能是否滿足研究與業界使用的需求。

B. Comments on any further improvement on the robotic mannequin shape design.

關於機器人模特兒的外形設計改進的建議

C. Participant personal information.

被訪人個人資料。

PART B: Comments on the shape design of the robotic mannequin

對機器人模特兒的外形設計的意見

Please circle the option which most fit for your feeling to the robotic mannequin design.

Robotic mannequin shape design 機器人模特兒的外形設計	Please Circle one option 請圈出一個選擇				
	Strongly Disagree 非常不同意	Disagree 不同意	Neutral 中立	Agree 同意	Strongly Agree 非常同意
The shape of the robotic mannequin is very close to the real human body within the design size variation range. 在設計尺寸變化範圍內，機器人模特兒總是能夠真實的模擬出人體的外形。				✓	
The design size variation range of robotic mannequin is sufficient for the research and industry use. 設計尺寸變化範圍可以滿足研究與業界的需要。					✓
The size input function is user-friendly 尺寸變化控制操作簡單。			✓		
The robotic mannequin can simulate most of different the human body types. 機器人模特兒可以模仿大部分的體形。				✓	
The dimension precision is good enough. 尺寸精度滿足需要。				✓	

Part C: Comments on any further improvement on the robotic mannequin

shape design

任何關於機器人模特兒的外形設計改進的建議

PART C: Participant personal information.

被訪人個人資料

Name: Mrs Cheung

Occupation: ☒ teacher ☒ researcher ☐ specialist or engineer from the textile

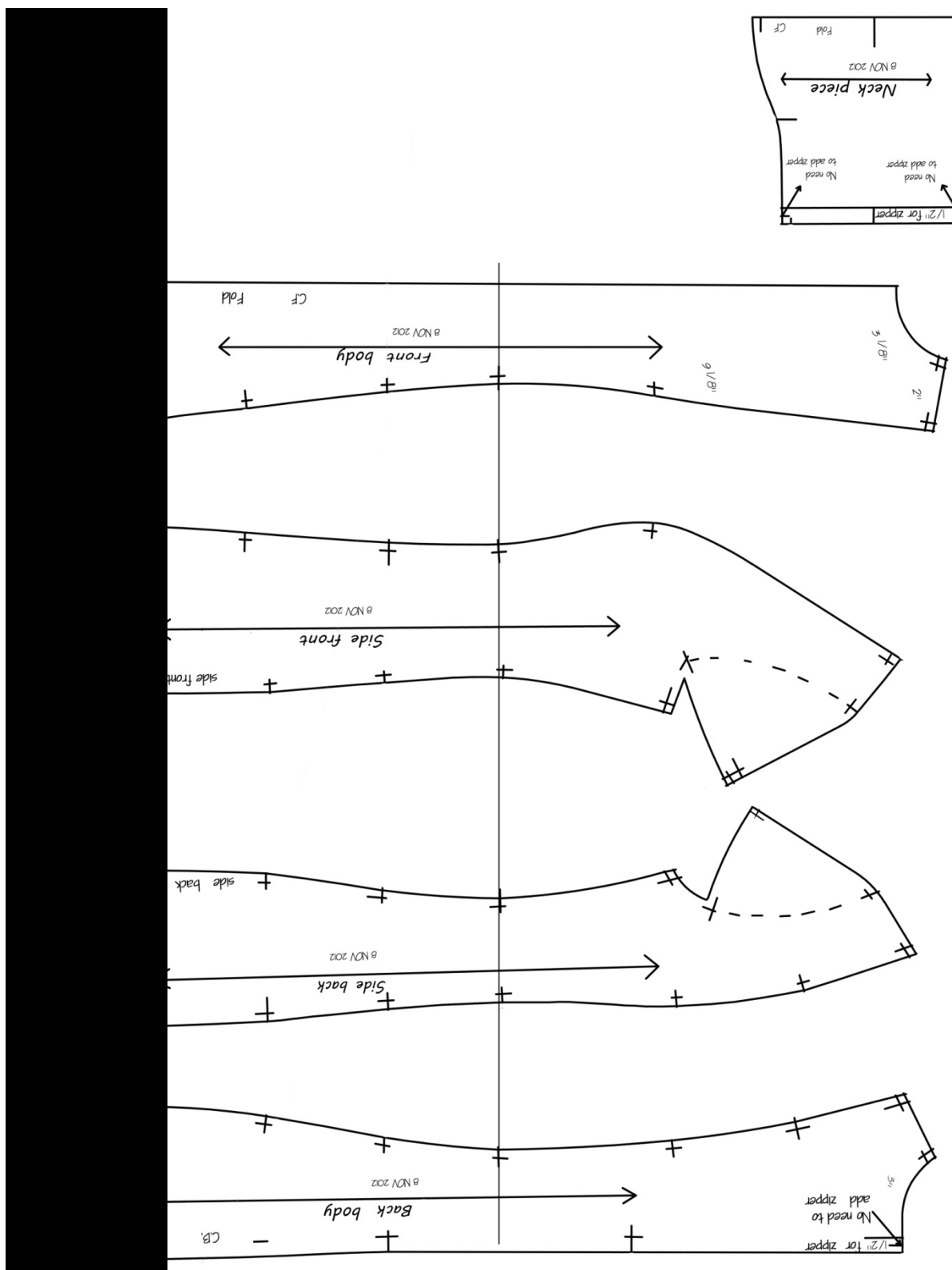
industry

☐ others (please specify_____)

THANK YOU VERY MUCH FOR YOUR COORERATION

多謝您的合作和寶貴意見

Appendix III. Cladding pattern



Bibliographies

- Alvanon mannequins [Online]. Available: www.alvanon.com/M01_S01.html [Accessed 2013].
- Alvanon website [Online]. Available: http://www.alvanon.com/M01_S03.html [Accessed 2012].
- Andreetto, M., Brusco, N. and Cortelazzo, G. M. 2004. Automatic 3D modeling of textured cultural heritage objects. *Image Processing, IEEE Transactions on*, 13, 354-369.
- Angelo, J. A. 2007. *Robotics: a reference guide to the new technology*, Greenwood Publishing Group.
- Arthur, E. R. 1974. Dressform. Google Patents.
- Asimow, M. 1962. *Introduction to design*, Prentice-Hall Englewood Cliffs.
- Böhler, W. and Marbs, A. 2002. 3D scanning instruments. *Proceedings of the CIPA WG*, 6, 9e18.
- Barhak, J. and Fischer, A. 2001. Parameterization for reconstruction of 3D freeform objects from laser-scanned data based on a PDE method. *The Visual Computer*, 17, 353-369.
- Barra, M. and Ralston, J. 2007. Adjustable dress form system. US Patent 20,070,275,632.
- Beatie, B. A. The American Heritage Dictionary of the English Language (review).
- Ben Azouz, Z., Rioux, M., Shu, C. and Lepage, R. 2005. Characterizing human shape variation using 3-d anthropometric data. *The Visual Computer*.
- Bentham, M., Bingham, G., Bruner, D. and Demers, M. 2004. Configurable mannequin form. US Patent 20,040,222,249.
- Beraldin, J. A., Picard, M., El-Hakim, S., Godin, G., Valzano, V. and Bandiera, A. Year. Combining 3D technologies for cultural heritage interpretation and

-
- entertainment. *In*, 2005. CiteSeer, 108-118.
- Bernardini, F., Chandrajit, L. B., Chen, J. and Daniel, R. S. 1999. Automatic reconstruction of 3D CAD models from digital scans. *International Journal of Computational Geometry & Applications*, 9, 327-369.
- Beutel, A. 2011. NASA's Mars Science Laboratory Launch Rescheduled for Nov. 26 [Online]. [Accessed 2012].
- Black, R. 1996. *Design and manufacture: an integrated approach*, Macmillan.
- Boyd, C. 2010. Terminator bots aim to give web shppers the right fit [Online]. Available: <http://www.bbc.com/news/technology-10687701> [Accessed 2012].
- Brenneke, C., Wulf, O. and Wagner, B. Year. Using 3d laser range data for slam in outdoor environments. *In: Intelligent Robots and Systems, 2003.(IROS 2003). Proceedings. 2003 IEEE/RSJ International Conference on, 2003. IEEE*, 188-193.
- Brosnan, M. 1947. *Display world*.
- Capek, K. 1920. Rossum's universal robots. *Prague, CZ*.
- Carbone, V., Carocci, M., Savio, E., Sansoni, G. and De Chiffre, L. 2001. Combination of a vision system and a coordinate measuring machine for the reverse engineering of freeform surfaces. *The International Journal of Advanced Manufacturing Technology*, 17, 263-271.
- Carrere, C., Istook, C., Little, T., Hong, H. and Plumlee, T. 2000. Automated garment development from body scan data. *National Textile Center Annual Report I*.
- Cheverud, J., Gordon, C., Walker, R., Jacquish, C., Kohn, L., Moore, A. and Yamashita, N. 1988. Anthropometric Survey of US Army Personnel: Correlation Coefficients and Regression Equations, Part 3 Simple and Partial Correlation Tables--Female. NATICK/TR-90/033 and 90/034. Natick, MA: US Army Natick Research, Development, and Engineering Center. AD.
- Claas, S. J. 1994. Mannequin-type clothing display assembly composed of rubberized acrylic material. US Patent 5,310,099.
- Colborne, R. 1996. *Visual merchandising: The business of merchandise presentation*,

Cengage Learning.

- Costume, H. and Strege, G. 1999. The art of selling: a history of visual merchandising. [Online]. Available: https://kb.osu.edu/dspace/bitstream/handle/1811/44670/Art_of_Selling_A_History_of_Visual_Merchandising_lg.pdf?sequence=1 [Accessed 2012].
- D'apuzzo, N. Year. 3D body scanning technology for fashion and apparel industry. *In*, 2007a.
- D'apuzzo, N. Year. 3D body scanning technology for fashion and apparel industry. *In*: Proceedings of SPIE, the International Society for Optical Engineering, 2007b. Society of Photo-Optical Instrumentation Engineers, 64910O. 1-64910O. 12.
- D'aulaire, E. and D'aulaire, P. O. 1991. Mannequins: our fantasy figures of high fashion. *Smithsonian*, 22, 66-76.
- D'apuzzo, N. Year. Overview of 3D surface digitization technologies in Europe. *In*, 2006. 42-54.
- Davis, M. 1999. The Rise of The Realistic Mannequin [Online]. Available: http://www.fashionwindows.com/mannequin_history/026femalerealism.asp [Accessed 2012].
- DINGS' electrical & mechanical Co., Ltd product brochure. 2012.].
- Dong, X. and Huang, R. 2006. Application of 3D laser scanning technology to geologic survey of high and steep slope. *Chinese Journal of Rock Mechanics and Engineering*, 25, 3629-3635.
- Faust, M. E. and Carrier, S. 2009. Discard 'One Size Fits All' Labels! Proposal for New Size and Body Shape Labels to Achieve Mass Customization in the Apparel Industry. *HANDBOOK OF RESEARCH IN MASS CUSTOMIZATION AND PERSONALIZATION*, Frank T. Piller, Michell M. Tseng, eds., World Scientific Publishing, 2009.
- Frank, P. I. and David, P. D. W. 1996. Fundamentals of heat and mass transfer. *John Wiley & Sons, Purdue University*, 683-684.
- Gao, Y., Zhao, Q., Hao, A., Sezgin, T. and Dodgson, N. 2010. Automatic construction of 3D animatable facial avatars. *Computer Animation and Virtual*

-
- Worlds*, 21, 343-354.
- Gerhardus, D. 2003. Robot-assisted surgery: the future is here. *Journal of Healthcare Management*, 48, 242-251.
- Golovinskiy, A., Kim, V. G. and Funkhouser, T. Year. Shape-based recognition of 3d point clouds in urban environments. *In*, 2009. IEEE, 2154-2161.
- Greenberg, I. 1935. Adjustable dress. Google Patents.
- Greenspan, R. 2003. Apparel sales apparent online [Online]. Available: www.cyberatlas.internet.com/markets/retailing/print/0,6061_2171361,00.html [Accessed 2010].
- Greenspan, R. 2003. Apparel sales apparent online. *CyberAtlas*, available at: www.cyberatlas.internet.com/markets/retailing/print/0,6061_2171361,00.html.
- Gronberg, T. 1997. Beware Beautiful Women: The 1920s shopwindow mannequin and a physiognomy of effacement. *ART HISTORY-OXFORD-*, 20, 375-396.
- Guidi, G., Beraldin, J. A. and Atzeni, C. 2004. High-accuracy 3D modeling of cultural heritage: the digitizing of Donatello's. *Image Processing, IEEE Transactions on*, 13, 370-380.
- Handbook, M. 1991. Anthropometry of U. S. Military Personnel. Department of Defense Document No. DOD-HDBK-743A. Released February 13.
- Hardaker, C. H. M. and Fozzard, G. J. W. 1997. Towards the virtual garment: three-dimensional computer environments for garment design. *International Journal of Clothing Science and Technology*, 10, 114-127.
- Hardaker, C. H. M. and Fozzard, G. J. W. 1998. Towards the virtual garment: three-dimensional computer environments for garment design. *International Journal of Clothing Science and Technology*, 10, 114-127.
- Hu, S., Zha, H. and Zhang, A. 2006. Modeling method for large-scale cultural heritage sites and objects using real geometric data and real texture data. *Journal of System Simulation*, 4, 035.
- Istook, C. L. and Hwang, S. J. 2001. 3D body scanning systems with application to the apparel industry. *Journal of Fashion Marketing and Management*, 5,

120-132.

Jense, G. J. 1989. Voxel-based methods for CAD. *Computer-Aided Design*, 21, 528-533.

Jiang, J. 1993. Mannequin with adjustable parts. US Patent 5,265,779.

K&L website [Online]. Available: <http://www.kennettlindsell.com/> [Accessed 2012].

Kakinuma, Y., Tsutsumi, E., Kondo, K., Mitani, J., Miyahara, S., Suzuki, H. and Yoshiyuki, I. 2008. Customized garment design supporting system for aged people using digital dress form model. *13th International Conference on Geometry and Graphics*. Dresden (Germany).

Kato, K. and Hirose, S. 2001. Development of the quadruped walking robot, TITAN-IX—mechanical design concept and application for the humanitarian de-mining robot. *Advanced Robotics*, 15, 191-204.

Khakimdjanova, L. and Park, J. 2005. Online visual merchandising practice of apparel e-merchants. *Journal of Retailing and Consumer Services*, 12, 307-318.

Kim, S. and Park, C. 2004. Parametric body model generation for garment drape simulation. *Fibers and Polymers*, 5, 12-18.

Kim, S. and Park, C. K. 2004. Parametric body model generation for garment drape simulation. *Fibers and Polymers*, 5, 12-18.

Kim, W. Y., Stuber, M., Börnert, P., Kissinger, K. V., Manning, W. J. and Botnar, R. M. 2002. Three-dimensional black-blood cardiac magnetic resonance coronary vessel wall imaging detects positive arterial remodeling in patients with nonsignificant coronary artery disease. *Circulation*, 106, 296-299.

Kouchi, M. and Mochimaru, M. 2002. Japanese body dimensions data 1997-1998. In: *Digital Human Laboratory*, N. I. O. a. I. S. a. T. (ed.).

Kruusmaa, M., Aabloo, A., Abels, A., Leinus, R., Haldre, H., Pällin, P. and Hindpere, E. 2010. Method and system for custom tailoring and retail sale of clothing. US Patent 20,100,070,384.

Law, J. M. 1997. *Puppets of Nostalgia: The Life, Death, and Rebirth of the Japanese Awaji Ningyo Tradition*, Princeton University Press.

-
- Lee, K. H., Woo, H. and Suk, T. 2001. Data reduction methods for reverse engineering. *The International Journal of Advanced Manufacturing Technology*, 17, 735-743.
- Loewenstein, K. L. 1983. *The Manufacturing Technology of Continuous Glass Fibers*, Amsterdam, Elsevier Science Publishers.
- Loker, S., Ashdown, S. and Schoenfelder, K. 2005. Size-specific analysis of body scan data to improve apparel fit. *Journal of textile and apparel, technology and management*, 4, 1-15.
- Ma, W. and He, P. 1998. B-spline surface local updating with unorganized points. *Computer-Aided Design*, 30, 853-862.
- Mantyla, M. 1990. A modeling system for top-down design of assembled products. *IBM Journal of Research and Development*, 34, 636-659.
- Moon, F. C. 2007. *The machines of Leonardo da Vinci and Franz Reuleaux: kinematics of machines from the Renaissance to the 20th century*, Springer Verlag.
- Nist, P. L. O. 1995. Early Clocks [Online]. Available: <http://web.archive.org/web/20080531063139/http://physics.nist.gov/GenInt/Time/early.html> [Accessed August 2012].
- Nof, S. Y. 1999. *Handbook of industrial robotics*, Wiley.
- Otto, K. N. and Wood, K. L. 2000. *Product design*, Prentice hall Englewood Cliffs, NJ.
- Paquette, S. 1996. 3D scanning in apparel design and human engineering. *Computer Graphics and Applications, IEEE*, 16, 11-15.
- Peers, J. 2004. *The fashion doll: from Béb  Jumeau to Barbie*, Berg Publishers.
- Petrak, S. and Rogale, D. 2006. Systematic representation and application of a 3D computer-aided garment construction method: Part I: 3D garment basic cut construction on a virtual body model. *International Journal of Clothing Science and Technology*, 18, 179-187.
- Pieraccini, M., Guidi, G. and Atzeni, C. 2001. 3D digitizing of cultural heritage.

- Journal of Cultural Heritage*, 2, 63-70.
- RB-150MG product homepage [Online]. Available: <http://trade.taobao.com/trade/detail/tradeSnap.htm?spm=a1z09.2.9.79.Buqq7k&tradeID=168744214367875> [Accessed 2013].
- Ronan, C. A. and Needham, J. 1978. *The Shorter Science and Civilisation in China*, Cambridge Univ Press.
- Rosheim, M. E. 1994. *Robot evolution: the development of anthropotics*, Wiley-Interscience.
- Rout, N., Zhang, Y. F., Khandual, A. and Luximon, A. 2010. 3D foot scan to custom shoe last. *Special Issue of International Journal of Computer and Communication Technology*, 1, 14-18.
- Sakagami, Y., Watanabe, R., Aoyama, C., Matsunaga, S., Higaki, N. and Fujimura, K. Year. The intelligent ASIMO: System overview and integration. *In*, 2002. IEEE, 2478-2483.
- Seo, H., Yeo, Y. and Wohn, K. 2006. 3D Body reconstruction from photos based on range scan. *Technologies for E-Learning and Digital Entertainment*, 849-860.
- Shih, N. J., Wang, H. J., Lin, C. Y. and Liao, C. Y. 2007. 3D scan for the digital preservation of a historical temple in Taiwan. *Advances in Engineering Software*, 38, 501-512.
- Simmons, K., Istook, C. L. and Devarajan, P. 2004. Female figure identification technique (FFIT) for apparel part I: describing female shapes. *Journal of Textile and Apparel, Technology and Management*, 4, 1-16.
- Simmons, K., Istook, C. L., Devarajan, P. and 2004. Female figure identification technique(FFIT) for apparel part I: describing female shapes. *Journal of textile and apparel, technology and management*, 4.
- Simmons, K. P. 2001. *Body measurement techniques: a comparison of three-dimensional body scanning and physical anthropometric methods*. North Carolina State University.
- Simmons, K. P. and Istook, C. L. 2003. Body measurement techniques: Comparing 3D body-scanning and anthropometric methods for apparel applications.

-
- Journal of Fashion Marketing and Management*, 7, 306-332.
- Slob, S. and Hack, R. 2004. 3D terrestrial laser scanning as a new field measurement and monitoring technique. *Engineering Geology for Infrastructure Planning in Europe*, 179-189.
- Sobh, T. M. and Xiong, X. 2012. *Prototyping of Robotic Systems: Applications of Design and Implementation*, Information Science Reference.
- Sokovic, M. and Kopac, J. 2006. RE (reverse engineering) as necessary phase by rapid product development. *Journal of Materials Processing Technology*, 175, 398-403.
- Solidwork 2012 online helps [Online]. 2012. Available: http://help.solidworks.com/2010/English/SolidWorks/cworks/LegacyHelp/Simulation/Meshing_topics/IDH_What_are_the_mesh_quality_checks_.html [Accessed 2012].
- Son, S., Park, H. and Lee, K. H. 2002. Automated laser scanning system for reverse engineering and inspection. *International Journal of Machine Tools and Manufacture*, 42, 889-897.
- Spiteri, C. J. 1990. *Robotics technology*, Saunders College Pub.
- T.S.C.V. 2008. How it's made: dress forms.
- Taylor, L. 2002. *The study of dress history*, Manchester University Press.
- Taylor, P. J. and Shoben, M. M. 1993. *Grading for the fashion industry: The theory and practice*, Stanley Thornes.
- Thesander, M. 1997. *Feminine Ideal*, Reaktion Books.
- Vassilev, T. I. 2000. Dressing virtual people. *Proceedings of Systemics, Cybernetics and Informatics*, 2000.
- Vepa, R. 2009. Biomimetic robotics: mechanisms and control. *Recherche*, 67, 02.
- Wang, C. 2005. Parameterization and parametric design of mannequins. *Computer-Aided Design*, 37, 83-98.
- Wang Zhi Li, W. D. K. 2003. *Ji xie she ji zhong he ke chen she ji*, Beijing, China

machine press.

Werghi, N. and Xiao, Y. Year. Posture recognition and segmentation from 3D human body scans. *In*, 2002. IEEE, 636-639.

Workman, J. and Lentz, E. 2000. Measurement specifications for manufacturers' prototype bodies. *Clothing and Textiles Research Journal*, 18, 251.

Xu, B., Huang, Y., Yu, W. and Chen, T. 2002. Body scanning and modeling for custom fit garments. *Journal of textile and apparel technology and management*, 2, 1-11.

Yau, H. T., Chen, C. Y. and Wilhelm, R. G. 2000. Registration and integration of multiple laser scanned data for reverse engineering of complex 3D models. *International Journal of production research*, 38, 269-285.

Yoshiura, H., Fujimura, K. and Kunii, T. L. 1984. Top-down construction of 3-D mechanical object shapes from engineering drawings. *Computer*, 17, 32-40.

Zappia, C. 2006. Fifty years of "ideal " beauty in fiberglass. *NYC Life*. New York.